UNIVERSIDADE DE SÃO PAULO

INSTITUTO DE GEOCIÊNCIAS

TAPHONOMY OF FOSSIL GROUPS FROM THE CRATO MEMBER (SANTANA FORMATION, ARARIPE BASIN, EARLY CRETACEOUS, NORTH-EAST BRAZIL): GEOBIOLOGICAL, PALAEOECOLOGICAL, AND PALAEOENVIRONMENTAL IMPLICATIONS

TAFONOMIA DE GRUPOS FÓSSEIS DO MEMBRO CRATO (FORMAÇÃO SANTANA, BACIA DO ARARIPE, EOCRETÁCEO, NE DO BRASIL): IMPLICAÇÕES GEOBIOLÓGICAS, PALEOECOLÓGICAS E PALEOAMBIENTAIS

Gabriel Ladeira Osés

Advisor: Prof. Dr. Setembrino Petri

MASTERS DISSERTATION

Programa de Pós-Graduação em Geoquímica e Geotectônica

São Paulo

2016

DEDICATION

I dedicate this dissertation to each person who helped me in my research, especially my family and advisors, who never spared efforts to give me freedom of thought, and my friends, who have always encouraged me to question myself, doubt my conclusions, and develop creativity.

ACKNOWLEDGEMENTS

I am very honoured to have known Professor Setembrino Petri (IGc-USP) and Professor Mírian Liza Alves Forancelli Pacheco (DBio-UFSCAR), who have both become great friends while advising me in my dissertation. Their humility and dedication are inspiring; their passion for Science is contagious; and their willingness to give students freedom of thought is fruitful. I have always had invaluable help during my research and own them my academic growth.

I acknowledge the Brazilian Council for Scientific and Technological Development (Process 154062/2014-6) for having provided my masters scholarship, and the Post-Graduation Program in Geochemistry and Geotectonics of the Institute of Geosciences of the University of São Paulo for logistics and financial support. I also thank the post-graduation secretaries for full support during my masters.

My sincere thanks also goes to Professor Thomas Rich Fairchild (IGc-USP), whose witty comments and sharp criticism make research routine lighter but, nevertheless, a high- quality enterprise. Professor Luiz Eduardo Anelli (IGc-USP) has always inspired me with insightful discussions. I also thank Professor Juliana Moraes de Leme Basso and Professor Paulo Eduardo de Oliveira (both from the IGc-USP) for having provided classroom assistant scholarships, and Ivone Cardoso Gonzales, Josefa Francisca Ferreira and all trainees of the Palaeontological Scientific Collection of the IGc-USP for their prompt help with infra-structure issues, facilitating research activities enormously. Samuel "Samuca" has always helped in dangerous rock cutting and Renato Carvalho in skilful thin-section preparation. I am also very grateful to Prof. Dr. Marcia de Almeida Rizzutto (IF-USP), Dr. Douglas Galante (LNLS), Prof. Dr. Fabio Rodrigues (IQ-USP), Prof. Dr. Adriana de Oliveira Delgado (UFSCAR), Rafael Parra Ribeiro (UNESP Sorocaba), and Prof. Dr. Elidiane Rangel (UNESP Sorocaba), who have made a great effort in both teaching and helping me with analytical techniques since the very early stages of my research. I am thankful to Izabel Ladeira ("English for You") for language revision, to Professor Mario Luis Assine (IGCE-UNESP), who have kindly provided a vectorized version of a map of the Araripe Basin, and to Bruno Becker Kerber (PPGERN-UFSCAR) for the palaeoenvironmental diagram of the Crato palaeolake.

I would like to thank my family, including my parents Ana and Julio, my brothers Guilherme and Mariana, my aunts Amália and Izabel, my uncle Hugo, and my grandmothers Lourdes and Rosa, for their kindness, inspiration and support throughout my life.

Last but not least, I thank the following friends for their faithful companionship, stimulating discussions, and unforgettable moments of joy: Gustavo Zanco Ramos (IGc-USP), Lucas Ferreira, Julio Inhasz, Danilo Lomonaco Vitorelli, Dr. Guilherme Raffaeli Romero (IG-UFPA), Gustavo Marcondes Evangelista Martins Prado (IGc-USP), Dr. Paula Andrea Sucerquia (DGeo-UFPE), Isabella Jorgenfeldt Viggiani, MSc. Luana Pereira Costa de Morais Soares (IGc-USP), Dr. Evelyn Aparecida Mecenero Sanchez Bizan (UFVJM), Silvio Yuji (FFCLRP-USP), MSc. Bruno Becker Kerber (PPGERN-UFSCAR), Dr. Cleber Calça, Dr. Cibele Gasparelo Voltani (IGCE-UNESP), Prof. Dr. Isaac Daniel Rudnitzki (IAG-USP), Evandro Silva (IQ-USP), MSc. Gabriel Araújo (IQ-USP), Dr. Giselle Utida, MSc. Rudney de Almeida Santos (IGc-USP), MSc. Victor Badaró (IGc-USP), and many others for whom I have immense gratitude.

I acknowledge scientists and institutions which helped in this research in each article.

Equipped with his five senses, man explores the universe around him and calls the adventure Science.

Edwin Powell Hubble

Table of Contents

Index of Figures

Chapter 3

Chapter 5

Reduction, M - Methanogenesis) on the left. The correspondent reactions are seen at figure bottom. Electron acceptor curves used in these respiration processes are depicted, showing electron acceptor depletion from right to left (indicated by arrow at figure top). Sediment depth is represented by vertical arrow. Either pyritized (upper diagram) or kerogenized (lower diagram) fossils are represented by an ellipsis, located in the correspondent simplified sediment geochemical zone (sulphidic or methanic). Curves of respiration geochemical products are depicted on the right, showing increase from left to right. We propose that BL (upper diagram) has been deposited at lower sedimentation rates than GL (lower diagram) facies, as evidenced by greater terrigenous clay/organic matter content and peloid levels in GL. Variable sedimentation rates are explained by transgressive-regressive climatic cycles[15]. As a consequence, carcasses in BL have remained longer in the sulphidic zone, whereas carcasses in GL have both entered more rapidly and spent more time in the methanic zone, respectively yielding pyritized and kerogenized labile-tissues. In addition, variable cement contents in different carbonate facies[38] plus clay in GL facies could have diminished sulphate percolation downwards, narrowing the sulphidic zone. The hypotheses we propose are based on references 6, 57. Microbial respiration process zonation and reactions, geochemical zonation, plus electron acceptor and geochemical product curves are based on reference 54…….79

Supplementary Figure 1. Geologic unit of the studied fossils. a, The Araripe Basin. **b**, Localization of the Araripe Basin in Brazil. **c**, Representative lithostratigraphic column of the Crato Member. **c** is modified from ref. 9…….91

Supplementary Figure 2. EDS point spectra. Thin sections GP/L 20 (**a**) and GP/L 16 (**b**) and specimens GP/2E 7786f (**c**) and GP/2E 7913e (**d**). **a**, 1 – calcite cement, 2 – bone, 3 – soft-tissue. **b**, 1 – calcite cement, 2 – bone, 3 – soft-tissue. **c**, Muscle microfabric composition: 1 – base of caudal fin, 2 – base of dorsal fin, 3 – muscles attached to vertebral column. **d**, 1 – microfabric, 2 – putative EPS……92

Supplementary Figure 3. Micro-Raman spectra of soft-tissues. a, Specimen GP/2E 9005. Soft-tissues are indicated by arrow heads. Scale bar is 30 mm. **b**, Spectrum of goethite (peaks at 235, 287, and 377 cm^{-1}) of BL fish GP/2E 7786f (Supplementary Figure 7). **c**, Spectrum of kerogen (D band – ca. 1366 cm^{-1}; G band – ca. 1583 cm^{-1}) of fossil in **a**. Intense bands (D and G bands) plus the lack of shoulder associated with the G band suggest that the analyzed material is both highly disordered and poorly

Abstract

Over the past decades, the so-called Fossil *Lagerstätten* have been in the core of discussions concerning the palaeobiological and geological history of the Earth. In particular, the Crato Member from the Santana Formation (Araripe Basin, north-east Brazil) is one of the most significant Cretaceous *Lagerstätten* since it records exceptionally well-preserved fossil invertebrates, vertebrates, and plants, deposited in palaeolake carbonate beds. The main aim of this dissertation is to shed light on the preservational processes responsible for the fossilization of insects and fishes still retaining 3D soft tissues. Petrographic thin sections and several palaeometric techniques – micro-Raman Spectroscopy, conventional X-ray Fluorescence (XRF), Synchrotron micro-XRF (SR-μXRF), Particle-Induced X-ray Emission (PIXE), Scanning Electron Microscopy (SEM), and Energy-Dispersive X-ray Spectroscopy (EDS) – have been employed to characterize the host rock, soft-tissue morphology and preservational fidelity, and fossil elemental and molecular compositions in centimetre to micrometre scale. The results reveal that while insects and fish soft-tissues found in the so called beige limestones (BL) are replaced by framboidal pyrite pseudomorphs (after pyrite oxidation) occurring together with putative bacterially-secreted extracellular polymeric substances (EPS), labile tissues of fishes from the grey limestones (GL) are kerogenized. In insects, there is a variation of framboid size inward the fossils, which is here interpreted as a product of the balance between diffusion and mineral nucleation rates. Moreover, the preferential distribution of Zn and Cu in pyritized insect/fish labile structures in comparison to their rock matrix is here considered as being the result of element fixation in bacterial biofilms. Zn concentrated in bones of kerogenized fishes and Fe/Cu occurring in their soft tissues are considered to have been incorporated during fish life. In the particular case of fishes, a model originally proposed for metazoan preservation in the Precambrian is here applied to explain the variation of fossilization between the BL and GL facies. Petrographic thin sections reveal that GL have generally higher clay/organic matter contents than BL, thus implying that burial rates might have been more intense in the former. This could have placed decaying carcasses more quickly in the methanogenesis sedimentary zone, in that way being kerogenized. On the other hand, carcasses deposited in the BL facies could have spent a

longer period in the sulphate-reduction zone, which would have accounted for pervasive pyritization. Additionally, microspar low porosity, cement and clay could have diminished both downward migrations of electron acceptors for anaerobic bacterial respiration processes – particularly sulphate-reduction (SR) and methanogenesis – and of their biogeochemical products, narrowing the SR zone, which would have lowered the impact of pyritization in some levels. While pyritization has recorded 3D muscle fibres, sarcolemma, putative cell nuclei, tendons and eyes, kerogenization has yielded connective tissues, integument and compressed/distorted muscle fibres. In conclusion, it is here proposed that palaeoenvironmental/geobiological-influenced facies have yielded fossils with a variable preservational-fidelity gradient, accordingly to each taphonomic pathway followed.

Key words: taphonomy, palaeometry, Early Cretaceous, Araripe Basin, Crato Member, exceptional preservation, taphonomic window, taphonomic model, preservational fidelity, fossil insects, fossil fishes, pyrite, kerogen.

Resumo

Nas últimas décadas, os *Lagerstätten* estiveram no centro das discussões relativas à história paleobiológica e geológica da Terra. Em particular, o Membro Crato da Formação Santana (Bacia do Araripe, Nordeste do Brasil) é um dos mais significantes *Lagerstätten* do Cretáceo já que registra invertebrados, vertebrados e plantas excepcionalmente preservados em sedimentos carbonáticos de um palaeolago. O principal objetivo desta dissertação é lançar luz sobre os processos de preservação responsáveis pela fossilização de insetos e peixes com tecidos moles em 3D. Lâminas petrográficas e diversas técnicas paleométricas – micro-Espectroscopia Raman, Fluorescência de raios-X (FRX) convencional, micro-FRX com fonte de luz sincrotron (RS-μFRX), emissão de Raios-X induzida por partículas (PIXE), microscopia eletrônica de varredura (MEV) e espectroscopia de energia dispersiva de Raios-X (EDS) – foram empregadas para caracterizar a rocha matriz, a morfologia e fidelidade de preservação dos tecidos moles e as composições elementares e moleculares dos fósseis em escala de centímetros e mícron. Os resultados revelam que, enquanto insetos e tecidos moles de

peixes encontrados nos denominados calcários beges (BL) são substituídos por pseudomorfos de pirita framboidal (após oxidação da pirita), os quais ocorrem juntamente com possíveis substâncias poliméricas extracelulares secretadas por bactérias (EPS), tecidos de peixes dos calcários cinza (GL) são querogenizados. Em insetos, existe variação de tamanho dos framboides para dentro dos fósseis, que é aqui interpretada como produto do equilíbrio entre as taxas de difusão e de nucleação dos minerais. Além disso, a distribuição preferencial de Zn e Cu em estruturas piritizadas de insetos e peixes em comparação com a sua matriz é aqui considerada como sendo o resultado da fixação de elementos químicos em biofilmes bacterianos. Zn concentrado nos ossos de peixes com querogenizados e Fe/Cu observados em seus tecidos moles são considerados como tendo sido incorporados durante a vida dos peixes. No caso particular de peixes, modelo originalmente proposto para a preservação de metazoários do Pré-cambriano é aqui aplicado para explicar a variação de fossilização entre as fácies BL e GL. Lâminas petrográficas revelam que os GL têm geralmente teor de argila/matéria orgânica maior do que os BL, implicando que as taxas de soterramento poderiam ter sido mais intensas nos GL. Isto teria colocado carcaças em decomposição mais rapidamente na zona sedimentar de metanogênese, sendo formado o querogênio. Por outro lado, carcaças depositadas na fácies BL poderiam ter passado período mais longo na zona de redução de sulfato, o que teria levado à piritização generalizada. Além disso, a baixa porosidade do microespato, o cimento e a argila poderiam ter diminuído a migração de aceptores de elétrons dos processos de respiração bacteriana anaeróbia – particularmente redução de sulfato (RS) e metanogênese – e de seus produtos biogeoquímicos, estreitando a zona de RS, o que teria reduzido a influência da piritização em alguns níveis. Enquanto que a piritização resultou na preservação de fibras musculares em 3D, sarcolema, possíveis núcleos celulares, tendões e olhos, a querogenização preservou tecidos conjuntivos, tegumento e fibras musculares distorcidas e compactadas. Em conclusão, é aqui proposto que fácies influenciadas por processos paleoambientais e geobiológicos produziram fósseis com gradiente diferencial de fidelidade de preservação de acordo com cada via tafonômica seguida.

Palavras-chave: tafonomia, paleometria, Eocretáceo, Bacia do Araripe, Membro Crato, preservação excepcional, janela tafonômica, modelo tafonômico, fidelidade de preservação, insetos fósseis, peixes fósseis, pirita, querogênio.

1. Introduction

The term Fossil *Lagerstätten* (or taphonomic windows) was coined by the German palaeontologist Adolf Seilacher 30 years ago and embraces rock deposits which are particularly rich in qualitative and quantitative fossil content (Seilacher et al., 1985). Therefore, according to these authors, Fossil *Lagerstätten* yield palaeobiological and taphonomic data which provide a broad and complete view of sedimentary facies genesis. Seilacher et al. (1985) also stressed that *Lagerstätten* rely on unique palaeoenvironmental, sedimentary, and diagenetic processes.

Several examples of fossil *Lagerstätten* record evidence of trends and patterns that shaped life on Earth: Archaean – Apex Chert (Schopf, 1993) and Strelley Pool Formation (Wacey et al., 2011), both from Australia, shed light on the very early steps of microbial life; Proterozoic – Mistaken Point, Canada (e.g. Narbonne, 2005), improved studies on the Ediacara biota; Cambrian – Burgess Shale, Canada (Briggs et al., 1994), whose fossils point out to biogeochemical marine transitions which took place in the Precambrian/Cambrian boundary (e.g. Callow and Brasier, 2009); Devonian – Rhynie Chert, Scotland, enabled palaeontologists to have a view of the very early stages of terrestrial plant evolution (e.g. Trewin, 2003); Jurassic – Solnhofen Limestone, Germany (e.g. Seilacher et al., 1985), on which the earliest bird *Archaeopteryx* was found; Eocene – Messel Shale, Germany (e.g. Schaal and Ziegler, 1992), whose high abundance of extraordinarily preserved fossil mammals, birds, insects, among others, enabled scientists to understand an early Cenozoic ecosystem.

Besides evolutionary and palaeoecological information, exceptionally well-preserved fossils also provide data for palaeobiogeographical inferences since they enable scientists to assess the temporal range of events of origin and extinction in different regions, contributing to the identification of radiations and extinctions (e.g. Martínez-Delclòs et al., 2004). Remarkable fossil preservation also yields evidence of soft tissues, enabling detailed morphologic research, and also evidence of the colour of extinct life forms, which raises palaeoecological research to a new stage of sophistication (McNamara, 2013). Furthermore, the study of fossil preservation modes is of paramount relevance since it provides information on the fidelity of preservation,

and chemical and mineralogical compositions of fossil samples, leading to innovative approaches to palaeoenvironmental, sedimentary, and geobiological research (e.g. Laflamme et al., 2011).

The fossil record is biased by palaeoenvironmental, biological, physical, geochemical, geobiological, and diagenetic factors, which affect palaeontological data interpretation (Allison and Bottjer, 2011). The area of Earth Sciences which deals with fossilization processes and fossil alteration is Taphonomy. Its importance relies on the capacity of yielding palaeoenvironmental, palaeoclimatic, palaeoecological, and sedimentary information, as well as of identifying modifications of original morphological features of organisms, improving taxonomic research, among other aspects (Allison and Bottjer, 2011).

Over the last few years, scientists have applied a broad range of cutting-edge non-destructive high-resolution imaging and geochemical techniques to unlock data kept in rare and/or exceptionally well-preserved fossils therefore raising novel questions to be answered. This branch of palaeontology is currently named Palaeometry (Riquelme et al., 2009; Delgado et al., 2014 – Appendix 1). For instance, Raman spectroscopy, Confocal Laser Scanning Microscopy (CSLM), Focused Ion Beam (FIB), Transmission Electron Microscopy (TEM), Nanoscale Secondary Ion Mass Spectrometry (nano-SIMS), among other approaches have been employed to assess the biogenicity, phylogeny, palaeoecology, and microtaphonomy of Precambrian microfossils (Schopf & Kudryavtsev 2009; Brasier et al., 2015); Time-of-Flight Secondary Ion Mass Spectrometry (ToF-SIMS) has been used to examine the presence of protein and blood traces (among other biomolecules, defining the field of molecular palaeontology; Briggs and Summons, 2014) on fossil vertebrates and invertebrates (Greenwalt et al., 2013; Bertazzo et al., 2015); X-ray Fluorescence (XRF) and Particle-Induced X-ray Emission (PIXE) have been extensively applied to taphonomic research (Bergmann et al., 2010; Riquelme et al., 2013; Gueriau et al., 2014); Synchrotron X-ray Microtomography (SR-µCT) has contributed to solving longstanding concerns on the taxonomic placement and palaeoecology of the Ediacaran fossil *Corumbella werneri* (Pacheco et al., 2015). Brazilian pioneers have been also conducting palaeometric work particularly regarding the taphonomy of the Santana Formation *Lagerstätte* (Filho et al., 2011; Buck, 2013; Osés, 2013; Delgado et al., 2014; Oliveira et al., 2015). In this

taphonomic window, the Crato Member (Early Cretaceous) records exceptionally well-preserved fossil invertebrates, vertebrates, and plants. Some issues regarding preservational processes of 3D insects and fish soft-tissues still remain open and circumscribe the aims of this dissertation.

2. The goals of the present research

The laminated limestones from the Crato Member, Santana Formation, Araripe Basin, north-eastern Brazil (Assine, 2007), is a worldwide famous *Lagerstätte*. It is known for its remarkably well-preserved fossil invertebrates (particularly insects), vertebrates (e.g. fishes, turtles, dinosaurs, and pterosaurs), and flora (spores, pollen, gymnosperms, basal flowering plants) (Martill et al., 2007a). Several cases of soft-tissue preservation have been hitherto reported on vertebrates (Davis and Martill, 1999; Fielding et al., 2005; Pinheiro et al., 2012) and insects (Delgado et al., 2014; Barling et al., 2015) recorded in the Crato Member limestones. This biota was preserved within an Aptian (Early Cretaceous) palaeolake during the last stages of the South America-Africa breakup and consists of the most complete window into the palaeobiology of a continental depositional palaeoenvironment from the Cretaceous (Martill et al., 2007a). However, the fossil record of this outstanding *Lagerstätte* still keeps unsolved geological and palaeobiological enigmas, such as the diversification of social insects, the early evolution of flowering plant, and the coevolution of insects and angiosperms (Labandeira and Eble, 2000; Soares et al., 2013).

Regarding the global relevance of the Crato Member, taphonomic research encompassing microscale morphological characterization and geochemical mapping is needed to resolve the very interesting issues concerning the processes and patterns of preservation which yielded fossils with such fine detailed morphological features. Following this rationale, the present masters dissertation has the following aims:

1- by means of palaeometric techniques on macro to microscale resolution, characterize and understand the fossildiagenetic mechanisms and processes, which led to the exceptional preservation of fossil insects and fishes from the Crato Member;

2- assess preservational patterns and propose taphonomic models;
3- discuss the possible role of microorganisms in the fossilization processes;
4- understand the palaeoenvironmental dynamics of the geological unit under study;
5- understand the role of palaeoenvironmental, palaeoecological, geobiological, and sedimentary interconnections in the Crato Member depositional environment, in the process of fossil preservation.

The results herein presented should contribute to improve the understanding of the fossilization processes that have operated in the Crato palaeolake. Beside this, they should help to interpret comparable preservational modes in other palaeoenvironments over the geologic time. This contribution sheds light on how the evolution of palaeoenvironmental conditions throughout time is related to exceptional fossil preservation, which records key changes in the history of life (e.g. Allison and Bottjer, 2011).

3. Geologic context

3.1. Basin evolution, stratigraphy and age

The Araripe Basin is located in northeastern Brazil (Fig. 1), consisting of part of the states of Ceará, Pernambuco, and Piauí. The Araripe Basin is a continental rift basin, bounded by NE and WNW faults, and formed during the opening of the South Atlantic Ocean by the reactivation of Precambrian faults (Fig. 1; Ponte and Ponte Filho, 1996; Assine, 2007).

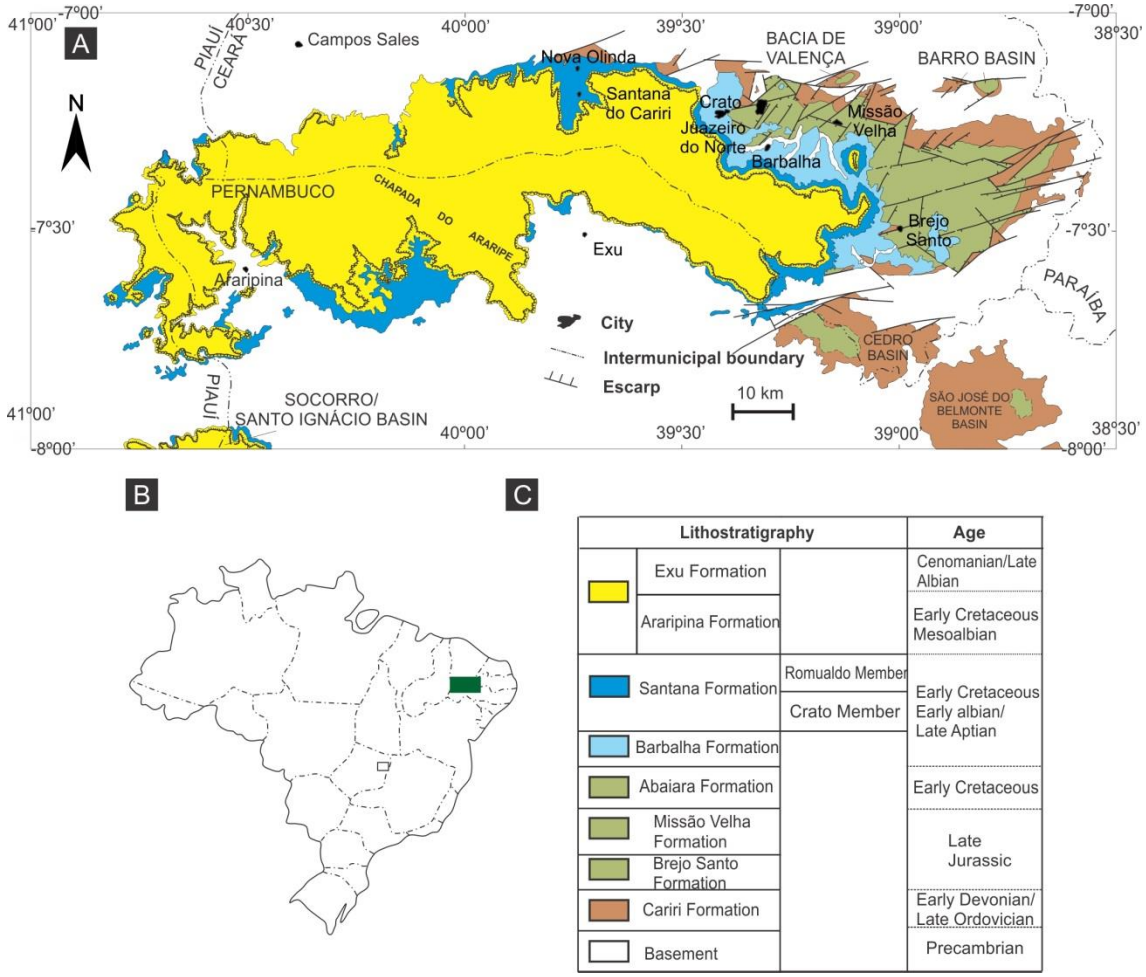

Figure 1. A, Geologic map of the Araripe Basin. **B,** Location of the Araripe Basin in the Brazilian territory. **C,** Simplified stratigraphic chart of the stratigraphy and age of the Araripe Basin. Modified after Assine (2007).

In the present contribution, the stratigraphic proposal for the Araripe Basin of Assine (2007) will be considered. Nevertheless, at some points of the text, other stratigraphic proposals may appear.

The base of the Araripe Basin is comprised by the Cariri Formation (Beurlen, 1962) (Late Ordovician/Early Devonian) (Assine, 2007). The tectonic-sedimentary evolution of the Araripe Basin is divided into four supersequences, from the base to the top (after Assine, 2007):

1- Pre-rift Supersequence: siliciclastic fluvial-lacustrine sediments from the Brejo Santo and the Missão Velha formations (Vale do Cariri Group), dated as Late Jurassic through ostracods and palynomorphs (Coimbra et al., 2002);

2- Rift Supersequence: deltaic, fluvial and lacustrine siliciclastic sediments from the Abaiara Formation (Vale do Cariri Group), which is attributed to the Early Cretaceous, based on ostracod biozonation (Coimbra et al., 2002);

3- Post-rift Supersequence: the Barbalha Formation, fluvial (siliciclasts)/lacustrine (pelites and carbonates) cycles and the Santana Formation, both units occurring within the Aptian-Albian Araripe Group (Coimbra et al., 2002). The lower succession of the Barbalha Formation comprises the "Batateira Beds", which represent a succession of fluvial, deltaic, and lacustrine palaeoenvironments.

The Santana Formation, with the Crato Member at its base, outcrops above the Barbalha Formation. The former unit is attributed to the Late Aptian based mainly on palynomorph biostratigraphy (Coimbra et al., 2002). At the top of the Crato Member, supratidal gypsum layers and shales, known as "Ipubi Beds" occur (Assine, 2007). Transgressive events led to the deposition of siliciclastic marine sediments, in which there are occurrences of shales with carbonate fossiliferous nodules of the Romualdo Member (Kellner, 2002), the top unit of the Santana Formation (Assine, 2007). Both "Ipubi Beds" and Romualdo Member are related to the Late Aptian-Early Albian interval, according to palynozones (Coimbra et al., 2002). Above the Romualdo Member, a marine coquina level occurs, which is covered by regressive freshwater facies (Beurlen, 1971), at the upper part of the Santana Formation. Mesoalbian Araripina Formation, located above the Santana Formation is a heterolitic facies of alluvial fan plains. This unit is overlaid by fluvial sediments of the Exu Formation (Araripe Group), located at the top of the Araripe Basin. The absence of microfossils makes it impossible to assign a specific age to this unit (Coimbra et al., 2002), although stratigraphic correlation suggests a possible Albian-Cenomanian age (Coimbra et al., 2002; Assine, 2007).

Neumann and Cabrera (2002) and Neumann et al. (2003) argued that the Aptian–Albian lacustrine sequences of the Araripe Basin have been deposited in a shallowing upward sequence (transgressive-regressive cycle), based on evidence for

recurrent cycles of six carbonate-siliciclastic facies comprising the “Batateira Beds”, the Santana Formation (Crato Member), and the “Ipubi Beds”. The latter two units are discussed below. The interplay of the lacustrine facies would have been controlled by the precipitation/evaporation balance and by the dynamics of fluvial drainage (Neumann et al., 2003).

Furthermore, Neumann et al. (2002) assumed that the Aptian-Albian lacustrine evolution of the Araripe Basin comprises four facies associations of the “Batateira Beds” and the Santana Formation (Crato Member only): marginal deltaic, internal terrigene, internal mixed and internal carbonate (C1 to C6), yielding interdigitated/interbedded siliciclastic and carbonate beds. These six carbonate beds evolved from the north to the south (unit C6 yielding the wider carbonate covering), while the palaeolake itself filled the basin from the opposite direction (Neumann et al., 2002). According to these authors, the carbonate units C1 to C6 correspond to the end of five minor transgressive cycles (C1, C2, C3/C4, C5, and C6), within a wider transgressive lacustrine sequence (“Batateira Beds” and Crato Member).

Castro et al. (2006) identified nine cycles of facies distributed among six depositional sequences, also comprising the “Batateira Beds” and the Santana Formation. Four cycles of facies were identified in the Crato Member: lacustrine limestone and bituminous shale (CF); deltaic shale, sandstone, and sigmoidal sandstone (FA-As); lacustrine marginal marl and sandy siltite (MA); and, fluvio-estuarine sandstone with cross-stratification and bioturbation (Axb). The top of sequence S2 has lacustrine limestones (CF), which represent a transgressive event. This sequence is overlaid by shales, sandstones, marls, siltites, and limestones (FA-AS, MA, CF) of sequence S3.1, deposited in deltaic and lacustrine settings. Above, sequence S3.2 is characterized by sandstones, shales, and limestones (Axb, FA, CF), which correspond to fluvio-estuarine, deltaic, and lacustrine facies. Sequence S3.3 is comprised by sandstones, limestones, and shales (As, CF) of deltaic and lacustrine origin. Castro et al. (2006) generally correlated their sequences (upper S2 to S3.3) to the Neumann et al. (2002) transgressive cycles C1 to C6, as shown in Fig. 2.

Transgressive Cycles	Depositional Sequences	Cycles of Facies	Lithology	Palaeoen-vironment
C6 (Lower S3.3)	S3.3	AS, CF	Sandstones, Shales, Limestones	Deltaic, Lacustrine
C5	S3.2	Axb, FA, CF	Sandstones, Shales, Limestones	Fluvio-estuarine, Deltaic, Lacustrine
C3/C4	S3.1	FA-AS, MA, CF	Shales, Sandstones, Marls, Siltites, Limestones	Deltaic, Lacustrine
C1/C2	S2 (Top)	CF	Limestones	Lacustrine

Figure 2. Correspondence of the transgressive cycles of Neumann et al. (2002) and the depositional sequences of Castro et al. (2006) for the Crato Member.

At this point, attention should be drawn to the Crato Member (Santana Formation). This unit outcrops only in the eastern portion of the Araripe Basin (Viana and Neumann, 2000), consisting of carbonates forming intermittent banks, which are up to 15 m thick, interbedded and interdigitated with marls, shales, sandstones, and siltstones (Viana and Neumann, 2000; Assine, 2007), as discussed above. In each carbonate unit (C1 to C6), basal clay-carbonate rhythmites (submicrofacies sm1) are overlaid by micritic laminated limestones (submicrofacies sm1-6) (Viana and Neumann, 2000; Silva et al., 2002; Neumann et al., 2003). Sm2 has ondulations and loop bedding structure; sm3 is characterized by peloids; sm4 has ondulations, micro-slumps, and micro-ripples; sm5 consists of fine parallel lamination; sm6 exhibits parallel/wave lamination and ostracods (Silva et al., 2002). Each carbonate unit has an average duration of 200.000-500.000 years (Neumann and Cabrera, 2002).

The laminated clay-carbonate rhythmite facies is characterized by couplets of light micritic laminae and dark laminae, the latter rich in terrigenous components (clay) and organic matter (including plant debris and ostracods; Neumann et al., 2003;

Heimhofer et al., 2010) associated to pyrite crystals. The content of C_{org} is less than 4% (Neumann et al., 2003). The calcite crystals (5-10 μm) are idiomorphic and include rhombohedral and polyhedral forms, withdissolution features (Heimhofer et al., 2010). Heimhofer et al. (2010) also reported framboidal pyrite and phyllosilicates and noticed high inter-grain porosity and low cement development. This palynomorph-poor facies, with salt pseudomorphs was deposited at a distal location under anoxic conditions (Neumann et al., 2002; 2003) since it is typical of inner lacustrine settings (Neumann et al., 2008). In turn, the fine laminated limestone facies is composed of pairs of light micritic laminae (low magnesium calcite; Silva et al., 2002) and dark laminae with disseminated pyrite (Heimhofer et al., 2010). The calcite crystals are 5-15 μm in length and, therefore, the laminated limestones are considered microspar (Heimhofer et al., 2010). In contrast with the clay-carbonate rhythmite facies, the laminated limestones show less inter-grain porosity due to well-developed spar cement and skeletal grains (Heimhofer et al., 2010). This facies has a lower contribution of detrital material and organic matter (C_{org} < 1%) than the clay-carbonate rhythmites (Neumann et al., 2003) and it includes ostracods and plant remains (Heimhofer et al., 2010). The laminated limestones were also deposited under the same conditions of the clay-carbonate facies (Neumann et al., 2003). In both facies, organic matter is either comprised by amorphous dispersed elements associated to the calcite or by pyritized branchlets of higher land plants (Neumann et al., 2003). These authors argued that regarding its composition and poor cell preservation, these branchlets might have undergone bacterial decay. Detrital quartz may also occur in both facies.

Non-laminated levels also occur in the Crato Member (Dias-Brito and Tibana, 2015). The laminated limestones are underlain by ostracod-rich organo-limestone laminites, which has mudstone/wackestone laminae. These are characterized by ostracods and peloids interlaminated with organic-clay laminae, which have ostracods and limestone nodules infilled with microbial spheres and ostracods (Dias-Brito et al., 2015).

3.2. Palaeoenvironment and diagenesis of the Crato Member carbonate units

The preserved area of the Crato palaeolake is about 7.500 km^2 wide. The biota thrived in a warm tropical–subtropical palaeoclimate, seasonally controlled by humid and dry cycles, leading to permanent density stratification owing to thermal heterogeneities along the water column (Neumann et al., 2003). The semiarid-arid conditions are supported by the predominance of the conifer family Cheirolepidiaceae. Still regarding the Crato palaeoflora, Ferns, Bennettitales, Gnetales, angiosperms, and large conifers covered areas around the waterbody (Neumann et al., 2003).

The deltaic body and the smooth inclination of the bottom relief have resulted in both interdigitation between siliciclastic and carbonate successions, and small scale sedimentary structures (micro-faulting and loop bedding; Neumann et al., 2002). The presence of faults, loop bedding, and slumps owns to minor syndepositional seismic activity (Silva et al., 2002). The lacustrine sequence thickness varies from 50 to 70 m (Silva et al., 2002).

Isotopic analyses of oxygen ($\delta^{18}O$ values between -5 ‰ and -7 ‰) performed in the Crato Member lowermost laminated limestones revealed that the depositional palaeoenvironment received meteoric ^{18}O-depleted waters and pointed to a freshwater waterbody (Heimhofer et al., 2010). Carbonate carbon isotopic data ($\delta^{13}C$ within -0.2 ‰ and 1.9 ‰) support that the palaeoenvironment was a stratified lake, poorly connected with external water sources, with stagnant bottom waters, reflecting the uptake of ^{12}C by microorganisms in the water column. Positive $\delta^{13}C$ values are due to limited mixing of ^{12}C in the water, although equilibrium with the atmosphere might also have played a role (Heimhofer et al., 2010). Alternatively, Heimhofer et al. (2010) also suggested the dissolution of marine carbonates and/or the isolation of the palaeolake as explanations for such $\delta^{13}C$ high positive values. Furthermore, these authors also alleged that the lack of fine cyclic patterns on isotope variation could be explained by the palaeoenvironmental stratification, although post burial homogenization cannot be ruled out. On the other hand, they claimed that overall differences do exist between clay-carbonate rhythmite and laminated limestone facies. Isotopic excursion to more negative $\delta^{18}O$ values from the former to the latter facies means an opening of the palaeoenvironment during highstand water levels simultaneously with laminated limestone deposition.

Neumann et al. (2003) suggested permanent water stratification in relation to O_2 (i.e. meromictic conditions; Fig. 3). Anoxic bottom conditions are supported by the occurrence of disseminated galena and sphalerite in the limestones as well as by the lack of bioturbators (Heimhofer and Martill, 2007). Water column stratification (yielding a bottom water monimolimnion and an upper water column mixolimnion, inhabited by aquatic insects, turtles, and fishes) could be explained by stagnation and/or high rates of surface water primary productivity providing a high flux of organic matter to the lake floor, the decay of which by aerobic bacteria reduced bottom water oxygen and, eventually, led to anaerobic conditions in deep waters (Heimhofer and Martill, 2007). This recycling of organic matter would have yielded low production of autochthonous organic matter in the lake bottom, further enhanced by stratification (Neumann et al., 2003). Alternatively, Catto et al. (2016) suggested that low organic matter preservation in some levels could be explained by bottom spells of freshwater, which could have oxidized organic matter. Additionally, a photic zone euxinia (PZE) could also have been seasonally established in the waterbody (Fig. 3), as evidenced by the presence of isorenieratene, a biomarker of Chlorobiacea, which thrives below the oxic-anoxic water column interface and performs photosynthesis using hydrogen sulphide instead of oxygen (Heimhofer and Martill, 2007).

The occurrence of salt pseudomorphs and xerophytic vegetation pollen support a semi-arid to arid palaeoclimate (Heimhofer and Martill, 2007), which is further evidenced by the low diversity of the palaeolake biota and by the low amount of organic matter recorded in the rocks, possibly owing to the chemical stratification (Neumann et al., 2003). The events of hypersalinity would have been possibly triggered by the dissolution of former precipitated evaporites, the evidence of which is supported by the presence of five types of halite pseudomorphs (Martill et al. 2007b). The high salinity could have been increased by the occasionally endorheic nature of the basin, while freshwater conditions would have been stablished near fluvio-deltaic river mouths (Neumann and Cabrera, 2002). Endorheic lacustrine basins have dynamic shores, with retrogradational and progradational cycles and enhanced chemical mineral precipitation owing to high evaporation rates plus low water input (Neumann and Cabrera, 2002; Neumann et al., 2008). These salinity fluctuations can be explained on palaeogeographical and palaeoclimatic grounds since, in the Early Cretaceous, the area was subjected to monsoon influence (Neumann and Cabrera, 2002). Martill et al.

(2007b) have pointed out that fluctuation in salinity levels could account for anoxia in the palaeolake.

Terrigenous sediments might have been restricted to marginal settings during carbonate deposition (low Al, K, Ti, and Si; Heimhofer et al., 2010). Heimhofer et al. (2010) enumerated factors which account for the precipitation of carbonate at lacustrine settings: terrigenous input, carbonate bioclasts, benthonic microbial influence, and microbially induced and/or mediated authigenic precipitation. The evidence of mass flow deposits in the Crato Member is scarce, except in one location, cited by Heimhofer and Martill (2007). Moreover, the lack of reworked calcite crystals further rules out the hypothesis of a terrigenous origin for the carbonate (Heimhofer et al., 2010). Additionally, the laminite is not predominantly built up by bioclastic particles, though ostracods do occur at some levels, particularly near the lake edge (Heimhofer et al., 2010; Dias-Brito and Tibana, 2015).

The presence of wrinkle and ripple like structures (Heimhofer and Martill, 2007; Martill and Wilby, 1993), similar to Microbially Induced Sedimentary Structures (MISS) (Noffke et al., 2001), suggests that the depositional surface was, at least, covered by patches of microbial mats or biofilms. However, only isolated slabs without precise stratigraphic location have been recovered (Heimhofer and Martill, 2007). Moreover, putative gas domes have also been reported (Martill et al., 2007b). However, owing to the fragmentary distribution of such evidence plus the lack of typical petrographic evidence, Heimhofer at al. (2010) have ruled out the role of a benthonic microbiota as the origin of the carbonate. Alternatively, these authors have suggested microbially induced and/or mediated authigenic precipitation of calcite crystals in the water column, which could have been seasonally controlled by temperature fluctuations and by blooms of autotrophic microorganisms (i.e. ‘whitings’; Fig. 3) (Heimhofer and Martill, 2007; Gierlowski-Kordesch, 2010). The carbonate deposition due to ‘whitings’ is controlled by rising water temperature during summer and autumn (Gierlowski-Kordesch, 2010) and by autotrophic microorganism proliferation due to a rise of nutrient supply (Heimhofer et al., 2007). The former factor leads to decreasing carbonate solubility, while the latter enhances carbonate nucleation rates and the uptake of CO_2 from the water, therefore contributing to calcite precipitation (Heimhofer et al., 2007). However, different authors have recently shown evidence for the activity of

benthonic microbial mats or biofilms at the edge of the palaeolake, where non-laminated clayey mudstones/wackestones rich in fibro-radiated spherules, microbial spheres, ostracods, gastropods, bivalves, and angular-shaped terrigenous quartz do occur (Dias-Brito and Tibana, 2015). Moreover, Catto et al. (2016) have further shown that microfossils and EPS are ubiquitous throughout the Crato Member beds, thus challenging Heimhofer et al. (2010) previous interpretation. Dolomitic structures, as observed in a Crato Member locality (Martill et al., 2008), might have been originated by sedimentation controls of carbonate at lacustrine settings particularly by water input and circulation, including groundwater (Gierlowski-Kordesch, 2010).

The preservation of the undisturbed fine lamination (Fig. 3) seems to have occurred by the following factors: deposition below normal wave base level, limited bottom current action, and lack of benthonic fauna (e.g. bioturbators plus absence of trace fossils; Heimhofer and Martill, 2007), though submicrofacies with ondulations and ripples do occur in some levels (Silva et al., 2002).

The absence of thermal action diagenetic features, such as degraded organic matter (e.g. palynomorphs display original colour), the lack of recrystallization of calcite crystals, cement-filled fractures, stylolites, pressure-solution features, and fractures, besides the occurrence of exceptional soft-tissue preservation, fit a low depth burial idea (Heimhofer and Martill, 2007; Heimhofer et al., 2010). This proposition is consistent with the low degree of compaction of the rocks, further supported by high porosity, particularly in the clay-carbonate rhythmites. This latter characteristic is explained by organic matter infilling the pores, which leads to low nucleation cement rates (Heimhofer et al., 2010). Furthermore, these authors pointed out that original stable mineralogy has possibly inhibited cement growth and recrystallization.

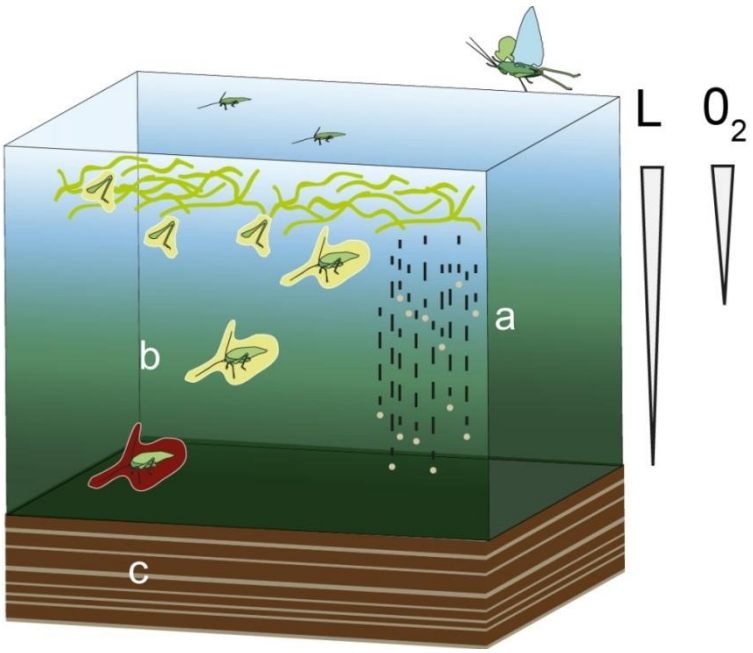

Figure 3. Diagram showing an inner setting of the Crato palaeolake. The palaeoenvironment was stratified with regard to O_2 (right side of the figure). Light intensity (L) is shown on the right. The calcite could have been precipitated during 'whitings' (a). A photic zone euxinia (PZE) was at least seasonally stablished below the oxic-anoxic interface of the water column (b). The lamination of the laminated limestone is undisturbed (c). Drawing by Bruno Becker Kerber.

4. Material and methods

The fossil specimens used in this research belong to the Scientific Palaeontological Collection of the Institute of Geosciences of the University of São Paulo (IGc-USP). The fossil insects are identified by the code **GP/1E** (invertebrate collection), while the fossil fishes are recognized by the prefix **GP/2E** (vertebrate collection). The following samples have been analyzed: GP/2E 9666, GP/2E 9005, GP/2E 9006, GP/2E 9014, GP/2E 7781g, GP/2E 7786f, GP/2E 7913e, GP/2E 7782j, GP/2E 7780e, GP/1E 9435, GP/1E 7105, GP/1E 8440, GP/1E 8397, GP/1E 8827, GP/1E 6820, GP/1E 10368, and GP/1E 9137. The complete list of samples and their correspondent thin sections can be found in Appendix 2.

The specimens were photographed in a Zeiss Stemi 2000-C stereomicroscope coupled to a Zeiss AxioCam ICc3 camera. The image acquisition was made in the software AxionVision 4.8.

In this research, different techniques were employed for studying external or internal parts of insects, both fish bones and soft tissues, and the host rock . The geochemical analyzes were performed systematically, being repeated in different points in a representative set of samples, when available. Here follow the techniques and methods employed in this research:

Petrographic thin sections

Thin sections perpendicular to the rock lamination and cross-sections of fish vertebral column, along with soft-tissues, were made. The aims were: (1) observe and characterize soft-tissue and bone morphology in cross-section, and (2) describe host carbonate petrography. Furthermore, since thin sections provide flat surfaces, they enabled accurate EDS and synchrotron micro-XRF mapping (discussed below). Therefore, two types of thin sections were made: (1) 30 µm-thick with cover slips used chiefly for mineral, texture, and structure description/identification, and (2) >30 µm (around 50 µm)-thick without cover slips used for geochemical analyses. For these, thicker thin sections (i.e. more rock volume) enhanced the measured signal (Davis and Martill, 1999), yielding high-quality geochemical maps.

Raman spectroscopy

When materials are illuminated by a monochromatic visible light source, incident photons interact with the molecular vibrations of the material (Neuville et al., 2014). As a consequence, scattered photons may have different energy in comparison to the incident photons, defining the Raman scattering phenomenon. This energy shift is known as Raman shift, which is measured by a spectrometer, yielding a characteristic spectrum (i.e. graphic) of the material molecular vibrations. Raman spectroscopy can be used for the chemical and mineralogical characterization of samples, being widely applied in mineral identification (Faria and Lopes, 2007; White, 2009) since it avoids most of the destructive procedures usually associated with conventional geochemical methods. In-situ analyzes were performed to investigate the minerals that have replaced original organic compounds during fossilization, with the advantage of having sub-

micron resolution and mapping capacity, as the spectrometer is coupled to a confocal microscope. The equipment setup included both a micro-Raman inVia Renishaw, coupled to a laser of 785 nm wavelength and another similar equipment coupled to a 532 nm wavelength laser. A CCD detector was used in both setups. The measurements were performed both at the Research Unity in Astrobiology, Laboratory of Astrobiology (NAP/Astrobio-USP, Astrolab) and at the Laboratory of Molecular Spectroscopy (LME) of the Institute of Chemistry of USP. The Raman spectra were then analysed in the software Origin®8 and data were interpreted using the RRUFF database.

X-ray fluorescence (XRF)

XRF consists of the following principle: when materials are excited by a high-energy X-ray photon source, electrons move from inner to outer atom orbitals and, consequently, external electrons occupy the vacancy left inside (Verma, 2007). In response to this process, X-ray photons with the same energy of that lost (to occupy the internal orbital) by the outer electron are emitted. This energy value is the energetic difference between the two orbitals involved. This X-ray emission is called fluorescence, being the energy value characteristic of the excited atomic element. XRF is used to characterize the elemental composition of samples. This is a very useful technique since it enables measuring several elements simultaneously, in a non-destructive way, not requiring high amounts of sample (Verma, 2007). XRF was employed in fossils and their host rock to characterize elemental composition and its distribution, aiming to understand the meaning of the latter. In this way, it was possible to test whether elements are representative of the original composition of the organisms or the result of fossilization processes. The analyses were performed at the Institute of Physics of USP (IF-USP), using a portable mini Amptek X-ray tube of Ag anode and a Silicon Drift Detector (SDD - X-ray semiconductor detector). Data processing was performed using the software WinQXAS, RUMP, and Microsoft Excel®.

Synchrotron micro-XRF (SR-µXRF) point analysis and mapping were performed with the same objectives as conventional XRF (discussed above). Moreover, specific characterization of phosphorus was made to quantify this element in the rock matrix and in fossil insects, aiming to assess preservational processes. In comparison to the employed conventional XRF, SR-µXRF has the advantage of µm-scale spectra collection, plus mapping mode, enabling the detailing of very fine structures and the

characterization of elemental distribution among them. In addition, SR-μXRF enables the measurement of elements with concentrations below the detection limit of conventional XRF. Phosphorus analysis was performed in the soft X-ray spectroscopy (SXS) beamline, and point/map characterization of several elements were made in the XRF beamline of the Brazilian Synchrotron Light Laboratory (LNLS).

Particle-induced X-ray emission (PIXE)

The physical principles behind PIXE are very similar to XRF, but in the former, the excitation is made by protons or other particles with charge (Verma, 2007). The PIXE technique is employed in qualitative and quantitative elemental analysis of materials and was used for the same purpose as the XRF. However, PIXE is different from XRF in regard to the following aspects (Verma, 2007): it is a surficial technique, that is, protons interact with atoms in a shallow sample area (ca. tens of microns); the efficiency for detecting elements with X-ray energies higher than Ca is better than XRF; and, compared to XRF, PIXE has a greater detection sensitivity. Furthermore, the equipment available allows sample mapping and has a smaller diameter beam in comparison with the portable (conventional) XRF equipment, allowing investigation of smaller structures. The analysis was performed in the external beam setup of the 1.7 MV-tandem accelerator of the Laboratory of Materials and Ionic Beams (LAMFI) of the IF-USP.

Scanning electron microscopy (SEM) and energy-dispersive X-ray spectroscopy (EDS)

A SEM is basically composed of an electron gun and electromagnetic lenses (Leng, 2008). The electron probe scans lines along the sample surface, which emits electrons that are captured by a detector. Then, an image is built based on the correlation between scanned points and points in a screen. SEM was used to yield very detailed images at micrometric scales of fossil ultrastructures, including the morphology of both preserved soft tissues and minerals replacing the specimens.

EDS is based on the same physical principles of XRF, but X-ray emission is triggered by a high energy electron beam (Leng, 2008). EDS microanalysis was employed to evaluate the elemental composition of the samples – particularly light elements, such as oxygen and carbon – yielding point spectra and maps, the latter

revealing a correlation between structures and composition. The analyzes, including secondary (yielding topographic contrast) and backscattered (yielding elemental contrast) electron micrographs, were performed at the Brazilian Nanotechnology National Laboratory (LNNano) and at the Laboratory of Technological Plasmas (LaPTec) of the São Paulo State University, using a JEOL JSM-6010 LA microscope and also a FEI Quanta 650 FEG microscope, both coupled to EDS equipment. In the former SEM, an X-ray Dry SD Hyper (EX-94410T1L11) detector with resolution of 129 to 133 eV for the Mn Kα line at 3000 cps was used. In order to avoid surface charging, some samples were coated with a thin layer of gold-palladium using a DESK-V HP Cold Etch/Sputter system. Whenever possible, EDS analysis was not used in coated samples, and EDS mapping was performed in thin sections, to avoid misinterpretation of elemental composition.

Obs.: Details on experimental setup are found in the following chapters (articles).

5. Article "Deciphering the Preservation of Fossil Insects: a Case Study from the Crato Member, Early Cretaceous of Brazil".

Deciphering the Preservation of Fossil Insects: a Case Study from the Crato Member, Early Cretaceous of Brazil

Gabriel Ladeira Osés[1], Setembrino Petri[1], Bruno Becker Kerber[2], Guilherme Raffaeli Romero[3], Márcia de Almeida Rizzutto[4], Fabio Rodrigues[5], Douglas Galante[6], Tiago Fiorini da Silva[7], Jessica Curado[8], Elidiane Cipriano Rangel[9], Rafael Parra Ribeiro[9], Mírian Liza Alves Forancelli Pacheco[10]

[1]Institute of Geosciences, University of São Paulo, São Paulo, São Paulo, Brazil
[2]PPGERN, Federal University of São Carlos, São Carlos, São Paulo, Brazil
[3]Institute of Geosciences, Federal University of Pará, Belém, Pará, Brazil
[4]Institute of Physics, University of São Paulo, São Paulo, São Paulo, Brazil
[5]Institute of Chemistry, University of São Paulo, São Paulo, São Paulo, Brazil
[6]Brazilian Synchrotron Light Laboratory, Campinas, São Paulo, Brazil
[7]Max Planck Institute for Plasma Physics, Germany
[8]Department of Physics, FEI Academic Centre, São Bernardo do Campo, São Paulo, Brazil
[9]Laboratory of Technological Plasmas, São Paulo State University, Sorocaba, São Paulo, Brazil [10]Department of Biology, Federal University of São Carlos, Sorocaba, São Paulo, Brazil

Corresponding author:
Gabriel Osés
Rua do Lago, 562, Cidade Universitária, São Paulo, SP, 05508-080, Brazil
Email address: gabriel.oses@usp.br

Abstract

Exceptionally well-preserved three-dimensional insects with fine details and even labile tissues are ubiquitous in the Crato Member Konservat Lagerstätte (northeastern Brazil). Here we investigate the preservational pathways which yielded such specimens. We employed high resolution techniques (EDXRF, SR-SXS, SEM, EDS, micro Raman, and PIXE) to understand their fossilisation on mineralogical and geochemical grounds. Pseudomorphs of framboidal pyrite, the dominant fossil microfabric, display size variation when comparing cuticle with inner areas or soft tissues, which we interpret as the result of the balance between ion diffusion rates and nucleation rates of pyrite through the originally decaying carcasses. Furthermore, the mineral fabrics are associated with structures that can be the remains of extracellular polymeric substances (EPS). Geochemical data also point to a concentration of Fe, Zn, and Cu in the fossils in comparison to the embedding rock. Therefore, we consider that biofilms of sulphate reducing bacteria (SRB) had a central role in insect decay and mineralisation. Therefore, we shed light on exceptional preservation of fossils by pyritisation in a Cretaceous limestone lacustrine palaeoenvironment.

Introduction

Exceptionally preserved biotas have been recorded since the Precambrian (e.g. Chen et al., 2014). They comprise taphonomic windows (Konservat-Lagerstätten of Seilacher, Reif & Westphal, 1985), which provide essential evidence for understanding major issues regarding evolution and palaeoecology of ancient ecosystems (e.g. Raff et al., 2008). In fact, organisms with low potential of preservation are very promising as taphonomic windows since once they retain fine morphological aspects, this implies in high taxonomic fidelity, representative of an ancient biological community (Briggs et al., 2016).The high preservational fidelity of insects from the Crato Member (Santana Formation, northeastern Brazil) defines it as a taphonomic window for an Early Cretaceous ecosystem (Soares et al., 2013). Due to this kind of unique record, we know that the evolutionary history of the insects was characterised by major radiation and extinction events in the Cretaceous (Nicholson et al., 2015), when the diversification of social insects (Jarzembowski and Ross, 1996; Engel et al., 2007) and the radiation of flowering plants (Lidgard & Crane, 1988) took place. The latter has impacted insect evolution thereafter (Jarzembowski and Ross, 1996; Labandeira, 2014).

Within the palaeolacustrine setting of the Crato Member, several insect groups display exceptional preservation of nonbiomineralised tissues on a micron-scale as well as gross morphological features (Delgado et al., 2014; Barling et al., 2015). Whilst previous studies have considered the preservation of these organisms (Heimhofer & Martill, 2007; Menon & Martill, 2007; Delgado et al., 2014; Barling et al., 2015), microtextural and geochemical analyses have not been performed, nor has a detailed taphonomic model been proposed. Based on imaging, geochemical, and mineralogical analyses, this paper presents data that supports the central role of microorganisms in the fossilisation of the Crato Member insects. We propose a preservational pathway able to predict interconnections between geobiological and taphonomic processes operating in the exceptional preservation of these insects, which have yielded 3D replicas with mineralised internal soft tissues.

Geological Setting

The fossil insects used in this study are from the Crato Member (Santana Formation, Araripe Basin) located in northeastern Brazil (Fig. 1). It is a continental rift basin, bounded by NE and WNW faults (Assine, 2007), formed during the opening of the South Atlantic Ocean (Brito-Neves, 1990; Assine, 2007).

The base of the Araripe Basin is comprised by the Cariri Formation, proposed by Beurlen (1962) (Late Ordovician/Early Devonian) (Assine, 2007). Four supersequences are recognised in the Araripe Basin (following Assine, 2007): 1- Pre-rift Supersequence: siliciclastic fluvial-lacustrine sediments from both the Brejo Santo and Missão Velha formations, dated to the Late Jurassic by ostracodes and palynomorphs (Coimbra, Arai & Carreño, 2002); 2- Rift Supersequence: deltaic, fluvial and lacustrine siliciclastic sediments from the Abaiara Formation, attributed to the Early Cretaceous based mainly on ostracode biozonation (Coimbra, Arai & Carreño, 2002); 3- Post-rift Supersequence: Barbalha Formation, with two fluvial (siliciclasts)/lacustrine (pelites and carbonates) cycles and the Santana Formation, both units occurring within the Araripe Group and Aptian-Albian in age (Coimbra, Arai & Carreño, 2002). The lower succession of the Barbalha Formation comprises the “Camadas Batateira”, which represent the first evidence of an anoxic lacustrine cycle. In the Araripina Formation, heterolitic facies of alluvial fan plains of the Mesoalbian occur. This unit is overlaid by fluvial sediments of the Exu Formation (Araripe Group), located in the top of the

Araripe Basin, whose age is uncertain due to the absence of microfossils (Coimbra, Arai & Carreño, 2002), although its stratigraphic position suggests an Albian-Cenomanian age (Coimbra, Arai & Carreño, 2002; Assine, 2007).

The Santana Formation is divided in two members. The Crato Member, the most basal unit, outcrops only in the east portion of the Araripe Basin (Viana & Neumann, 2000). Its Late Aptian age is based mainly on palynomorphs (Coimbra, Arai & Carreño, 2002). This unit consists of carbonates, forming intermittent banks, more than 20 meters thick (Assine, 2007). These carbonates are divided into six levels, each one with basal clay-carbonate rhythmites overlaid by micritic laminated limestones, where the fossil insects from this study occur (Viana & Neumann, 2000). These lithologies were deposited in a lacustrine palaeoenvironment. The carbonate levels are interbedded with shales (occasionally rich in organic matter), sandstones, and siltstones (Viana & Neumann, 2000).

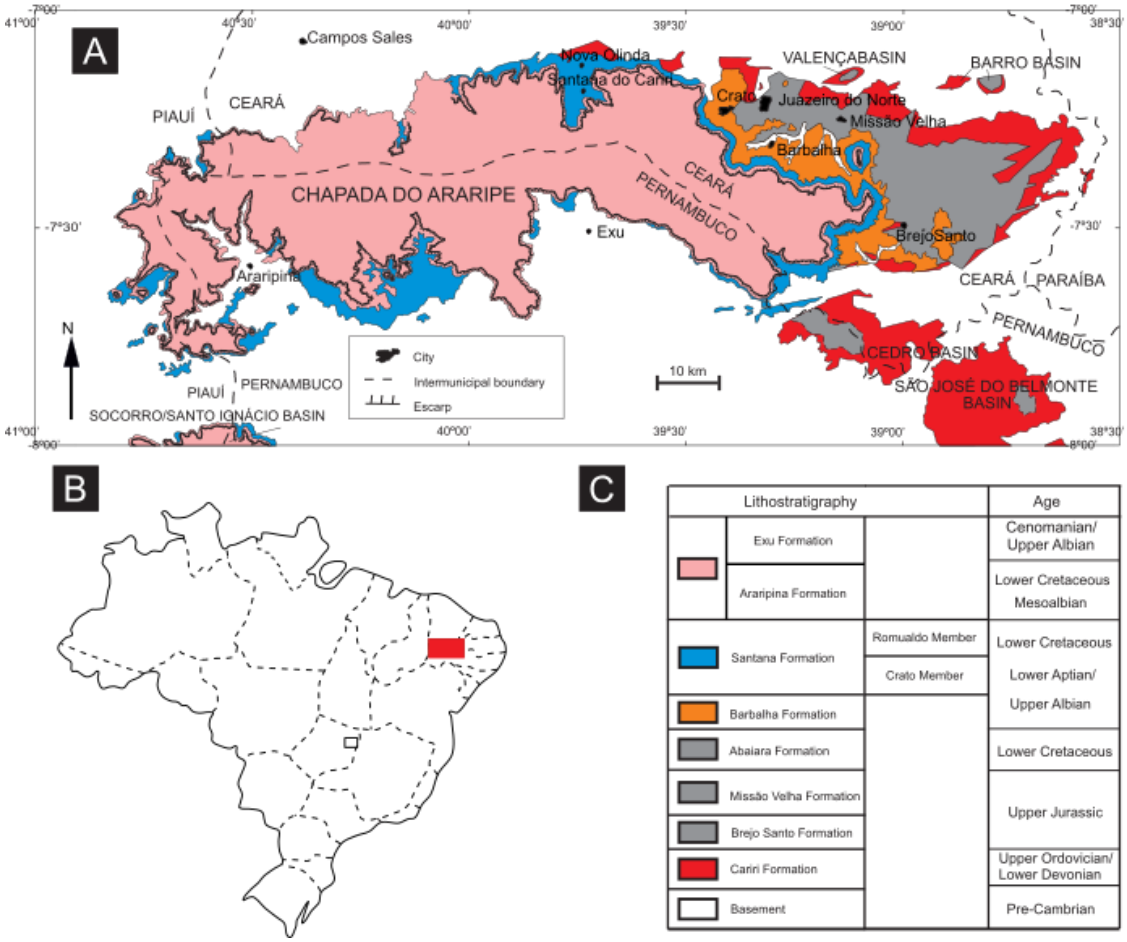

Figure 1: Geological setting of the Crato Member. (A) Geological Map of the Araripe Basin. (B) Position of the Araripe Basin in the Brazilian territory. (C) Simplified stratigraphic chart of the Araripe Basin. Modified from Assine (2007).

In the top of the Crato Member, supratidal gypsum layers and shales, known as the "Camadas Ipubi" occur (Assine, 2007). Transgressive events led to the deposition of siliciclastic marine sediments, with shales with carbonatic fossiliferous nodules from the Romualdo Member (Kellner, 2002), the Santana Formation top stratigraphic unit (Assine, 2007). Both "Camadas Ipubi" and Romualdo Member comprise the Late Aptian-Early Albian interval, defined by palynozones (Coimbra, Arai & Carreño, 2002). Above the Romualdo Member, a level with marine shell beds occurs, which is covered by regressive freshwater facies (Beurlen, 1971), in the upper part of the Santana Formation.

Materials and Methods

The specimens analysed ("GP/1E") are deposited in the Scientific Palaeontological Collection of the Institute of Geosciences of the University of São Paulo (Brazil). No permits were required for the described study since it was performed after specimens had been deposited in the above mentioned scientific collection. The results herein presented comprise the analyses of the following samples: GP/1E 7105, GP/1E 8440, GP/1E 8397, GP/1E 8827, GP/1E 6820, GP/1E 10368, and GP/1E 9137.

The analyses were made with complementary paleometrical techniques (Delgado et al., 2014) on weathered samples, in order to validate the results of several techniques.

Samples were initially observed and photographed in a Zeiss Stemi 2000-C stereomicroscope coupled to a Zeiss AxioCam ICc3 camera. The image acquisition was made in the software AxionVision 4.8.

Micro morphological analyses of the fossil insects were conducted by scanning electron microscopy (SEM) in a JEOL JSM-6010 LA microscope and also in a FEI Quanta 650 FEG microscope, both coupled to an energy dispersive X-ray spectroscopy (EDS) equipment. In the former microscope, an X-ray Dry SD Hyper (EX-94410T1L11) detector with resolution of 129 to 133 eV for the Mn Kα line at 3000 cps was used. To avoid surface charging during SEM inspections samples were coated with a thin layer of gold-palladium using a DESK-V HP Cold Etch/Sputter system. The micrographs were then taken using the secondary electron detector of the microscopes (except one micrograph, which was taken using the backscattered electron detector of

the JEOL JSM-6010 LA microscope). All spectroscopic analyses were performed on three main regions of the samples: inside the carcasses, on the cuticle, and on the surrounding rock matrix. EDS point and mapping spectra were employed to highlight qualitative elemental heterogeneities among these three regions. The results obtained with EDS were carefully analysed and interpreted since EDS point analysis may lack spatial representativeness and EDS mapping is a qualitative approach, which may be affected by sample topographic irregularities.

Energy dispersive X-ray fluorescence (EDXRF) analyses were performed for rapid elemental characterisation of heavier elements, previously to EDS in order to select samples to this latter technique. The portable EDXRF equipment consisted of a mini Amptek X-ray tube of Ag anode and a Silicon Drift Detector (SDD - X-ray semiconductor detector) of 125 eV FWHM for the 5.9 keV line of Mn. The measurements were carried out with 30 kV voltage and 5 μA of tube current and with an excitation/detection time of 100 s.

The quantitative detection of phosphorus in the samples was performed in vacuum, at the soft X-ray spectroscopy (SXS) beamline of the Brazilian Synchrotron Light Laboratory (Abbate et al., 1999), following the work of Leri et al. (2006).

The elemental mapping of a whole sample was made by the application of particle induced X-ray emission (PIXE). The analysis was performed in the external beam setup of the 1.7 MV-tandem accelerator of the University of São Paulo. A 2.4 MeV energy proton beam (1 mm in diameter) was used at the sample surface to induce the emission of characteristic X-rays, detected by an AMPTEK XR-100CR (450 μm thickness, 4.6 mm^2 area, 0.5 mil Be-window, and 165 eV energy-resolution at 5.9 keV, and additional X-ray absorber of 300 μm to avoid high counting rates). The sample was positioned in front of the external beam setup by a robotic sample holder that sequentially moved the sample to cover the fossil area by a matrix of analysed spots (0.7 mm steps in both directions). In each point, the sample holder stands during the detector acquisition time, which in the case of this study was 15 s with a beam current of 10 nA, and saves an X-ray spectra for each point. The maps were created using the peak area (background removed) and the position of each measured point tracked by the robotic sample holder.

The mineralogical composition of both fossils and laminated limestone was analysed by Raman spectroscopy in a confocal micro Raman inVia Renishaw

equipment, coupled to a laser of 785 nm wavelength and 300 mW power and a laser of 633 nm wavelength and 17 mW power, and a CCD detector. The Raman spectra were analysed in the software Origin®8.

Results and Discussion

Microtextural Characterisation of the Fossils

SEM analysis revealed that fossil exoskeletons (Fig. 2) are preserved by sub-spherical to spherical closely-packed grains, with diameters mainly in the range of 5 to 10 µm (Fig. 3A), which are formed by anhedral to euhedral nanocrystals (Fig. 3B-D). The outer cuticle surface retains fine morphological details (Fig. 3A; Barling et al., 2015), built by the close-packing of these grains (Fig. 3A-D; Grimes et al., 2002). The cuticle is also replaced by polygonal lamellar sometimes porous structures likely filled with nanocrystals similar to the ones forming the sub-/spherical grains and with an anhedral microcrystalline mineral phase, with less than 1 µm (Fig. 3D).

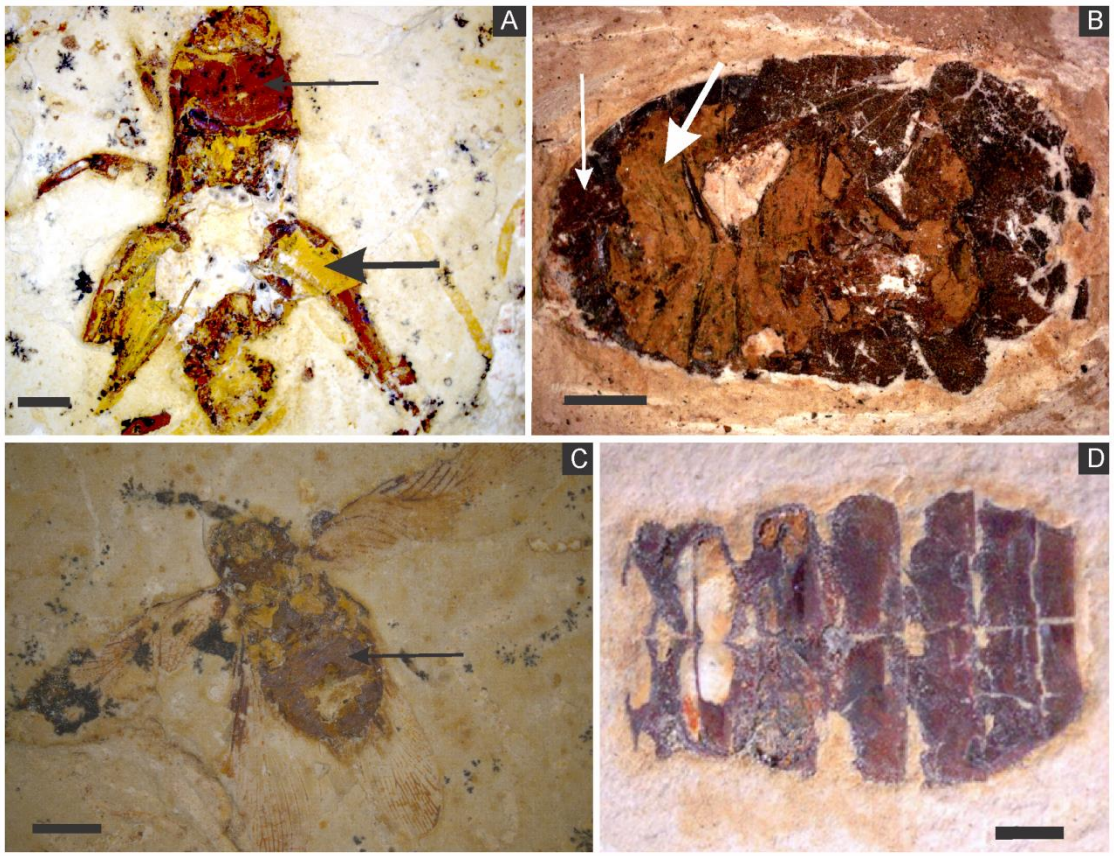

Figure 2: (A) orthopteran GP/1E 7105. (B) hemipteran GP/1E 8440. (C) blattodea GP/1E 9137. (D) specimen GP/1E 6820, cuticle of an undetermined insect. In A-C, exoskeleton is indicated by narrow arrows and internal part is indicated by wide arrows. The brown, yellow, and orange-brown colours represent the alteration of originally

precipitated pyrite (Barling et al., 2015). Scale bars = 2 mm (A-C), 1 mm (D). Figure A was modified from Delgado et al. (2014).

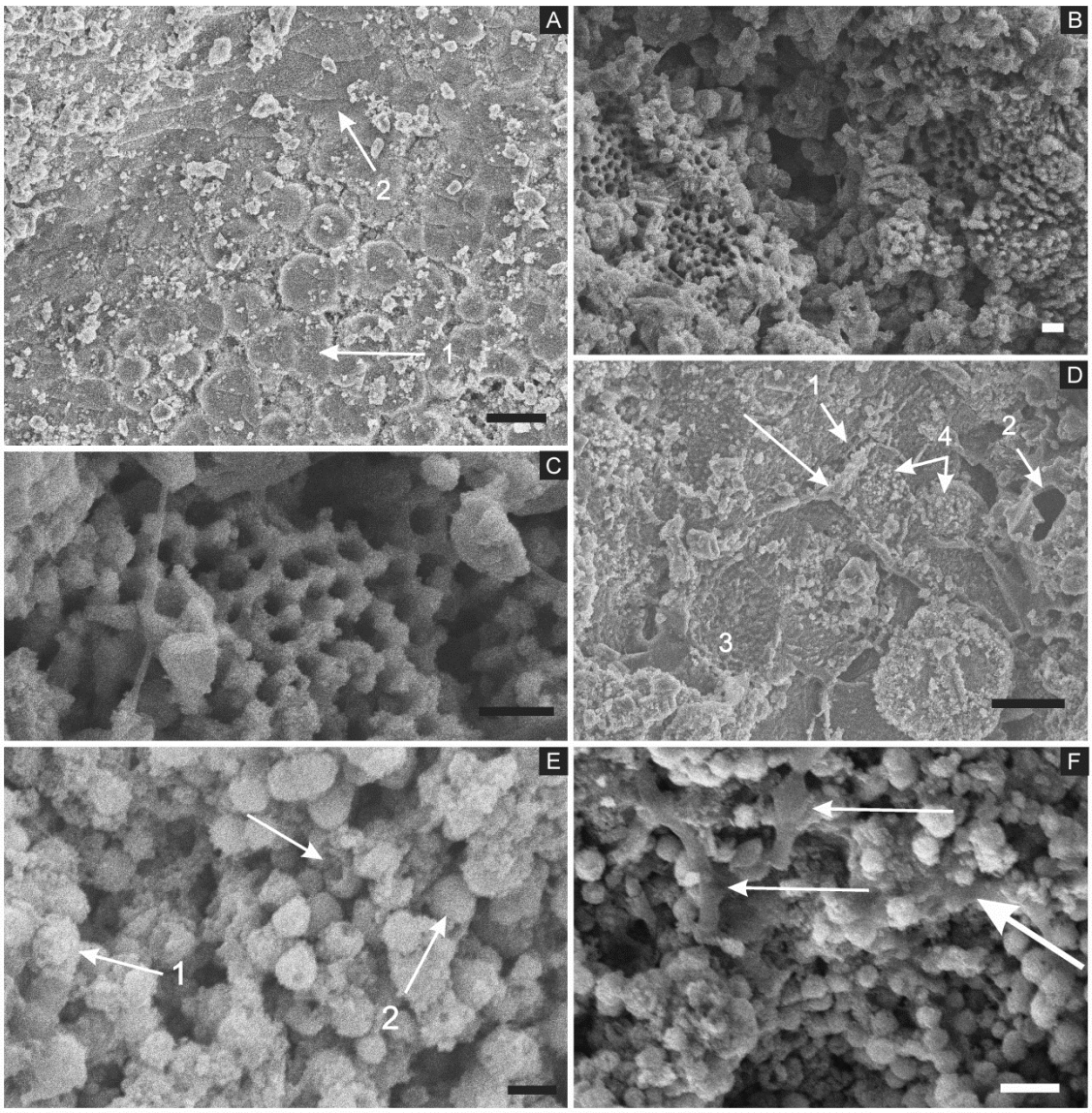

Figure 3: Scanning electron microscopy analysis for mineral characterisation of samples. (A) blattodea GP/1E 9137 (Fig. 2C). Sub-spherical to spherical grains merge (1), yielding a levelled surface (Grimes et al., 2002), which retains details of the outer cuticle area (2; e.g. Barling et al., 2015). Scale bar = 10 µm. (B) GP/1E 8440 (Fig. 2B). Dissolution cavities delimited by a mineralised template formerly occupied by crystals. Scale bar = 2 µm. (C) GP/1E 8440 (Fig. 2B). Detail of the microtexture depicted in B. Scale bar = 2 µm. (D) GP/1E 9137 (Fig. 2C). In the cuticle, polygonal structures delimited by lamellae (arrow) occur. These are likely composed by very fine grained pseudomorphs after pyrite. The lamellae are porous in some portions (1 and 2). The

polygonal structures are filled with nanocrystals similar to the ones forming the sub-spherical to spherical grains (3) and with anhedral pseudomorphs of microcrystalline pyrite (< 1 μm) (4). Scale bar = 10 μm. (E) GP/1E 8397 (Fig. 6A). The microfabrics of the internal cavities are formed by sub-spherical to spherical generally loosely-packed grains (of approximately 1 μm in diameter), formed by nanocrystals (1) and sometimes have smoothed surface (2). The latter is likely an oxidation feature of the former type. The arrow depicts oxidation feature. Scale bar = 1 μm. (F) GP/1E 7105 (Fig. 2A). Some grains infilling internal cavities are embedded in a smooth matrix (wide arrow) and form clusters without a defined shape. "Weblike" structures are indicated by narrow arrows. These features are interpreted as preserved extracellular polymeric substances (EPS). Scale bar = 2 μm. A-F are secondary electron micrographs. A: Beam energy: 10 kV, work distance: 11 mm, spot size: 15; B: Beam energy: 10 kV, work distance: 8 mm, spot size: 15; C: Beam energy: 10 kV, work distance: 8 mm, spot size: 15; D: Beam energy: 10 kV, work distance: 11 mm, spot size: 15. E: Beam energy: 10 kV, work distance: 8 mm, spot size: 15. F: Beam energy: 10 kV, work distance: 8 mm, spot size: 15.

The inner portion of the fossils (Fig. 2) is filled with sub-spherical to spherical generally loosely-packed grains of approximately 1 μm in diameter, formed by nanocrystals (Fig. 3E and F). These grains sometimes have smoothed corroded surfaces and are partially disintegrated or covered by a fuzzy mineral phase (Fig. 3E; as showed by Barling et al., 2015 in Fig. 13E). Cuticle-replacing grains have dissolution cavities formerly occupied by crystals, which left empty templates after oxidation (Fig. 3B and C; similar to Fig. 3B and 3D of MacLean et al., 2008). Taking together, such evidence reinforces oxidation.

In some parts of both cuticle and internal cavities, individual grains are embedded in a smooth matrix, forming clusters that vary in size and shape and are connected by "weblike" structures (Fig. 3F).

Geochemical Analyses

Elemental analyses revealed that iron is more concentrated in fossils than in rock matrix, while calcium and strontium are more concentrated in rock (Figs. 4-6; Fig. S1).

The preferential distribution of these elements is in accordance with the presence of iron compounds replacing the fossils and the calcitic composition of the rock matrix (Barling et al., 2015). Zinc, copper, and lead appear in a higher concentration in the fossils than in the laminated limestone (Figs. 5, 7, Fig. S1). Lead and zinc may be attributed, respectively, to galena and sphalerite (Heimhofer & Martill, 2007). Concentrations of copper in fossils may point to the original precipitation of sulphides along with pyrite, galena and sphalerite, reflecting reducing conditions (Heimhofer & Martill, 2007).

The low abundance of potassium, aluminium, silicon (Figs. 5, 6), plus oxygen in the samples can be attributed to an aluminium silicate, probably k-feldspar, which occurs in the laminated limestones (Heimhofer et al., 2010), or even to clay minerals formed after feldspar weathering. PIXE mapping of elemental distribution revealed high concentrations of manganese in the rock matrix (Fig. S1), indicating that disseminated pyrolusite does occur (Heimhofer & Martill, 2007).

We also showed higher concentrations of phosphorus in the fossils (50.000-60.000 ppm; associated to some areas filled with inner grains (Fig. 5C and D)), as briefly mentioned by Delgado et al. (2014), than in the limestone (700-800 ppm). The observed positive correlation between the concentration of calcium and phosphorus (Fig. 5) is consistent with the presence of apatite in the samples. EDS elemental mapping of mineral fabrics and "weblike" structure (Fig. 7) revealed a marked preferential concentration of carbon in the latter.

Raman spectroscopy analysis indicated the presence of goethite or amorphous hematite in fossils (Fig. 8; Faria & Lopes, 2007). Therefore, iron and oxygen detected by other techniques can be associated to these iron oxides/hydroxides, also documented by Barling et al. (2015) and Grimaldi & Maisey (1990).

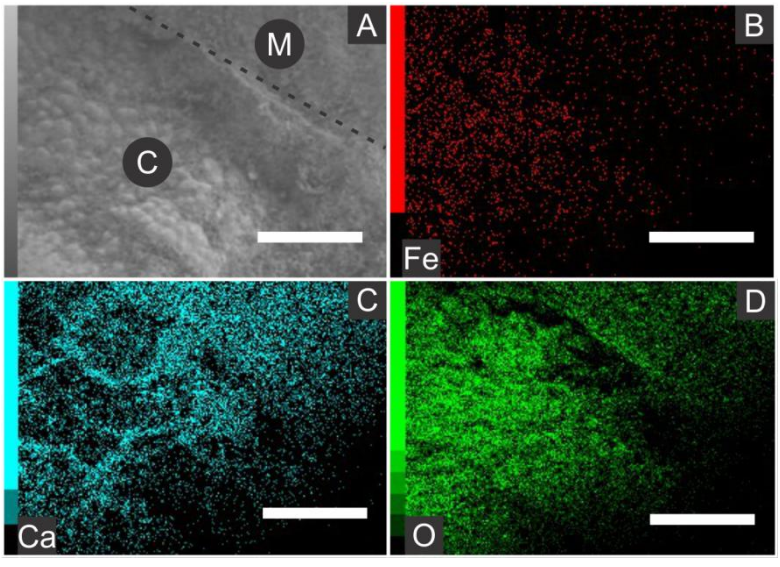

Figure 4: Energy dispersive X-ray spectroscopy elemental maps of the specimen GP/1E 8440 (Fig. 2B). (A) Scanning electron microscopy secondary electron micrograph of the specimen (matrix (M) and cuticle (C)). Beam energy: 10 kV, work distance: 8 mm, spot size: 65. (B) iron. (C) calcium. (D) oxygen. Scale bars = 0.5 mm.

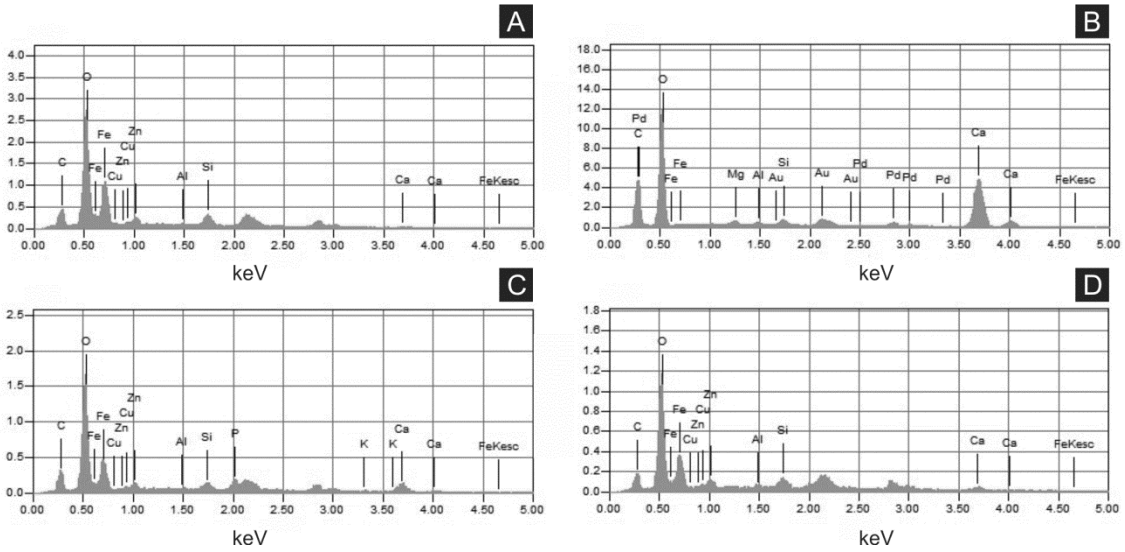

Figure 5: Energy dispersive X-ray spectroscopy point spectra. (A) GP/1E 8440 (Fig. 2B). Cuticle. (B) GP/1E 7105 (Fig. 2A). Matrix. (C-D), GP/1E 8397 (Fig. 6A). Internal part of the fossil.

Preservation of Fossil Insects

Microcrystals of framboidal pyrite or even of framboid pseudomorphs can be subhedral to anhedral, as for example observed in fresh biofilms (Maclean et al., 2008) and replacing Chengjiang *Cricocosmia* worm (Gabbott et al., 2004). In samples here analysed, cuticle sub-/spherical grain shape is sometimes obscured, possibly by grain collapse after weathering (Barling et al., 2015), although Fig. 6A of Delgado et al. (2014) depicts grain shape. Moreover, it is still possible to recognise often regular euhedral to subhedral microcrystal templates (Fig. 3 B,C) and anhedral microcrystals (Fig. 6A, inset, of Delgado et al., 2014). With such evidence in mind, pyrite framboids can be actually defined as spherical to sub-spherical textures formed by microcrystals often regular in shape and size (Canfield and Raiswell, 1991; Butler and Rickard, 2000). Therefore, we follow Delgado et al. (2014) in their interpretation that cuticle-replacing microfabrics are composed of framboid pseudomorphs, while inner grains are herein considered pseudomorphs after microframboidal pyrite (microframboid *sensu*

Sawlowicz, 1993). Indeed, microfabrics are mainly composed of iron and oxygen (Figs. 4 and 5), as also reported by Delgado et al. (2014). Additionally, the polygonal lamellae structures associated with pseudomorphs of pyrite crystals (Fig. 3D) could be interpreted as pyrite overgrowths around originally precipitated pyrite framboids (e.g. Fig. 1D of Grimes et al., 2002).

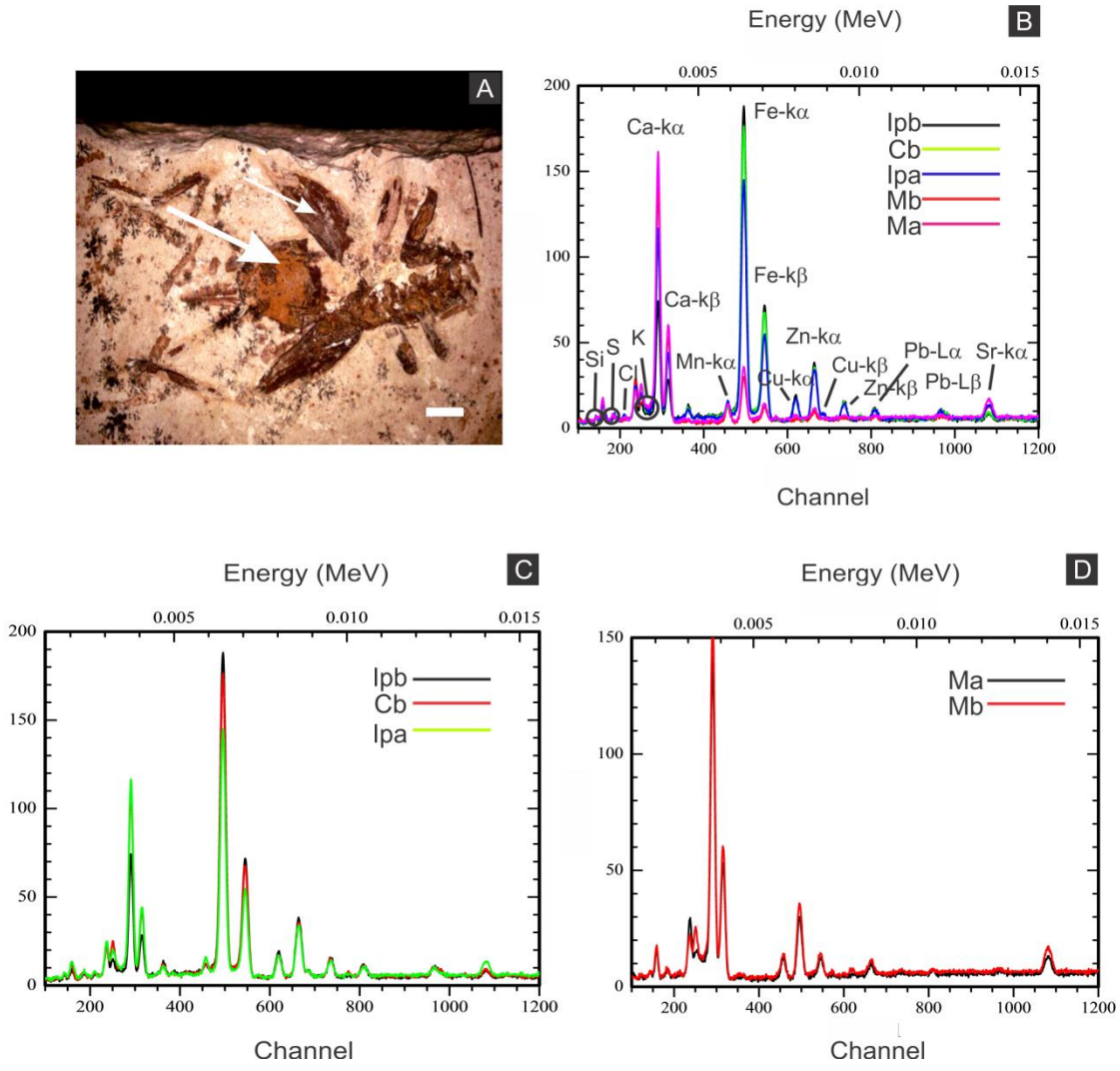

Figure 6: X-ray fluorescence spectra (EDXRF). (A) orthopteran GP/1E 8397. Cuticle is indicated by narrow arrow, while internal portion is indicated by wide arrow. Scale bar = 2 mm. (B-D), EDXRF spectra of specimen in A (a) and of specimen GP/1E 8440 (b) (Fig. 2B). Ip = internal portion, C = cuticle, and M = rock matrix. See (B) for element/peak correlation for all three spectra (B-D).

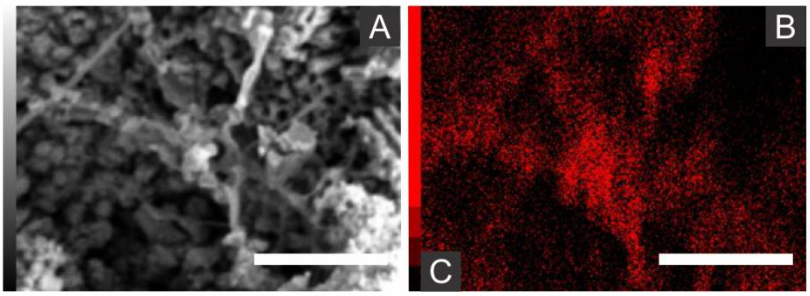

Figure 7: Energy dispersive X-ray spectroscopy elemental map of a "weblike" feature. (A) GP/1E 8827 (Fig. S1). Scanning electron microscopy secondary electron micrograph of the "weblike" (putative preserved extracellular polymeric substances) feature and the surrounding pyrite pseudomorphs. Beam energy: 10 kV, work distance: 11 mm, spot size: 65. (B) Carbon map of the region showed in A. The colour pattern (carbon distribution) may, alternatively, reflect sample topographic irregularities. Scale bars = 5 µm.

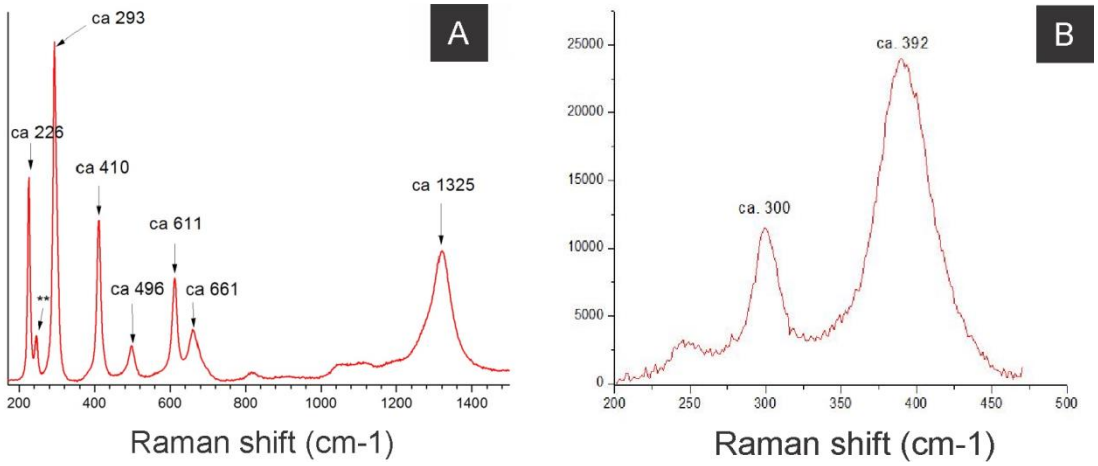

Figure 8: Raman spectra of insect cuticle. (A) spectrum of an iron oxide/hydroxide (amorphous hematite or limonite (Faria & Lopes, 2007)) of cuticle in Fig. 2D (** = ca 245). (B) spectrum of goethite of the cuticle of the fossil GP/1E 8440 (Fig. 2B). A laser source of 785 nm was used in B and other laser source of 633 nm was used in A. A: magnification = 20x, exposure time = 20s, accumulation number = 30, laser power = 1%; B: magnification = 50x (long working distance), exposure time = 10s, accumulation number = 30, laser power = 0.05%.

In comparison to the Crato Member insects, other similarly preserved palaeobiotas include Jehol biota insects, composed of framboids between 6-15 μm (Wang et al., 2015), but lacking microframboids. In Crato Member insects, it was possible to differentiate the pyritic microtexture replacing cuticles from that infilling internal cavities or replacing soft tissues (Delgado et al., 2014). This difference was not observed in the Jehol specimens. When cuticle is preserved in these specimens, it is composed of isolated microcrystals (Wang et al., 2012), while Crato Member exoskeletons are composed of coarse framboid pseudomorphs.

Some of the filamentous structures associated with microfabrics could be interpreted as soft-tissue decay amorphous products, as reported in a taphonomic experiment carried out by Briggs and Kear (1993) using decaying shrimps. However, several observations support that these structures, which seems to have been originally flexible and pliable, are putative remaining fragmentary extracellular polymeric substances (EPS) (Figs. 3F and 7; e.g. Fig. 10F in Toporski et al., 2002; Fig. 3A in MacLean et al., 2008; Fig. 3F in Wang et al., 2012), confirming other current interpretations (e.g. Delgado et al, 2014):

1- these structures occur in fossils and were not found in the matrix (Toporski et al.,2002), although EPS has been both found associated to calcite and microfossils in the host rock and related to calcite genesis (Catto et al., 2016);

2- Figure 7A, for instance, shows that even after SEM vacuum the "weblike" structure has not collapsed, as it would otherwise be expected since samples were not prepared to avoid the collapse of recent hydrated structures (Défarge et al., 1996);

3- if these structures were modern contamination, one would expect the presence of bacteria, however it does not happen. This observation is coherent with pyritisation being slower than bacteria decay, thus hindering bacteria preservation. This would be possible by faster mineralisation processes, such as phosphatisation (Briggs, 2003; Briggs et al., 2005);

4- the structures are structurally organised with mineral fabrics since putative EPS involves them and microfabrics are embedded in a smooth matrix (Fig. 3F), as already mentioned, enabling grain cohesion, accordingly to the EPS definition of Characklis and Wilderer (1989);

5- we actually expect the occurrence of EPS in the context of organomineralisation, such as the precipitation of framboidal pyrite;

6- finally, the association of high abundance of carbon to EPS (Fig. 7) is also well documented in the Jehol biota fossil insects (Wang et al., 2012). Barling et al. (2015) suggested that silica halos surrounding and partially covering Crato Member fossil insects might be attributed to preserved bacterial biofilms, although they have not provided additional morphological and/or geochemical evidence to support this interpretation.

The above discussed presence of pseudomorphs of framboidal pyrite replacing insects, in association with putative EPS, strengthens the hypothesis that biofilm-forming heterotrophic sulphate-reducing bacteria precipitated pyrite, accounting for the preservation of our fossils (Briggs, 2003; Peterson, Lenczewski & Scherer, 2010; Wang et al., 2012; Delgado et al., 2014; Barling et al., 2015). Indeed, biofilms develop organic templates and suitable chemical microenvironmental conditions for the nucleation, growth and aggregation of pyrite crystals in framboids (MacLean et al., 2008). This explains mineral fabrics with empty cavities in the insects, originally filled with pyrite crystals, likely outlined by an organic template (Fig. 3B, C; very similar to Plate 14, Fig. 15 of Love, 1965 and to Fig. 3B and 3D of MacLean et al., 2008). Additionally, the relationship between decaying organic matter and pyrite growth (Brock, Parkes & Briggs, 2006; Raff et al., 2008) has already been supported, for instance, by the presence of organic matter in framboids (Maclean et al., 2008), and the infilling of microfossils (Szczepanik, Sawłowicz & Bak, 2004) and of vertebrate bones (Peterson, Lenczewski & Scherer, 2010) by framboids. Actually, the same happens with the Crato Member insects, thus endorsing the influence of SRB activity to mineralisation during carcass decay. Finally, biofilms create geochemical gradients, controlling ion diffusion rates, directly affecting mineralisation (Briggs, 2003; Peterson, Lenczewski & Scherer, 2010; MacLean et al., 2008; Raff et al., 2008) and, hence promoting active organomineralisation (*sensu* Dupraz et al., 2008). This has already been evidenced by taphonomic experiments with decaying shrimp carcasses (Sagemann et al., 1999), which revealed that geochemical gradients are rapidly developed by oxygen and pH decrease, and sulphate reduction is triggered by anaerobic bacterial decay, leading to iron sulphide formation and soft-tissue preservation.

We propose that during early diagenesis, sulphate-reducing bacteria reduced sulphate (SO_4^{2-}) to hydrogen sulphide (H_2S) (Heimhofer & Martill, 2007) and, possibly, ferric iron (Fe^{3+}) to ferrous iron (Fe^{2+}) (Colemann et al., 1993; Gabbott et al., 2004;

Popa, Kinkle & Badescu, 2004; Heimhofer & Martill, 2007) dissolved in pore water solutions, leading to pyrite formation, which is generally controlled by the amount of dissolved sulphate, reactive iron minerals and available decay-prone organic matter (Berner, 1984; Skei, 1988; Sawlowicz, 1993). This process led to exoskeleton mineralisation (e.g. Orr, Briggs, Kearns, 2008). Moreover, the diffusion of pore water solutions into and through insect carcasses also provided ions for SRB, which in turn infested the insects (e.g. Briggs et al., 2005), mediating the precipitation of minerals, mainly microframboidal pyrite, which covered the internal soft tissues (Fig. 9 and Fig. 13E of Barling et al., 2015). Microframboidal pyrite also infilled internal cavities (Figs. 3E, F) with remaining organic matter derived from partially decayed soft tissues (Orr, Briggs & Kearns, 2008; Pan, Sha & Fürsich, 2014). Therefore, distinct soft tissues had variable preservational potentials (Briggs & Kear, 1993; Duncan & Briggs, 1996) and/or fossilisation processes varied along carcasses (Gabbott et al., 2004). The preservational process is summarised in Fig. 10.

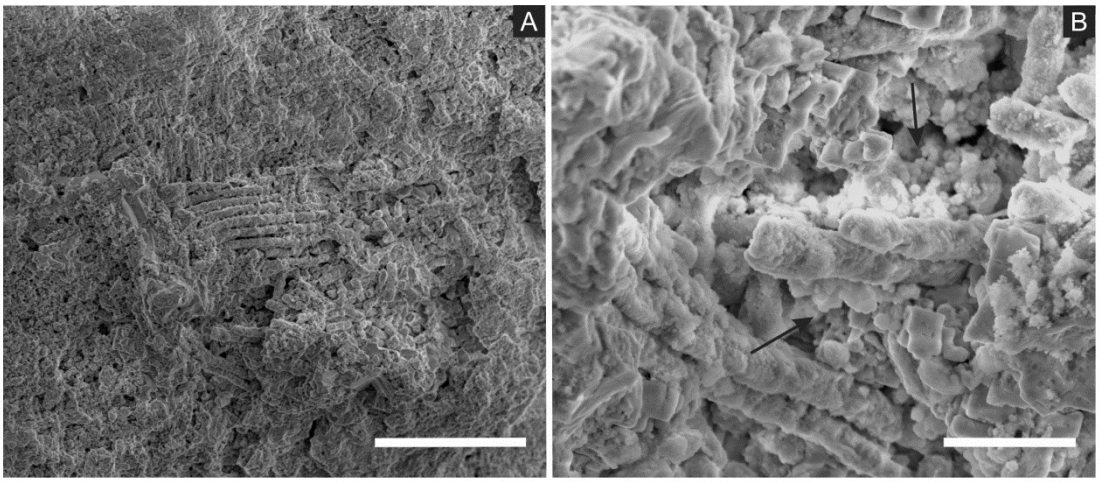

Figure 9: Scanning electron microscopy micrographs of putative muscular fibres. (A-B) GP/1E 7105 (Fig. 2A). (A) putative muscular fibres in a broken portion of the cuticle. Scale bar = 50 µm. (B) microfabric (arrows) associated with the putative muscular fibres. Scale bar = 10 µm. A-B are secondary electron micrographs. A: Beam energy: 5.000 kV, spot size: 3.0, work distance: 14.5 mm; B: Beam energy: 10.00 kV, spot size: 3.0, work distance: 14.4 mm.

The occurrence of coarse framboidal pyrite and fine microframboidal pyrite pseudomorphs can be interpreted as the result of the balance between ion (iron and sulphate) diffusion and pyrite nucleation rates (Sagemann et al., 1999; Butler &

Rickard, 2000; Gabbott et al., 2004). Initially, several pyritic nuclei likely formed owing to an initial high oversaturation of iron and sulphate present in pore water solutions, thus yielding framboids, as proposed for framboid formation in Chengjiang biota fossils and in Jehol biota insects (Gabbott et al., 2004; Ohfuji & Rickard, 2005; Wang et al., 2012; Schiffbauer et al., 2014). Moreover, the barrier created by the cuticle, the biofilms (around and inside carcasses), and the already formed authigenic pyrite crystals presumably restricted ion diffusion (lower than nucleation rate) (e.g. MacLean et al., 2008) and, thus, also favoured the precipitation of framboidal pyrite, instead of isolated crystals (Gabbott et al., 2004). Nevertheless, in comparison to innermost carcass areas, the cuticle received a continuous influx of iron and sulphate from the sediment, which favoured coarse framboid formation, while finer microframboidal pyrite precipitated within the inner cavities of the carcasses owing to the decreasing influx of iron and sulphate inward. Indeed, initial pyrite saturation and ion diffusion timing can control mineral size (Sawlowicz, 1993; Gabbott et al., 2004; Schiffbauer et al., 2014). Furthermore, the high decay potential of labile internal tissues (e.g. muscles; Fig. 9) also led to an increase in H_2S saturation (Schiffbauer et al., 2014) and, thus, high nucleation rates and microframboid formation inside the insect carcasses, as suggested by Gabbott et al. (2004) to the preservation of the Chengjiang biota.

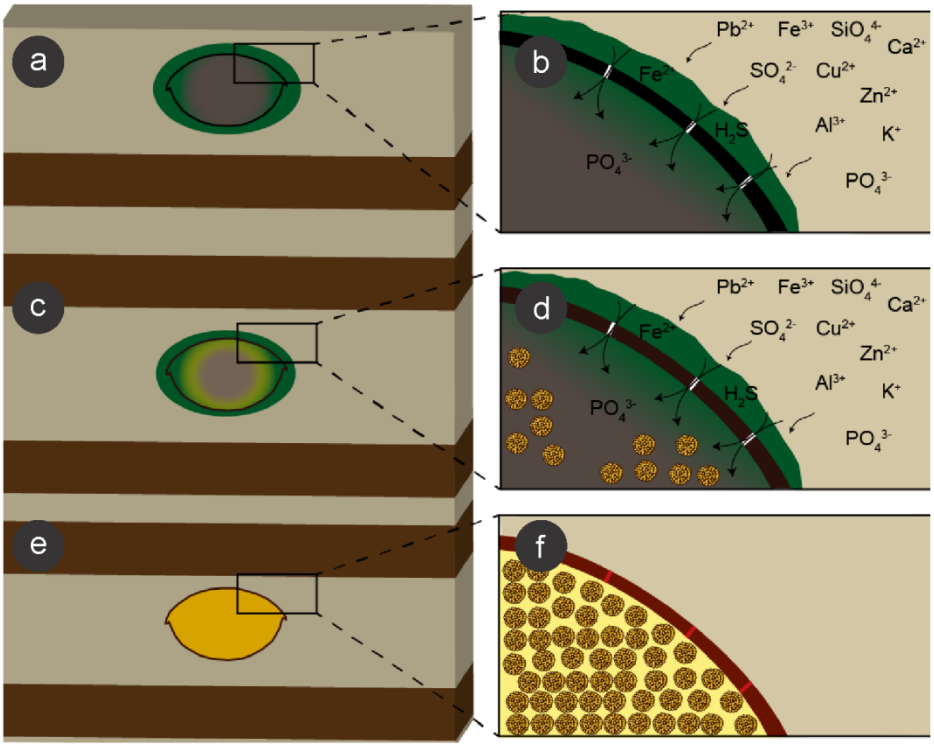

Figure 10: Process of preservation of the Crato Member fossil insects. After final burial (a), ions present in sediment pore water solutions were concentrated in biofilms of sulphate reducing bacteria (SRB) (green) around and within decaying carcasses. Both ions and bacteria entered insects through microcracks (putatively generated by compaction) in the cuticle (black) (b). These bacteria reduced sulphate and, possibly iron (III), resulting in framboidal pyrite formation, which replaced cuticle (brown; c, d). Within the carcasses, labile tissues (grey) were also replaced and replicated (or at least covered) by microframboidal pyrite (c, internal yellow halo and d, internal yellow spheres). Total carcass collapse was initially avoided by structural strength of both cuticle and internal soft tissues and later prevented by early lithification of both exoskeleton and internal soft tissues (e, f), thus yielding three-dimensional replicas. Microcracks were also filled with pyrite (f, red segments in the mineralised cuticle).

Geochemical analyses revealed the preferential concentration of copper, zinc, and lead in fossils in comparison to the surrounding matrix. The different abundance of some elements between fossils and their embedding rock has been extensively attributed to the activity of bacterial biofilms, which envelop decaying carcasses and leads to their mineralisation (Wilby et al., 1996; Toporski et al., 2002; Westall et al., 2006; Laflamme et al., 2011). Copper, zinc, and lead are able to bond to organic matter (Šípková et al., 2013). Alternatively, the preferable association of copper and zinc to the carcasses can be attributed to bacterial activity. Indeed, chitinous substrates buried in sediments are able to remove heavy metals from contaminated environments, a process mediated by bacteria (Kan et al., 2013). In this sense, the high chemical affinity of copper and zinc with chitin (Neugebauer, 1986) further explains the presence of these metals associated with the insects. Moreover, the adsorption of Cu^{2+} to chitin varies in response to pH gradients (Gonzalez-Davila & Millero, 1990), which is controlled by biofilms, as already mentioned. The higher lead concentration in the fossils than in the limestone may be related to the association of this element with iron oxide/hydroxides, as reported in an *Archaeopteryx* sample (Bergmann et al., 2010), although no causal relationship has been attributed to explain this preferential association. This may also be explained by SRB activity on and within the insect carcasses yielding authigenic precipitation of galena (Lambrez et al., 2000).

Local variations of pH created during anaerobic decay control mineralisation, with acid conditions leading to phosphate precipitation, while higher pH values accounts for carbonate mineralisation (Briggs & Wilby, 1996; Sagemann et al., 1999). In this vein, other authors suggested that the preservation of internal non-cuticular soft tissues of the Crato Member insects has occurred by phosphatisation (e.g. Barling et al., 2015), similarly to the preservation of labile tissues within a Jurassic horseshoe crab (Briggs et al., 2005), although direct quantitative evidence has not been revealed until SXS data herein provided. The preferential association of apatite to the fossils also points to microbial activity during fossilisation, as noticed elsewhere (Briggs et al., 2005). Only calcium poor continental waters have enough high concentrations of phosphate in solution to enable phosphatisation (Martínez-Delclòs, Briggs & Peñalver, 2004), which was not the case of the Crato Member palaeolake. Therefore, alternative sources, such as the decay of organic matter (Allison, 1988; Briggs, 2003) might have resulted in a high offer of phosphorus (and phosphate) for fossil insect phosphatisation. This process may have been facilitated by the activity of phosphate solubilizing bacteria (Kan et al., 2013; Martínez-Delclòs, Briggs & Peñalver, 2004).

The diffusion of solutions within decaying carcasses was likely controlled by the lithification rate and, possibly, by exoskeleton microcracks generated by compaction (Figs. 10 and 11). This latter process is an explanation for the preservation of internal tissues in a Jurassic horseshoe crab (Briggs et al., 2005), wherein the infestation of bacteria was also facilitated by predation or diseases. Indeed, predation and partial disarticulation of some insects could have facilitated bacteria infestation and the diffusion of ion rich solutions. This mechanism could account for the occurrence of partially disarticulated and fragmented fossil insects, but still with fine details preserved (e.g. Barling et al., 2015) and with some degree of three-dimensionality due to early mineralisation.

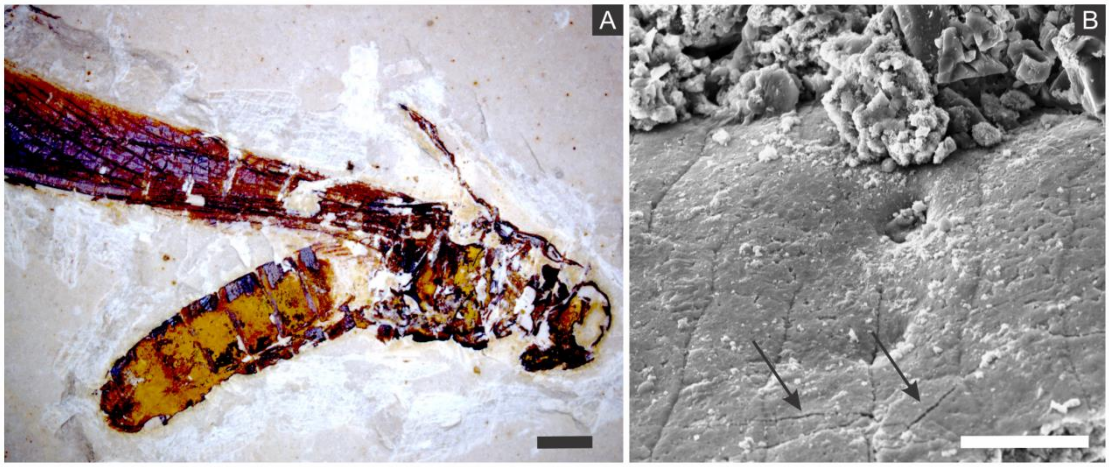

Figure 11: Microcracks in the cuticle of a specimen. (A) Orthopteran GP/1E 10368. Scale bar = 2 mm. (B) Scanning electron microscopy secondary electron micrograph showing microcracks in the cuticle (arrows). Scale bar = 10 µm. Beam energy: 10.00 kV, spot size: 3.0, work distance: 11.2 mm.

The small size of the microframboidal pyrite pseudomorphs (~1 µm in diameter) explains the high fidelity of internal soft-tissue preservation (Briggs, 2003; Delgado et al., 2014), as observed in a taphonomic experiment carried out by (Briggs & Kear, 1993). We suggest that total carcass collapse by sediment compaction (Wang et al., 2012) was initially prevented by exoskeleton and internal tissue mechanical resistance to compression (Orr, Briggs & Kearns, 2008; Pan, Sha & Fürsich, 2014). Thereafter, further compaction was likely prevented by carcass mineralisation, yielding three-dimensional insect replicas (Fig. 11), as suggested for the Jehol biota insects (Wang et al., 2012; Pan, Sha & Fürsich, 2014).

The exceptional preservation of Crato Member insects reflects palaeoenvironmental conditions. Isotopic analyses of carbonate carbon and oxygen performed in the Crato Member basalmost laminated limestones revealed that the depositional palaeoenvironment was a freshwater stratified lake poorly connected with external water sources, with stagnant, anoxic, and at least episodic hypersaline bottom waters (Heimhofer & Martill, 2007; Martill, Loveridge & Heimhofer, 2007; Heimhofer et al., 2010). Water column stratification may have been related to stagnation and/or high rates of surface water primary productivity providing a high amount of organic matter, the decay of which by aerobic bacteria reduced bottom water oxygen and eventually led to anaerobic conditions in deep waters (Heimhofer & Martill, 2007).

Furthermore, the occurrence of salt pseudomorphs and xerophytic vegetation pollen supports a semi-arid to arid palaeoclimate (Heimhofer & Martill, 2007).

Melendez et al. (2012) proposed the influence of photic zone euxinia (PZE) to the preservation of biomarkers and to exceptional fossil preservation (Heimhofer & Martill, 2007). The isorenieratene biomarker was reported in the Crato Member laminated limestones by Heimhofer & Martill (2007). This pigment is used by green sulphur bacteria (Chlorobiaceae) in anoxygenic photosynthesis (Schwark, 2013). This implies that the palaeoenvironment was, at least, temporarily stratified in relation to O_2 and H_2S yielding euxinic photic zone (EPZ), being H_2S likely produced by SRB within the sediment (Heimhofer & Martill, 2007). Following this rationale, degradation was diminished after carcasses entered the EPZ since the blockage of autolysis is triggered by reduction and/or anoxic conditions (Raff et al., 2008).

Moreover, the palaeoenvironmental stratification in respect of oxygen and salinity likely favoured fossil preservation (Heimhofer et al., 2007). The absence of burrowers (together with grazers and scavengers) in the palaeolake owing to its stratification (Heimhofer & Martill, 2007; Menon & Martill, 2007) accounts for the lack of bioturbation, which have favoured mineralisation. Indeed, diffusion of O_2, sediment hydration, and aerobic decay of C_{org} were prevented (Callow & Brasier, 2009) resulting in a zone of ionic saturation, heterotrophic anaerobic activity, then yielding the early precipitation of authigenic minerals, like phosphates and pyrite (Gehling, 1999; Callow & Brasier, 2009; Laflamme et al., 2011; G. L. Osés et al., unpublished data). Similarly, bioturbation was proposed as a control for the pyritisation of insects from the also lacustrine Jehol biota (Wang et al., 2012; Pan, Sha & Fürsich, 2014). In addition to the lack of bioturbation, the protection of the water-sediment interface against storms likely contributed to substrate anoxia (Gehling, 1999; Heimhofer & Martill, 2007). Furthermore, the development of SRB biofilms around insect carcasses at the palaeolake bottom, followed by carcass mineralisation, would have been enabled, for instance, by the lack of grazers in the water-sediment interface (Menon & Martill, 2007). Indeed, the importance of microorganisms, of high salinity, and of the lack of scavengers to the preservation of three-dimensional fossil insects was already noticed by Duncan and Briggs (1996) for the preservation of Riversleigh (Tertiary, Australia) 3D insects. The role of microbial mats to three-dimensional insect preservation in

palaeolakes was then extended to the Jehol biota and the Crato Member (Wang et al., 2012; Barling et al., 2015).

Nevertheless, the above discussed factors cannot fully explain pyritisation. The Crato Member fossil insects are typically found in laminated limestone facies with a poor content of organic matter (Neumann et al., 2003). Jehol biota pyritised insects (Wang et al., 2012) and Chengjiang biota pyritised arthropods, sponges, brachiopods, and other organisms (Gabbott et al., 2004) are also exclusive to organic-poor lithologies. In this way, the formation of pyrite is concentrated in the carcasses and not widespread within the sediment (Gabbott et al., 2004), which, therefore, we extend to the Crato Member.

The fossil insects from the Crato Member are the first record of these organisms in lacustrine laminated limestones preserved by pyrite without a volcanogenic sediment origin, as it has been suggested for the preservation of the Jehol biota insects (Wang et al., 2012; Pan, Sha & Fürsich, 2014). These authors argued that iron and sulphur were nourished by volcanic material, deposited at a siliciclastic-bearing lacustrine system. Nevertheless, Wang et al. (2012) considered the role of heterotrophic bacteria as central for insect pyritisation, which was put on debate by Pan, Sha & Fürsich (2014). However, for the Crato Member, sulphate was likely provided by evaporites (Martill et al., 2007).

Finally, SEM, EDS, EDXRF, PIXE, and Raman analyses (Figs. 3-6, 8, Fig. S1) suggest that the supergene oxidation and/or hydration of pyrite resulted in the formation of iron oxides/hydroxides (Sawlowicz & Kaye, 2006; Menon & Martill, 2007; Wang et al., 2012; Delgado et al., 2014; Pan, Sha & Fürsich, 2014).

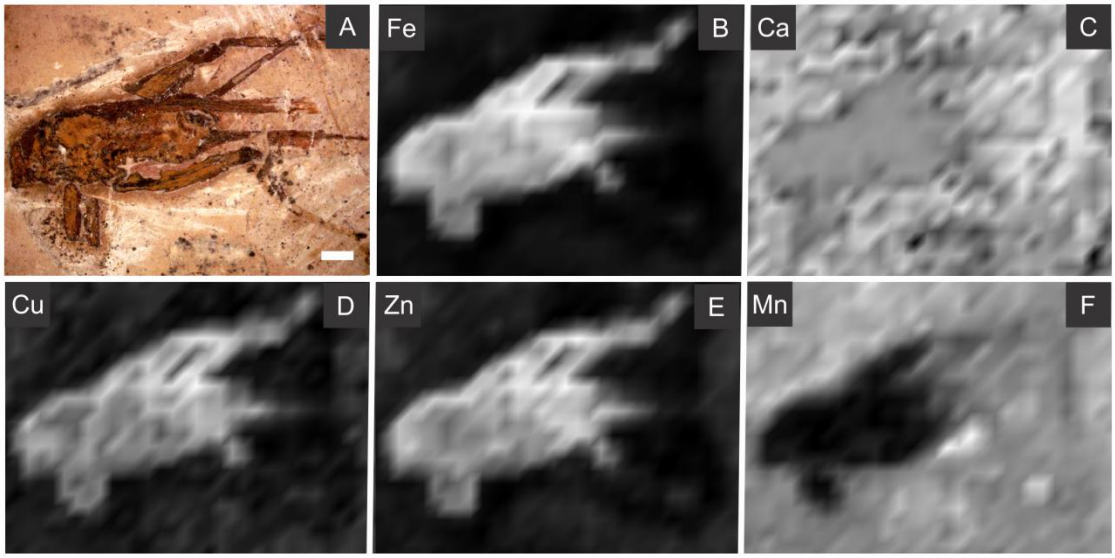

Supplemental Figure S1. Particle induced X-ray emission analysis of the orthopteran GP/1E 8827. A, specimen analysed. Scale bar = 2 mm. B, iron. C, calcium. D, copper. E, zinc. F, manganese. Observe that the lighter portions of the elemental maps show higher concentrations of the analysed elements.

Conclusions

The results of imaging and geochemical techniques suggest that Crato Member fossil insects have been preserved by framboidal pyrite. Based on such evidence, we propose that the diffusion of pore water solutions to and through insect carcasses and their envelopment and infestation by bacteria created microenvironmental geochemical conditions which led to the mineralisation (mainly pyritisation) of insect cuticles and internal soft tissues. These geobiological/taphonomic processes have yielded three-dimensional replicas of insects, keeping morphological details of delicate features (e.g. muscle fibres), which can shed light on taxonomy, systematics, and palaeoecology.

Despite of pyrite genesis being ubiquitous, pyritisation of labile tissues is rare and restricted to few examples in the fossil record (e.g. Briggs, Bottrell & Raiswell, 1991; Gabbott et al., 2004; Wang et al., 2012). Indeed, the exceptional preservation of the Crato Member fossil insects confirms the importance of the following factors to the formation of *Lagerstätten*: early diagenetic precipitation of pyrite (Gabbott et al., 2004; Wang et al., 2012; Barling et al., 2015) under stratified lake conditions with low energy and without bioturbators (Gehling, 1999; Wang et al., 2012), associated with microbial activity (Duncan & Briggs, 1996; Wang et al., 2012; Delgado et al., 2014; Barling et al.,

2015; Catto et al., 2016), and fine sediments (Gehling, 1999) with low organic matter contents (Neumann et al., 2003).

Acknowledgements

We would like to thank the Brazilian Council for Scientific and Technological Development (Proc. 154062/2014-6) for providing a master scholarship for the author Gabriel L. Osés. We also thank the Department of Federal Police of Brazil for intelligence service and proactive initiatives, which have diminished the illegal international trade of fossils from the Santana Formation, in the last years. These actions have increased the palaeontological collections of Brazilian universities (e.g. University of São Paulo) in thousands of specimens, providing an unprecedented amount of exceptionally well preserved fossils for Brazilian researchers and foreign collaborators, hence contributing to the development of Brazilian palaeontological research. Most of this material is already legally available for research. We are very grateful to the huge effort made by the staff headed by Professor Paulo Eduardo de Oliveira, Professor Juliana Moraes de Leme Basso, and Ivone Cardoso Gonzales, which improved the infrastructure of the Scientific Palaeontological Collection of the Institute of Geosciences from the University of São Paulo (São Paulo, Brazil), enabling proper fossil storage and organisation. We would like to acknowledge the Astrobiology Laboratory (Institute of Astronomy, Geophysics, and Atmospheric Sciences, University of São Paulo, USP) for Raman analyses (equipment update was funded by the São Paulo Research Foundation, FAPESP, project 2012/18936-0), the Institute of Physics (USP) for EDXRF analyses (equipment acquisition was supported by FAPESP, process 2012/00202-0), the Laboratory of Materials and Ionic Beams (Institute of Physics, USP) for PIXE analyses, the Laboratory of Technological Plasmas (São Paulo State University) and the Brazilian Nanotechnology National Laboratory for having kindly offered their SEM equipment under the Quanta 15068, 16826, 16923, and 18363 proposals, and finally, the Brazilian Synchrotron Light Laboratory for SXS analyses under the SXS 14563 proposal. We are also grateful to Professor Martin David Brasier, *in memorian*, for his stimulating and insightful ideas and to Professor Thomas Rich Fairchild and the graduate student Gustavo Evangelista Prado for enlightening discussions. We thank Professor Mario Luis Assine for having kindly offered a vectorised version of his geologic map of the Araripe Basin. We also thank Evandro

Pereira da Silva for technical support during Raman spectra acquisition, Evelyn Aparecida Mecenero Sanchez for support in figure preparation, and Hugo Silva Pires Junior for skilful sample preparation. We are also thankful for the language revision made by Izabel Maria da Silva Ladeira from English for You (São Paulo, Brazil).

References

Abbate M, Vicentin FC, Compagnon-Cailhol V, Rocha MC, Tolentino HCN. The soft X-ray spectroscopy beamline at the LNLS: technical description and commissioning results. J Synchrotron Radiat. 1999; 6 (5): 964-972.

Allison PA. Phosphatized soft-bodied squids from the Jurassic Oxford Clay. Lethaia. 1988; 21 (4): 403-410.

Assine ML. Bacia do Araripe. Bol. Geoc. Petr. 2007; 15 (2): 371-389.

Barling N, Martill DM, Heads SW, Gallien F. High fidelity preservation of fossil insects from the Crato Formation (lower Cretaceous) of Brazil. Cret Res. 2015; 52 (B): 605-622.

Bergmann U, Morton RW, Manning PL, Sellers WI, Farrar S, Huntley KG, et al. *Archaeopteryx* feathers and bone chemistry fully revealed via synchrotron imaging. Proc Natl Acad Sci U S A. 2010; 107 (20): 9060-9065.

Berner RA. Sedimentary pyrite formation: an update. Geochim Cosmochim Acta. 1984; 48: 605-615.

Beurlen KA. Geologia da Chapada do Araripe. An Acad Bras Cienc. 1962; 34 (3): 365-370.

Beurlen K. As condições ecológicas e faciológicas da Formação Santana na Chapada do Araripe (Nordeste do Brasil). An Acad Bras Cienc. 1971; 43: 411-415.

Briggs D. The role of decay and mineralization in the preservation of soft-bodied fossils. Annu Rev Earth and Planet Sci. 2003; 31: 275-301.

Briggs DEG, Bottrell SH, Raiswell R. Pyritization of soft-bodied fossils: Beecher's Trilobite Bed Upper Ordovician, New York State. Geology. 1991; 19: 1221-1224.

Briggs DEG, Kear AJ. Fossilization of soft tissue in the laboratory. Science. 1993; 259: 1439-1442.

Briggs DEG, McMahon S. The role of experiments in investigating the taphonomy of exceptional preservation. Palaeontology. 2016; 59: 1-11.

Briggs DEG, Moore RA, Shultz JW, Schweigert G. Mineralization of soft-part anatomy and invading microbes in the horseshoe crab *Mesolimulus* from the Upper Jurassic lagerstätte of Nusplingen, Germany. Proc Biol Sci. 2005; 272: 627–632.

Briggs DEG, Wilby PR. The role of the calcium carbonate-calcium phosphate switch in the mineralization of soft-bodied fossils. J Geol Soc London. 1996; 153: 665-668.

Brito-Neves BB. A Bacia do Araripe no contexto geotectônico regional. In: Atas do I Simpósio sobre a Bacia do Araripe e Bacias Interiores do Nordeste; 1990. 1: 21-33.

Brock F, Parkes RJ, Briggs DEG. Experimental pyrite formation associated with decay of plant material. Palaios. 2006; 21: 499-506.

Butler IB, Rickard D. Framboidal pyrite formation via the oxidation of iron (II) monosulphide by hydrogen sulphide. Geochim Cosmochim Acta. 2000; 64 (15): 2665-2672.

Callow RHT, Brasier MD. Remarkable preservation of microbial mats in Neoproterozoic siliciclastic settings: Implications for Ediacaran taphonomic models. Earth-Sci. Rev. 2009; 96: 207–219.

Canfield DE, Raiswell R. Pyrite formation and fossil preservation. In: Allison PA, Briggs DEG, editors. Topics in Geobiology. Plenum Press; 1991, pp. 337–387.

Catto B, Jahnert RJ, Warren LV, Varejao FG, Assine ML. The microbial nature of laminated limestones: lessons from the Upper Aptian, Araripe Basin, Brazil. Sediment Geol. 2016; doi: 10.1016/j.sedgeo.2016.05.007.

Characklis WG, Wilderer PA. Glossary. In: Characklis WG, Wilderer PA (eds) Structure and function of biofilms. Wiley, Chichester; 1989. pp. 369-371.

Chen L, Xiao S, Pang K, Zhou C, Yuan X. Cell differentiation and germ-soma separation in Ediacaran animal embryo-like fossils. Nature. 2014; 516: 238-241.

Coimbra JC, Arai M, Carreño AL. Biostratigraphy of lower Cretaceous microfossils from the Araripe Basin, northeastern Brazil. Geobios. 2002; 35 (6): 687-698.

Coleman ML, Hedrick DB, Lovley DR, White DC, Pye K. Reduction of Fe (III) in sediments by sulphate-reducing bacteria. Nature. 1993; 361: 436-438.

Défarge C, Trichet J, Jaunet A-M, Robert M, Tribble J, Sansone FJ. Texture of microbial sediments revealed by cryo-scanning electron microscopy. J Sediment Res. 1996; 66 (5): 935-947.

Delgado A de O, Buck PV, Osés GL, Ghilardi RP, Rangel EC, Pacheco MLAF. Paleometry: a brand new area in Brazilian science. Mater Res. 2014; 17: 1434-1441.

Duncan IJ, Briggs DEG. Three-dimensionally preserved insects. Nature. 1996; 381: 30-31.

Dupraz C, Reid RP, Braissant O, Decho AW, Norman RS, Visscher PT. Processes of carbonate precipitation in modern microbial mats. Earth-Sci Rev. 2008; 96 (3): 141-162.

Engel MS, Grimaldi D & Krishna K. Primitive termites from the Early Cretaceous of Asia (Isoptera). Stuttgarter Beiträge zur Naturkunde, Serie B (Geologie und Paläontologie). 2007; 371: 1-32.

Faria DLA, Lopes FN. Heated goethite and natural hematite: can Raman spectroscopy be used to differentiate them? Vib Spectrosc. 2007; 45: 117-121.

Gabbott SE, Xian-guang H, Norry MJ, Siveter DJ. Preservation of early Cambrian animals of the Chengjiang biota. Geology. 2004; 32 (10): 901-904.

Gehling JG. Microbial mats in terminal Proterozoic siliciclastics: ediacaran death masks. Palaios Res. Rep. 1999; 14: 40-57.

Gonzalez-Davila M, Millero FJ. The adsorption of copper to chitin in seawater. Geochim Cosmochim Acta. 1990; 54*:* 761-768.

Grimaldi D, Maisey J. Introduction. In: Gimaldi D, editor. Insects from the Santana Formation, Lower Cretaceous, of Brazil. Bull. AMNH; 1990. pp. 1-15.

Grimes ST, Davies KL, Butler IB, Brock F, Edwards D, Rickard D, et al. Fossil plants from the Eocene London Clay: the use of pyrite textures to determine the mechanism of pyritization. J Geol Soc. 2002; 159: 493-501.

Heimhofer U, Ariztegui D, Lenniger M, Hesselbo SP, Martill DM, Rios-Netto AM. Deciphering the depositional environment of the laminated Crato fossil beds (early Cretaceous, Araripe Basin, north-eastern Brazil). Sedimentology. 2010; 57: 677-694.

Heimhofer U, Martill DM. The sedimentology and depositional environment of the Crato Formation. In: Martill DM, Bechly G, Loveridge R, editors. The Crato fossil beds of Brazil: window to an ancient world. Cambridge University Press; 2007. pp. 44-62.

Jarzembowski EA, Ross AJ. Insect Origination and Extinction in the Phanerozoic. In: Hart MB, editor. Biotic Recovery from Mass Extinction Events. Geological Society Special Publication; 1996, nº 102, pp. 65-78.

Kalliokoski J, Cathles L. Morphology, mode of formation, and diagenetic changes in framboids. Bull Geol Soc Fin. 1969; 41: 152—133.

Kan J, Obraztsova A, Wang Y, Leather J, Scheckel KG, Nealson KH. Apatite and chitin amendments promote microbial activity and augment metal removal in marine sediments. Open J. Met. 2013; 3: 51-61.

Kellner AWA. Membro Romualdo da Formação Santana, Chapada do Araripe, CE: um dos mais importantes depósitos fossíliferos do Cretáceo brasileiro. In: Schobbenhaus C, Campos DA, Qeiroz ET, Winge M, Berbert-Born MLC, editors. Sítios geológicos e paleontológicos do brasil, Departamento Nacional da Produção Mineral/Companhia de Pesquisa de Recursos Minerais/Comissão Brasileira de Sítios Geológicos e Paleobiológicos; 2002. pp. 121- 130.

Labandeira C. Why did Terrestrial Insect Diversity Not Increase During the Angiosperm Radiation? Mid-Mesozoic, Plant-Associated Insect Lineages Harbor Clues. In: Pontarotti P, editor. Evolutionary Biology: Genome Evolution, Speciation, Coevolution and Origin of Life. Springer International Publishing Switzerland; 2014, pp. 261-299.

Laflamme M, Schiffbauer JD, Narbonne JM, Briggs DEG. Microbial biofilms and the preservation of the Ediacara biota. Lethaia. 2011; 44: 203-213.

Lambrez M, Druschel GK, Thomsen-Ebert T, Gilbert B, Welch SA, Kemner KM, et al. Formation of sphalerite (ZnS) deposits in natural Biofilms of sulfate-reducing bacteria. Science. 2000; 290: 1744-1777.

Leri AC, Hay MB, Lanzirotti A, Rao W, Myneni SCB. Quantitative determination of absolute organohalogen concentrations in environmental samples by X-ray absorption spectroscopy. Anal Chem. 2006; 78: 5711-5718.

Lidgard S, Crane PR. Quantitative analyses of the early angiosperm radiation. Nature. 1988; 331: 344-346.

Love LG. Micro-organic material with diagenetic pyrite from the lower Proterozoic Mount Isa shale and a carboniferous shale. Proc York Geol Soc. 1965; 35 (2), 9: 187-202.

MacLean LCW, Tyliszczak T, Gilbert PU, Zhou D, Pray TJ, Onstott TC, et al. A high-resolution chemical and structural study of framboidal pyrite formed within a low-temperature bacterial biofilm. Geobiology. 2008; 6: 471–480.

Martill DM, Loveridge RF, Heimhofer U. Halite pseudomorphs in the Crato Formation (early Cretaceous, late Aptian) Araripe Basin, northeast Brazil: further evidence for hypersalinity. Cret. Res. 2007; 28 (4): 613-620.

Martínez-Delclòs X, Briggs DEG, Peñalver E. Taphonomy of insects in carbonates and amber. Palaeogeogr. Palaeoclimatol. Palaeoecol. 2004; 203: 19-64.

Martínez-Delclòs X, Martinell J. The oldest known record of social insects. J Paleontol. 1995; 69: 594-599.

Melendez I, Grice K, Trinajstic K, Ladjavardi M, Greenwood P, Thompson K. Biomarkers reveal the role of photic zone euxinia in exceptional fossil preservation: an organic geochemical perspective. Geology. 2012 Nov 06. doi:10.1130/G33492.1.

Menon F, Martill DM. Taphonomy and Preservation of Crato Formation Arthropods. In: Martill DM, Bechly G, Loveridge R, editors. The Crato fossil beds of Brazil: window to an ancient world. Cambridge University Press; 2007. pp. 79-96.

Neugebauer E. The krill chitin and some aspects of metals transport in antarctic sea water. Pol Polar Res. 1986; 371-376.

Neumann VH, Borrego AG, Cabrera I, Dino R. Organic matter composition and distribution through the Aptian-Albian lacustrine sequences of the Araripe Basin, northeastern Brazil. Int J Coal Geol. 2003; 54: 21-40.

Nicholson DB, Mayhew PJ, Ross AJ. Changes to the Fossil Record of Insects Through Fifteen Years of Discovery. PLoS ONE. 2015; 10(7): e0128554. doi:10.1371/journal.pone.0128554.

Ohfuji H, Rickard D. Experimental syntheses of framboids—a review. Earth-Sci Rev. 2005; 71: 147-170.

Orr PJ, Briggs DEG, Kearns S. Taphonomy of exceptionally preserved crustaceans from the upper Carboniferous of southeastern Ireland. Palaios. 2008; 23: 298-312.

Pan Y, Sha J, Fürsich FT. A model for organic fossilization of the early Cretaceous Jehol lagerstätte based on the taphonomy of ‘‘*Ephemeropsis trisetalis*’’. Palaios. 2014; 29: 363-377.

Peterson JE, Lenczewski ME, Scherer RP. Influence of microbial biofilms on the preservation of primary soft tissue in fossil and extant archosaurs. PLoS ONE. 2010; 5 (10): e13334. doi:10.1371/journal.pone.0013334.

Popa R, Kinkle BK, Badescu A. Pyrite framboids as biomarkers for iron-sulfur systems. Geomicrobiol J. 2004; 21 (3): 193-206.

Raff EC, Schollaert KL, Nelson DE, Donoghue PCJ, Thomas C-W, Turner FR, et al. Embryo fossilization is a biological process mediated by microbial biofilms. Proc Natl Acad Sci U S A. 2008; 105 (49): 19360–19365.

Sagemann J, Bale SJ, Briggs DEG, Parkes RJ. Controls on the formation of authigenic minerals in association with decaying organic matter: an experimental approach. Geochim Cosmochim Acta. 1999; 63 (7/8): 1083–1095.

Sawlowicz Z. Pyrite framboids and their development: a new conceptual mechanism. Geol Rundsch. 1993; 82: 148-156.

Sawlowicz Z, Kaye TG. Replacement of iron sulphides by oxides in the dinosaur bone from the Lance Fm. (Wyoming, USA) – preliminary study. Min. Pol. Spec. Pap. 2006; 29, 184-187.

Schiffbauer JD, Xiao S, Cai Y, Wallace AF, Hua H, Hunter J. A unifying model for Neoproterozoic–Palaeozoic exceptional fossil preservation through pyritization and carbonaceous compression. Nat Commun. 2014; 5: 5754. doi: 10.1038/ncomms6754.

Schwark L. Exceptional preservation of microbial lipids in Paleozoic to Mesoproterozoic sediments. Geology. 2013; 41: 287-288.

Seilacher A, Reif W-E, Westphal F. Sedimentological, ecological and temporal patterns of fossil lagerstätten. Philos Trans R Soc Lond B Biol Sci. 1985; 311: 5-23.

Šípková A, Száková J, Tlustoš P. Affinity of Selected Elements to Individual Fractions of Soil Organic Matter. Water, Air & Soil Pollution. 2013; 225: 1802.

Skei JM. Formation of framboidal iron sulfide in the water of a permanently anoxic fjord-Framvaren, South Norway. Mar Chem. 1988; 23: 345-352.

Soares LPCM, Kerber BB, Osés GL, de Oliveira AM, Pacheco MLAF. Paleobiologia e evolução: o potencial do registro fossilífero brasileiro. R Esp. 2013; 2: 24-40.

Szczepanik P, Sawłowicz Z, Bak M. Pyrite framboids in pyritized radiolarian skeletons (Mid-Cretaceous of the Pieniny Klippen Belt, Western Carpathians, Poland). An Soc Geol Pol. 2004; 74: 35–41.

Toporski JKW, Steele A, Westall F, Avci R, Martill DM, McKay DS. Morphologic and spectral investigation of exceptionally well-preserved bacterial biofilms from the Oligocene Enspel formation, Germany. Geochim Cosmochim Acta. 2002; 66: 1773–1791.

Viana MS, Neumann VH. O Membro Crato da Formação Santana: riquíssimo registro de fauna e flora do Cretáceo. In: Schobbenhaus C, Campos DA, Qeiroz ET, Winge M, Berbert-Born MLC, editors. Sítios geológicos e paleontológicos do brasil, 5. Departamento Nacional da Produção Mineral/Companhia de Pesquisa de Recursos Minerais/Comissão Brasileira de Sítios Geológicos e Paleobiológicos; 2000. pp. 113-120.

Wang B, Zhao F, Zhang H, Fang Y, Zheng D. Widespread pyritization of insects in the early Cretaceous Jehol biota. Palaios. 2012; 27: 707-711.

Westall F, de Vries ST, Nijman W, Rouchon V, Orberger B, Pearson V, et al. The 3.466 Ga ‘Kitty’s Gap Chert,’ an early Archean microbial ecosystem. Geol Soc Am Spec Pap. 2006; 405: 105–131.

Wilby PR, Briggs DEG, Bernier P, Gaillard C. Role of microbial mats in the fossilization of soft tissues. Geology. 1996; 24 (9): 787-790.

6. Article "Deciphering pyritization-kerogenization gradient for fish soft-tissue preservation".

Deciphering pyritization-kerogenization gradient for fish soft-tissue preservation

Gabriel L. Osés*[1], Setembrino Petri[1], Cibele G. Voltani[2], Gustavo M. E. M. Prado[1], Douglas Galante[3], Marcia A. Rizzutto[4], Isaac D. Rudnitzki[5], Evandro P. da Silva[6], Fabio Rodrigues[6], Elidiane C. Rangel[7], Paula A. Sucerquia[8], M. L. A. F. Pacheco[9]

[1]Instituto de Geociências, Universidade de São Paulo - Rua do Lago 562, 05508080, Cidade Universitária, São Paulo-SP, Brazil - E-mail: gabriel.oses@usp.br, spetri@usp.br, gustavo.dino@gmail.com.

[2]Instituto de Geociências e Ciências Exatas, Universidade Estadual Paulista – Avenida 24A 1515, 13506900, Rio Claro-SP, Brazil - E-mail: voltani@rc.unesp.br.

[3]Laboratório Nacional de Luz Síncrotron – Rua Giuseppe Maximo Scolfaro 10.000, 13083-970, Campinas-SP, Brazil - E-mail: douglas.galante@lnls.br.

[4]Instituto de Física, Universidade de São Paulo - Rua do Matão 1371, 05508090, Cidade Universitária, São Paulo-SP, Brazil - E-mail: rizzutto@if.usp.br.

[5]Instituto de Astronomia, Geofísica e Ciências Atmosféricas, Universidade de São Paulo - Rua do Matão 1226, 05508090, Cidade Universitária, São Paulo-SP, Brazil - E-mail: idrgeo@gmail.com.

[6]Instituto de Química, Universidade de São Paulo – Avenida Prof. Lineu Prestes 748, 05508080, Cidade Universitária, São Paulo-SP, Brazil - E-mail: evandro.pereira.silva@usp.br, farod@iq.usp.br.

[7]Laboratório de Plasmas Tecnológicos, Universidade Estadual Paulista – Avenida Três de Março 511, 18087-180, Sorocaba-SP, Brazil - E-mail: elidiane@sorocaba.unesp.br.

[8]Departamento de Geologia, Universidade Federal de Pernambuco - Avenida Acadêmico Hélio Ramos s/n, 50740530, Cidade Universitária, Recife-PE, Brazil - E-mail: psucerquia@gmail.com.

[9]Departamento de Biologia, Universidade Federal de São Carlos – Rodovia João Leme dos Santos, Km 110, 18052780, Sorocaba-SP, Brazil - E-mail: forancelli.ufscar@gmail.com.

Abstract

Soft-tissue preservation provides palaeobiological information otherwise lost during fossilization. In Brazil, the Early Cretaceous Santana Formation has fishes with integument, muscles, connective tissues, and eyes still preserved. Thin-section petrography, geochemistry, and electron microscopy have been employed to test if such labile structures are the result of distinct palaeoenvironment-controlled pathways. Our study reveals that soft-tissues were pyritized or kerogenized in different facies, yielding distinct preservational fidelities. Indeed, new data provide the first record so far of vertebrate pyritized muscles and eyes. We propose that distinct sedimentation rates yielded two different facies in which buried carcasses underwent varied residence times in sulphate-reduction and methanogenesis zones, thus yielding pyritized or kerogenized soft-tissues, as suggested by Ediacaran fossil preservation.

Introduction

Exceptionally preserved fossils register palaeobiological novelties not encountered elsewhere in the geological record. Most questions can be answered through soft-tissue investigation in the so called Konservat-Lagerstätten[1]. Among these deposits, the Mesozoic rocks from the Santana Formation (Araripe Basin, north-east Brazil) stand out for their unique fossil content, often exquisitely preserved[2].

The Crato Member (Supplementary Figure 1) records fossils that make it one of the Early Cretaceous most diversified palaeontological deposit. The vertebrate occurrences include pterosaurs, anurans, turtles, birds, among others[2], with soft-tissue preservation[3,4]. Regarding fishes, *Dastible crandalli* (Supplementary Note 1) is the most abundant, occurring throughout the entire unit. However, its palaeoecology is still controversial. Despite that previous studies have briefly assessed taphonomic aspects[5], several issues remain undebated. For instance, specimens with black carbonaceous and orange iron oxide/hydroxide soft-tissues are commonly found, respectively in grey (GL) and beige (BL) limestones. Previous works on insect preservation have claimed this preservational difference is due to rock weathering[2], which is not supported by our evidence concerning fishes.

Here, we hypothesize that fishes have followed distinct preservational pathways, according to palaeoenvironmental/facies variation. To test this hypothesis, we present independent lines of evidence, including thin-section light microscopy, as well as

geochemical and electron microscopy analyzes. The results reveal that fishes have been either pyritized or kerogenized. We propose that sedimentation rates have varied in regard to distinct facies, implying different carcass residence-time either in sulphate-reduction (SR) or methanogenesis sedimentary microbial zones, resulting in both different taphonomic pathways and preservational fidelities. Hence, we suggest that the Crato Member fish fossilization can be interpreted by the kerogenization-pyritization gradient model for Neoproterozoic-Paleozoic metazoan preservation[6].

Results

Fishes from BL present P concentrated in bones, while Ca is dominant in bones and in carbonate matrix (Fig. 1a,b). A high abundance of P and Ca in decayed soft-tissue area is explained by the presence of ribs in this region. It was also possible to measure Pb correlated to the fossil as well as minor signals of S and metals that are commonly chelated by organic matter such as Fe, Cu, and Zn along soft-tissue regions (Fig. 1b).

A BL fish has calcite-filled ($CaCO_3$) bone cavities, hydroxyapatite ($Ca_5(PO_4)_3(OH)$) in bones, and goethite ($FeO(OH)$) replacing soft-tissues surrounding vertebrae (Fig. 1d,e and Supplementary Figures 2 and 3). These results support EDXRF data. The same bone composition is confirmed for fish preserved in GL (Figs. 1f-h, Fig. 2a,b). In contrast, soft-tissues are composed of C and S, revealing that they are carbonaceous (Fig. 1h). Furthermore, Mn is abundant in both matrix and cement (Supplementary Figure 4), Fe and Cu are more concentrated in soft-tissue regions (Fig. 2a-c), and Zn is more concentrated in bones (Fig. 2a,d).

In the carbonaceous fish, distinct cement types do occur (Supplementary Figure 5). Moreover, soft-tissues consist of a thick hard dark material, which occur consistently along the body (Fig. 1f). Almost every bone, in cross-section, is enveloped by dark opaque amorphous to sinuous laminated material with alternating light/dark bands, locally convoluted (Fig. 2e-g), composed of fibres (Fig. 2f,g). Sometimes, black, beige, brown, and green bands alternate yielding a fibrous aspect (Fig. 2h,i). We interpret these features as preserved soft-tissue with muscle fibres (cells). In some regions, both soft-tissues and bones present a degraded aspect (Fig. 2j). Carbonaceous fibres are poorly preserved and have no discernible microfabrics (Fig. 2k).

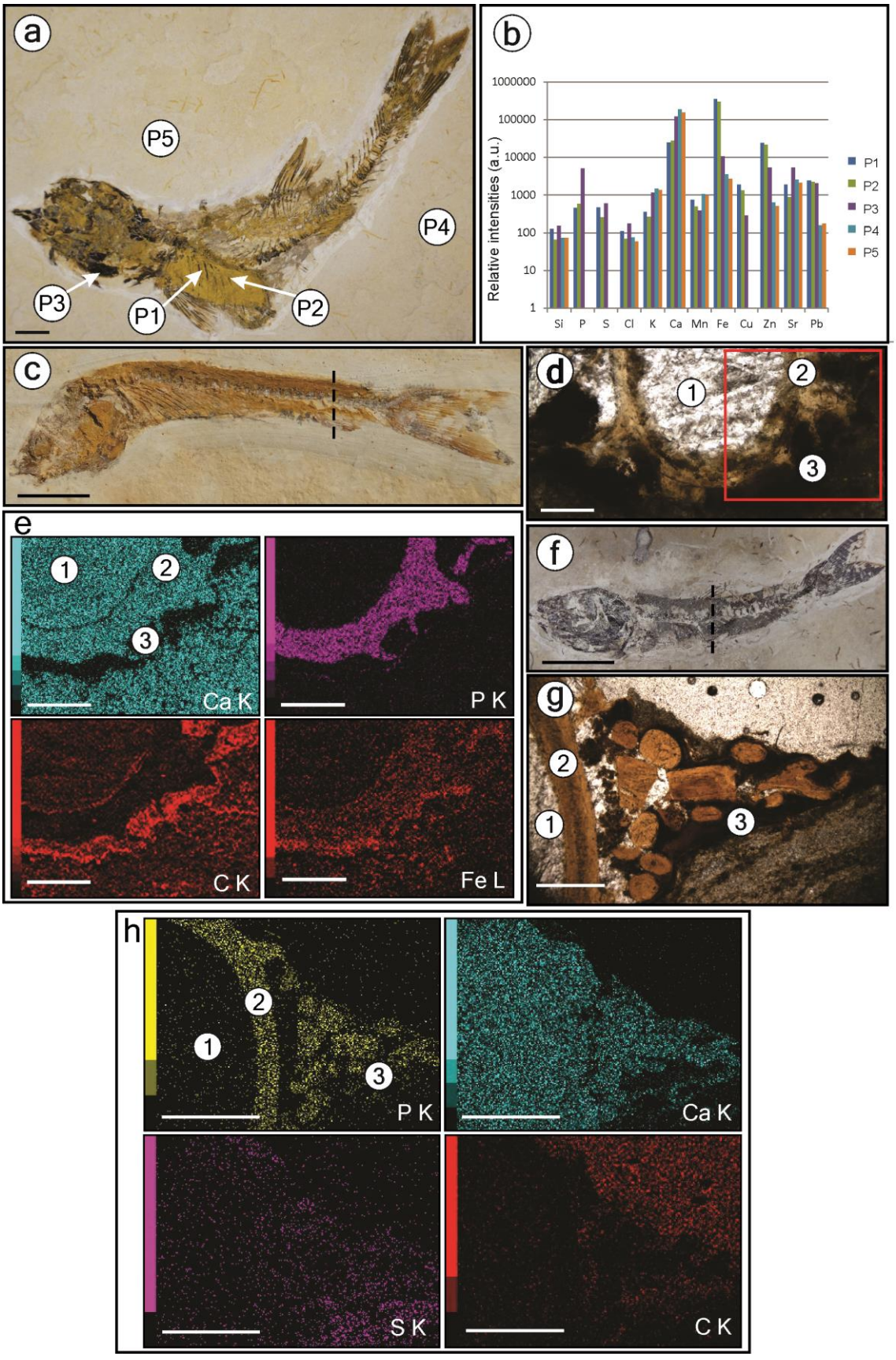
a
P5
P4
P3
P1
P2
b
Relative intensities (a.u.)
1000000
100000
10000
1000
100
10
1
Si P S Cl K Ca Mn Fe Cu Zn Sr Pb
P1
P2
P3
P4
P5
c
d
1
2
3
e
1
2
3
Ca K
P K
C K
Fe L
f
g
1
2
3
h
1
2
3
P K
Ca K
S K
C K

Figure 1. Geochemistry of the Crato Member fossil fishes. a, Specimen GP/2E 9014 from BL with points (P1, P2 – decayed soft-tissue area; P3 – bones; P4, P5 – matrix) analyzed in **b**. **b**, EDXRF results of the selected points in fossil depicted in **a**. **c**, Fossil GP/2E 7781g. The dashed line indicates the approximate direction of thin section in **d**. **d**, Thin section (GP/L 20) of specimen in **c** depicting calcite cement filling vertebrae (1), vertebrae (2), and soft-tissues (3) around vertebrae. The red square delimits the area analyzed in **e**. **e**, Energy dispersive X-ray (EDS) maps of several elements distributed among the three main regions (1-3) in **d**. **f**, Specimen GP/2E 9666 from grey limestones (GL). The approximate direction of thin section (in **g**) extraction is marked by dashed line. **g**, Thin section (GP/L 16) of specimen in **f** showing calcite cement (1), vertebrae (2), soft- tissues (3). **h**, EDS maps of elemental distribution over areas (1-4) selected in **g**. Scale bars: **a** – 1 cm; **c** – 0.5 cm; **d** – 0.1 mm; **e** – 0.1 mm; **f** – 1.5 cm; **g** – 0.5 mm; **h** – 1 mm.

Some regions possess a vesicle texture, formed by bodies of various shapes (Fig. 2l,m). They are locally oriented in a curved fashion, yielding apparently round pockets. These bodies resemble muscle fibres in cross-section[7]. They are surrounded by a light matrix resembling endomysium (i.e. collagenous connective tissue). The pockets can be interpreted as fascicles (i.e. muscle bundles), separated by something like perimysium, which is also a connective tissue of muscle fibres. Although these are rarely preserved in the fossil record, their presence can open new avenues for physiological research, including insights into muscular functions. Locally, the outer fish margin is outlined by broken scales interlayered with calcite and labile-tissue that we interpret as carbonaceous skin (Fig. 2n,o). Integument preservation (Supplementary Note 2) yields evolutionary, physiological, and palaeoecological information[8].

Patches of orange amorphous Fe oxide/hydroxide material are commonly seen in BL fossils (Fig. 1c). Most rarely, these regions have 3D muscle fibres already reported elsewhere[5]. Fibres are sometimes fragmented and locally degraded, which is likely to be the effect of decay (Fig. 3a). Sometimes gaps between fibres occur, being occupied by wide elongated flat soft structures interpreted as sarcolemma (i.e. muscle cell membrane; Fig. 3a,b). Such gaps have likely resulted from decay and dehydration/shrinkage of sarcolemma during fossilization. These hypotheses are

strengthened by the presence of sarcolemma in other orientations either than of fibre length, as reported elsewhere[9]. Some samples have fibres subparallel to the vertebral column, arranged in myomeres that are connected to the dorsal column area (Fig. 3c,d). Some fibres possess putative cell nuclei (Fig. 3d).

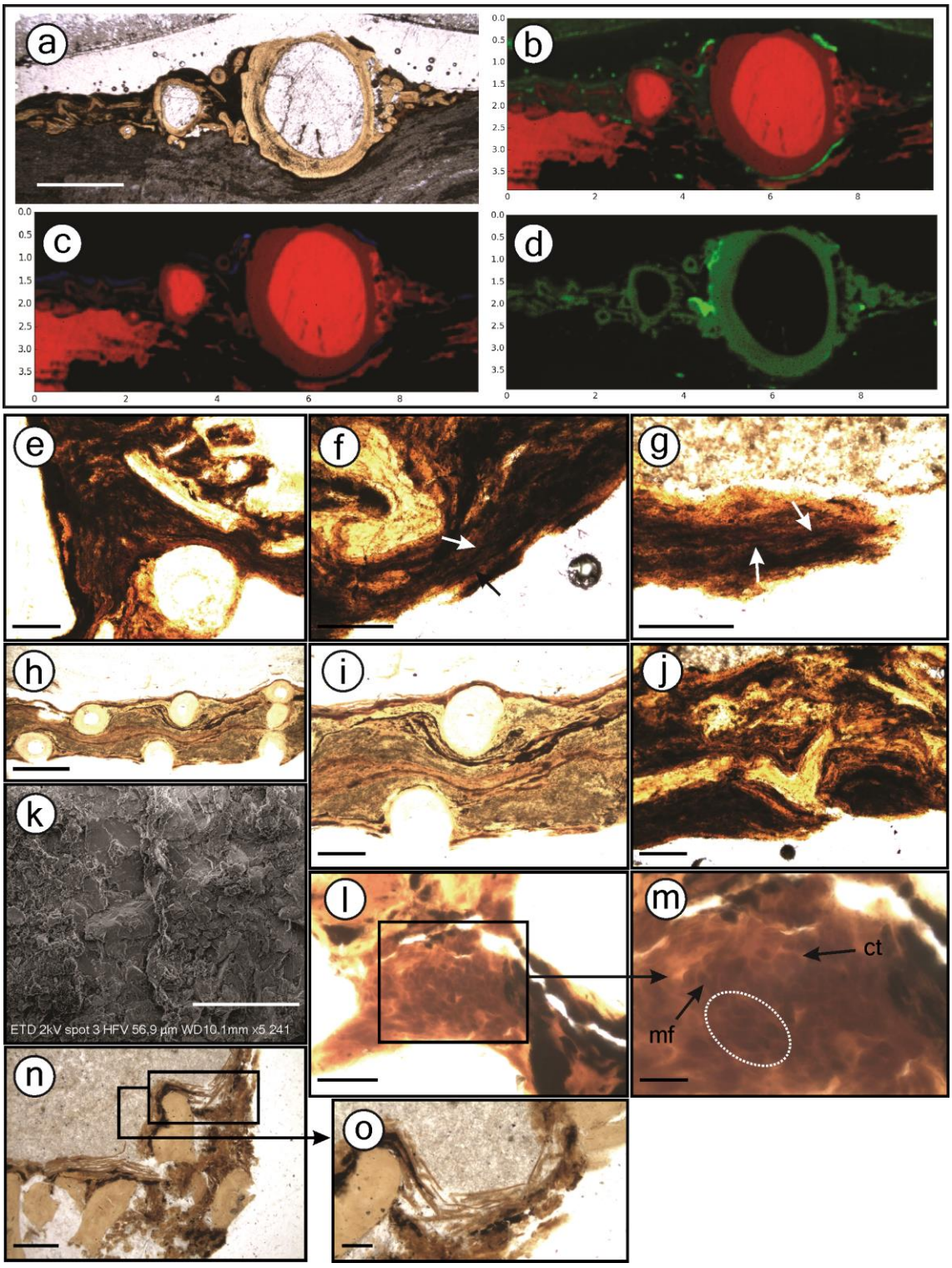

Figure 2. SR-µXRF maps, thin section images and SEM of fish (Fig. 1f) with preserved carbonaceous soft-tissues. a, Area mapped by SR-µXRF of the thin section GP/L 16. **b**-**d**, SR-µXRF maps. **b**, Ca – red, Fe – green. **c**, Ca – red, Cu – blue. **d**, Zn. Colour brightness is proportional to element concentration, and both map horizontal and vertical scale axes are in mm. Elemental maps of all elements (except for Zn) are in Supplementary Figure 4. Thin sections GP/L 16 (**e**-**g**, **j**) and GP/L 17 (**h**, **i**, **l**-**o**). Dark opaque sinuous laminated, locally convolute muscle tissues (**e**-**g**), composed of alternating, differently coloured light/dark bands (**h**, **i**). Muscle tissue is composed of dark fibres (**f**, **g**; arrows). **j**, Degraded soft-tissues and bones. **k**, SEM micrograph of muscle fibre detail. **l**,**m**, Muscle fibres (mf) in cross-section, depicting endomysium/perimysium-like connective tissues (ct) and muscle bundles (dashed ellipsis). **n**,**o**, Scales are interlayered with soft-tissues (black) and calcite cement. Scale bars: **e**-**g**, **i**, **j**, **n**, **o** – 0.2 mm; **h** – 0.5 mm; **k** – 20 µm; **l** – 0.1 mm; **m** – 0.02 mm.

We compared soft-tissues in distinct locations (Supplementary Figure 7). In the caudal fin base, fibres possess barely visible margins and are almost indistinguishable from each other (Fig. 3e). Fibres are composed of Fe oxide/hydroxide sub-spherical to spherical grains larger than 1 µm, locally merged and covered by a "fuzzy" coating (Fig. 3f,g). These grains replace muscles of the entire specimen. Similar grains, but smaller than 1 µm, are scattered within pores among larger grains (Fig. 3f). Furthermore, sometimes Fe oxide/hydroxide honeycomb-like texture formed by hollow spaces with subhedral to euhedral shape can be seen (Fig. 3g). We consider that the grains of up to 1 µm have likely filled those spaces, and have possibly been released after weathering oxidation[10]. The dorsal fin area depicts muscles arranged in layers along the specimen's depth, revealing how muscles are attached to the fin base and the way these muscles connect to those that run along/around the column (Fig. 3h). Micrographs of fish anteroposterior axis details muscular insertion to vertebrae surface (including tendons attaching muscles to bones), multiple stages of muscle decay around vertebra (Fig. 4a), and confirms fibre microfabric (Fig. 4b,c). These observations challenge previous analysis, which claimed that fibres are rather indistinct[5]. Furthermore, eye area is also preserved by Fe oxide/hydroxide microfabrics (Fig. 4d,e).

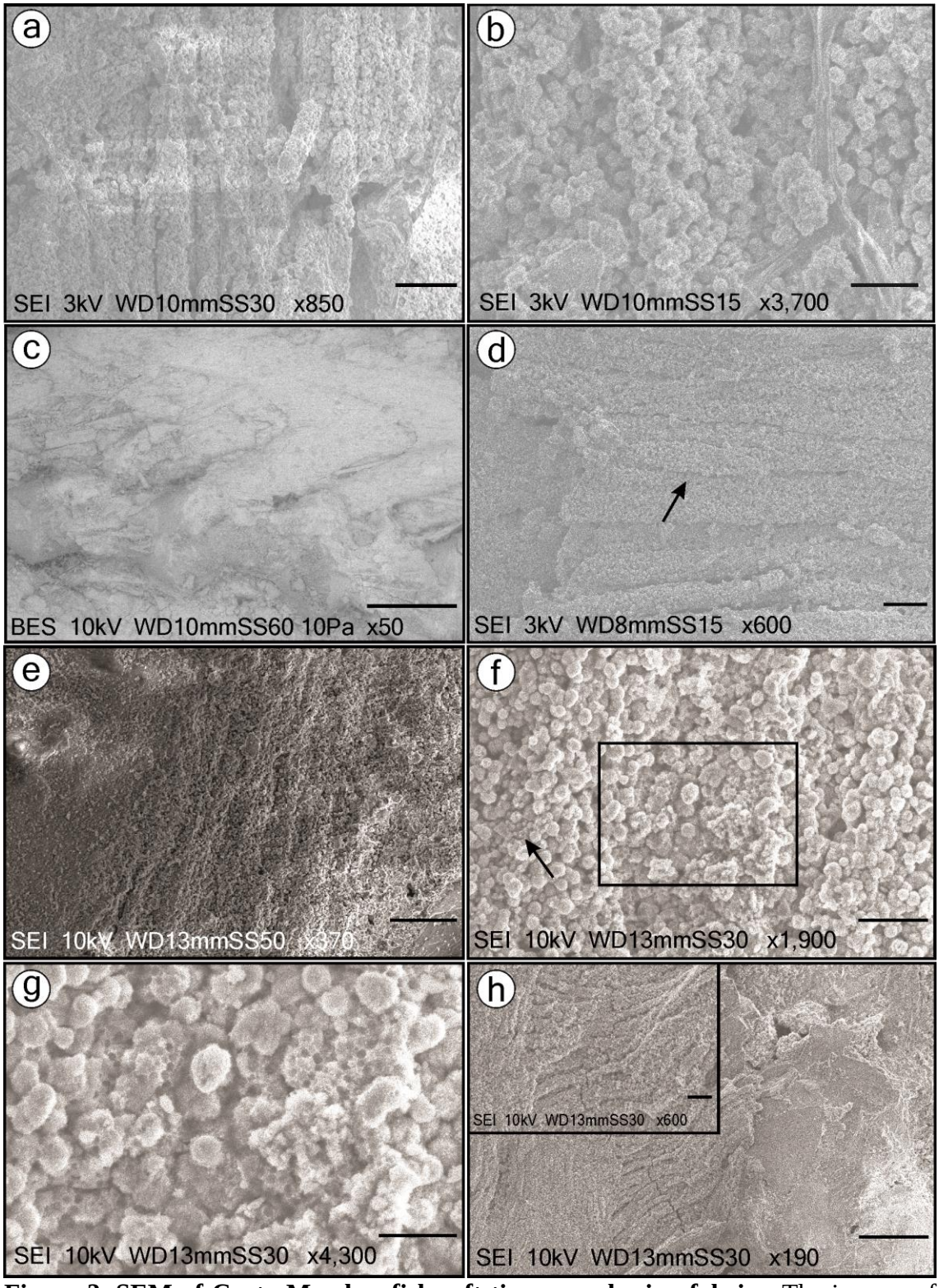

Figure 3. SEM of Crato Member fish soft-tissues and microfabrics. The images of specimens analyzed, and the localization of micrographs are depicted in Supplementary Figures 6 and 7. **a** depicts fragmented and locally excavated muscle fibres subparallel to vertebral column. Gaps between fibres are occupied by wide elongated flat soft-structures (sarcolemma), which also have orientations different from fibres. **b**, Detail of

sarcolemma. **c** shows myomeres with muscle fibres (Supplementary Figure 6). **d**, Possible nucleus (arrow). **e** depicts poorly-preserved muscle fibres, like diagonal ridges, at caudal fin base (Supplementary Figure 7). **f** shows that fibres are composed of Fe oxide/hydroxide (Supplementary Figure 2) sub-spherical to spherical grains with more than 1 µm (and occasionally less than this size, indicated by arrow), locally merged and covered by a "fuzzy" coating. The area highlighted in **f**, enlarged in **g**, depicts Fe oxide/hydroxide honeycomb-like texture (Supplementary Figure 2). **h**, Micrograph showing how muscles are attached to dorsal fin base *via* tendons and the way these muscles connect to those sub-parallel to column (Supplementary Figure 7). Inset details these observations. Microfabric composition is depicted in Supplementary Figure 2. Scale bars: **a**, **d**, inset in **h** – 20 µm; **b**, **g** – 5 µm; **c** – 500 µm; **e** – 50 µm; **f** – 10 µm; **h** – 100 µm.

In a BL fish, we identified a ribbon-like smooth structure with pliable aspect, shaping itself according to the microfabric relief underneath, resembling bacterially secreted extracellular polymeric substances (EPS; Fig. 4f). Indeed, it is richer in carbon content than microfabric (Supplementary Figure 2). Similar structures have been found in Crato insects[11]. In one specimen, we observed spherical spaces resembling external moulds of melanosomes, which will undergo further investigation.

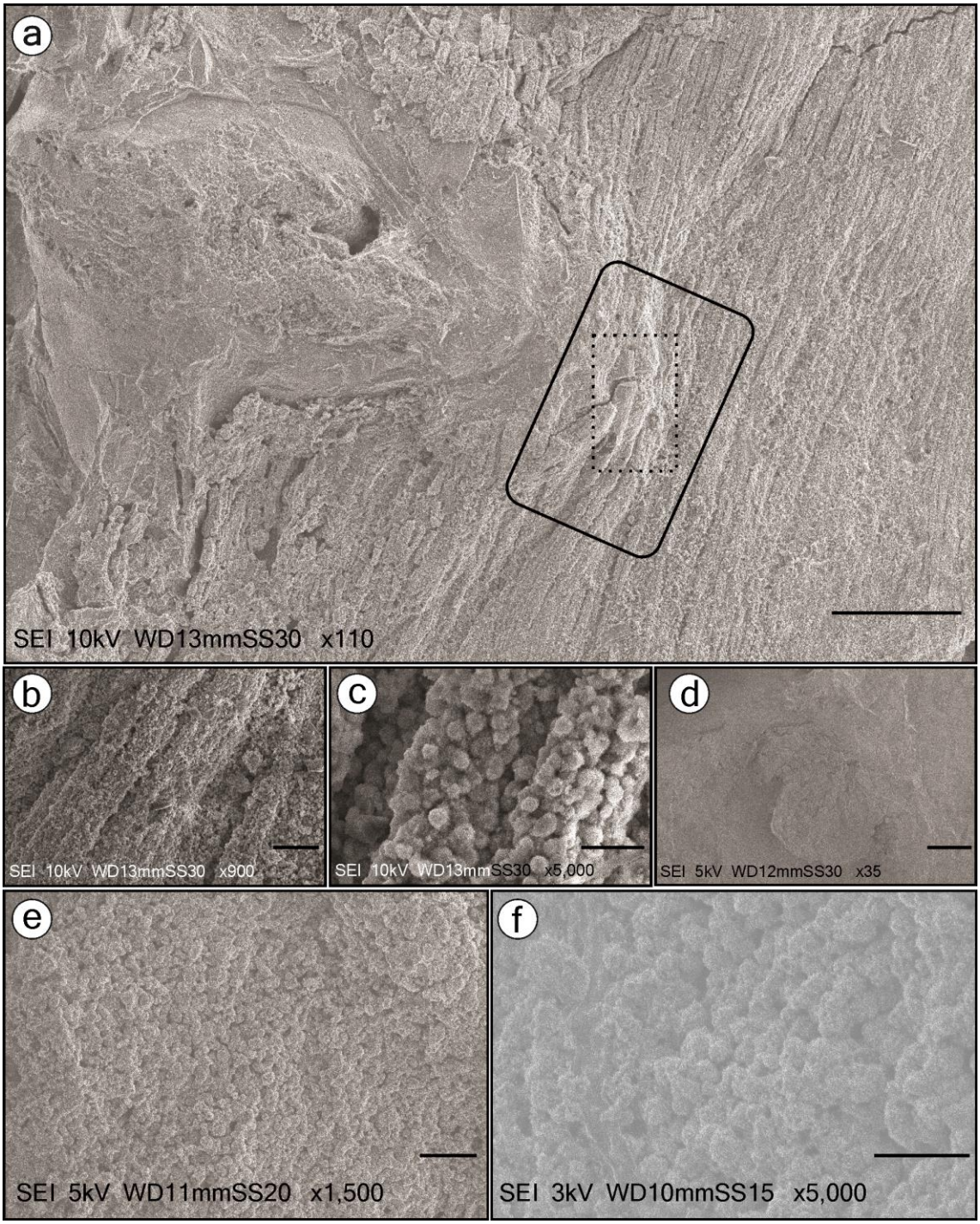

Figure 4. SEM of Crato Member fish soft-tissues, microfabrics and putative extracellular polymeric substances (EPS). The images of analyzed specimens, and the localization of micrographs are depicted in Supplementary Figures 7 and 8. **a-c**, Micrographs of fish anteroposterior axis (below dorsal fin; Supplementary Figure 7). Images reveal how muscles attach to vertebra (**a**), revealing preserved tendons (dashed rectangle in **a**), and muscles connected to tendons (big rectangle in **a**). **b**, **c** depict fibre microfabric (Supplementary Figure 2). **d** depicts eye preserved soft-tissues

(Supplementary Figure 8). **e** shows eye microfabric. **f**, Putative EPS covering grains (Supplementary Figure 9) in left half. Scale bars: **a** – 100 µm; **b** – 20 µm; **c** – 5 µm; **d** – 500 µm; **e** – 10 µm; **f** – 5 µm.

In Nova Olinda quarries, BL overlie GL[12,13]. BL have thin laminations (ca. 0.5 mm) of dark clay interlaminated with pale pure microspar laminae (Fig. 5a,c). Organic matter-rich dark lenses[14] are indistinctly scattered. BL microfacies most likely correspond to laminated limestones (LL)[15]. GL are composed of 1-3 mm thick layers[15]. Undulated dark-grey laminations rich in pyrite crystals[13] present fine blackish material (likely to be clay/organic matter impurities[13,15]), and sometimes peloids (Fig. 5b,d-g). Such laminations are interlaminated with paler microspar-dominated layers, including neomorphic sparry anhedral crystals[15]. GL facies is here interpreted as Sm1 microfacies (clay-carbonate rythmite, CCR), which has microfaults[15] (Supplementary Figure 5).

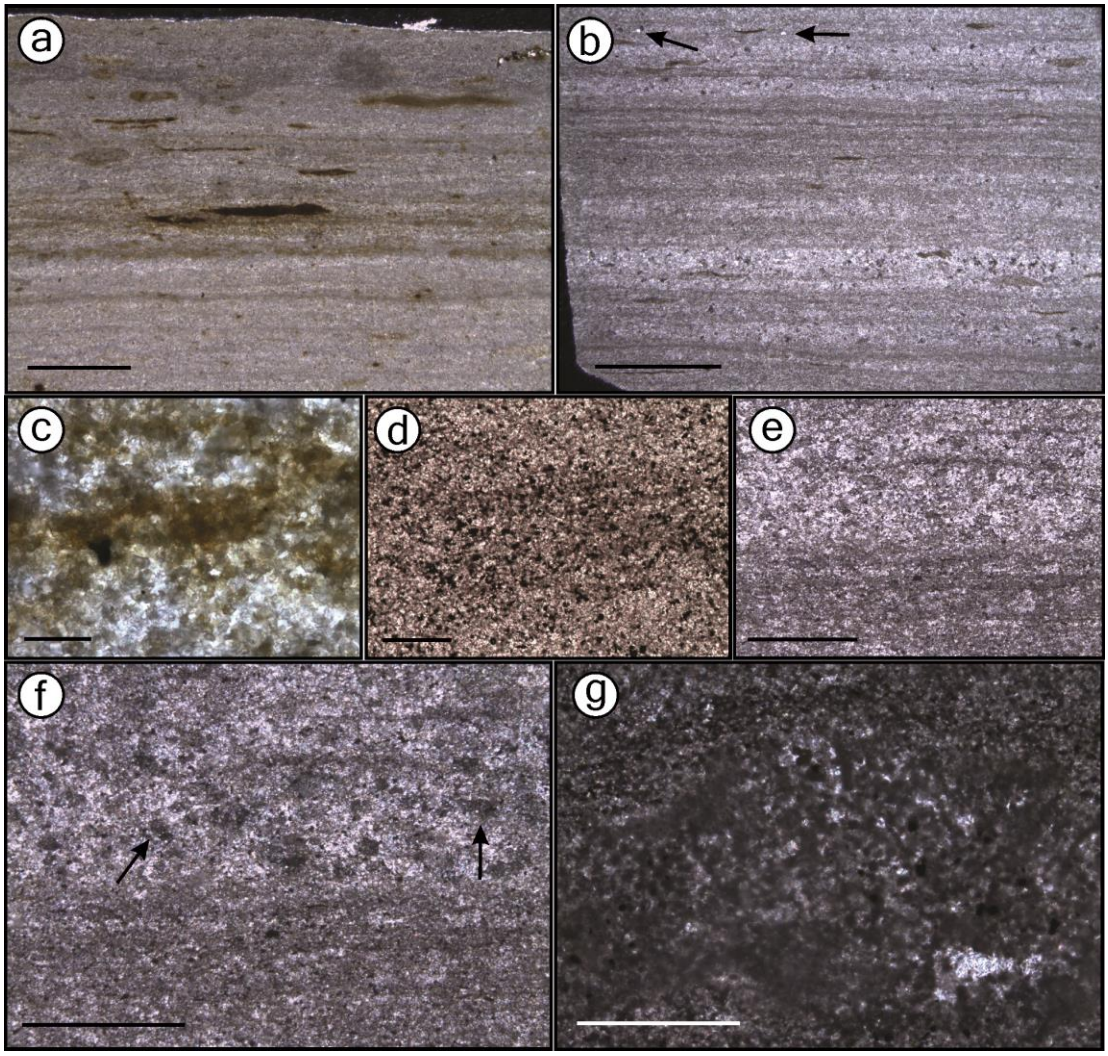

Figure 5. Thin sections of the beige limestone (BL) and the grey limestone (GL) microfacies. Thin sections GP/L 21 (**a**, **d**), GP/L 19 (**b**), GP/L 18 (**g**), GP/L 172 (**c**), and GP/L 16 (**e**, **f**). **a**, BL is composed of thin laminasets of diffuse dark clay laminae (detail in **c**), interlaminated with pale pure microspar laminae. Elongated dark to rounded organic matter-rich dark lenses[14] are indistinctly scattered. This facies is interpreted as the laminated limestone (LL) Sm5 microfacies[15]. **b**, GL is composed of dark-grey undulated laminasets formed by thin laminae with fine blackish scattered material, likely clay/organic matter impurities[13,15] (detail in **d**). Laminasets are interlaminated with paler microspar-dominated laminae. Scattered non-oriented detrital quartz is indicated by arrow. GL microfacies is interpreted as Sm1, a clay-carbonate rythmite (CCR)[15]. Besides GL having significantly fewer dark lenses than BL, the clay/organic matter-rich laminasets are more frequent, regularly distributed, thicker and have more and closer-packed laminae. **c**, Detail of BL dark laminae. **d**, Detail of GL dark laminae, showing concentration of pyrite[13]. **e**, Thin section of GL depicting microspar-dominated level (top) and clay-rich laminaset (bottom). **f**, Image in **e** with crossed-nicols showing neomorphic sparry crystals (arrows). **g**, GL clay-rich level with peloids. Scale bars: **a** – 1 mm; **b** – 2 mm; **c** – 0.02 mm; **d** – 0.1 mm; **e** – 0.5 mm; **f** – 0.5 mm; **g** – 0. 2 mm.

Discussion

Pyritized Fishes

In BL, the concentration of P together with Ca in bones, indicates that original hydroxyapatite is probably unaltered. Fe dominance in soft-tissues reflects iron oxides/hydroxides concentrated in these regions. Thus, the presence of S can be explained by sulphate resulting from pyrite oxidation. Arthropods in BL occur as hematite/goethite replacements after pyrite[11]. Similarly, we consider that fish soft-tissues in BL were originally preserved by pyrite, later oxidized[16], as previously suggested[5]. Microfabrics are composed of Fe oxide/hydroxide sub-spherical to spherical grains, which we interpret as framboidal pyrite pseudomorphs[17]. However, the fuzzy coating makes it difficult to assess whether grains are composed of microcrysts and their characteristics. Nevertheless, this composition is strengthened by the honeycomb-like texture that resembles framboids. Regarding the hollow spaces (formerly

microcryst filled), their morphology, size, and organization are regular[17]. The sphericity variation plus microcryst size/morphology depend on the framboid formation steps: nucleation/growth of iron monosulphides (mackinawite), transition to greigite, aggregation of greigite microcrystals, and conversion to pyrite[17], although greigite is not always required[18]. Size variation might reflect redox conditions, which influence framboid growth[19]. Framboids formed within H_2S rich waters are smaller (< 10 μm) than those from oxic/dysoxic basins (> 10 μm)[19]. The former seems to be our case, although caution must be taken into consideration in such interpretations[20]. Additionally, the observed framboid size variation requires variable pyrite nucleation rates and iron/sulphate diffusion balance over time[6,16,18]. Initially, labile-tissue high decay rates yield pyrite supersaturation, inducing nucleation, favouring framboid precipitation (high Eh)[18]. This diminishes organic matter availability for SRB over time, decreasing framboidal pyrite nucleation rates and, thus, sulphide fuels crystal growth[6], as suggested for the Eocene London Clay plants[21] and Cambrian animals[16].

Iron monosulphides nucleate due to sulphide supersaturation favoured by organic matter[17]. Indeed, framboids have been widely associated to decay[22,23] and researchers demonstrated the role of biofilms for framboid development[20,24]. Framboidal pyrite is found replacing Crato Member insects, which was interpreted as bacterially induced mineralization[11]. Framboidal pyrite is also ubiquitous in other Konservat-Lagerstätten[16,25,26]. Moreover, high abundance of Cu, Zn, and Pb in fish labile-tissues suggests microbial activity[27,28]. This condition may also reflect the incorporation of these metals into pyrite, which is favoured by high pyrite precipitation mainly in anoxic-sulphidic environments[29]. This is consistent with fish microfabrics and elemental sedimentary availability, supported by trace metal occurrence in the matrix (Fig. 1b). Taken together with geochemical and mineralogical evidence, putative EPS also point to bacterially-induced pyrite production. It is noteworthy that pyritization has occurred during lacustrine carbonate deposition, considering that sulphate is depleted in freshwater systems[30]. Pyritization is commonly recorded in siliciclastic marine deposits[16,25,31,32], and subordinately terrigenous lacustrine settings[33], from oxic[25,31,34] to dysoxic/anoxic[33] water columns.

Soft-tissue preservation depends mainly on early diagenetic authigenic mineralization[35] during anaerobic decay, when geochemical gradients[36] and chemical reactions involving several oxidants yield C_{org} mineralization[35]. However, pyritization

requires special conditions[37]. In this context, labile-tissues worked as C_{org} source for pyritization, while sediment provided iron and sulphate. Regarding palaeolake water column O_2 stratification[2,14,38], anoxic bottom waters yielded an either shallow or absent oxic zone with prevailing aerobic decay[34] and, thus, shallow bacterial iron/sulphate-reduction zones[39]. Shallow SRZ also have high iron concentrations, which enhances SR and pyritization[37]. At C_{org} decay sites, hydrogen sulphide (H_2S) is formed and subsequently fixed by Fe^{2+} through iron-monosulphide (FeS) formation, a process which occurs in sulphide-poor, Fe-rich porewaters[37], and widely explains pyritization[25,31]. In fact, gypsum, a possible sulphate source, does not occur in planar laminated microfacies[14], which we regard as BL. Therefore, muscles have likely provided intense SR, which must be high in non-marine settings to provide pyritization[37]. Indeed, less degraded C_{org} yields high sulphate-reduction rates[40]. Furthermore, sedimentary organic matter is low in BL, possibly owing to oxidation caused by bottom spells of freshwater[14], or by water stratification[41]. Otherwise, pyritization would have been widespread hindering fish mineralization[35], as proposed for the exceptional preservation at Ordovician Beecher's Trilobite Bed[31], Devonian Hunsrück Slate[25], and Cambrian Chengjiang Biota[16]. Anyway, the lack of scavengers and burrowers, owing to water column stratification, favoured exceptional preservation[2].

We observed that, in the same specimen, some regions have framboids not associated with soft-tissues whereas other regions have 3D muscles, particularly central trunk muscles surrounding the dorsal portion of the vertebral column, which is indeed the least decay-prone fish segment[42]. Myosepta (i.e. collagen boundary between myomeres) has not been preserved in our samples. Moreover, some fishes have fibres organized in myomeres, while others have non-organized muscle fibres, revealing a preservational gradient. Taphonomic experiments carried out on amphioxus, lampreys, and fishes have showed that ventral myomere portion is lost before dorsal one, and gaps develop between myomeres as they shrink after 6 decay-days[42] (Supplementary Figure 6). Interestingly, some specimens with good muscle fibre preservation have evidence for integument rupture (Supplementary Figure 6; Supplementary Note 2), which should have enhanced SRB and sulphate and Fe entrance within carcasses, followed by pyritization. In addition, preserved area extension and preservational fidelity are usually higher in smaller specimens, while bigger ones have only very localized poor soft-tissue preservation. This pattern is expected as smaller carcasses are more readily pyritized

owing to the following factors: iron and sulphate required contents are lower; and fixation of sulphide by iron[37] is faster owing to lower H_2S production due to the already lower amount of decay-prone organic matter. Regarding eye preservation, the lens (which seems to be present in our specimen) is the least decay-prone eye structure, lasting more than 300 days under decay, as revealed by taphonomic experiments on lampreys[42].

Surprisingly, fish muscles are not phosphatized. Since fish soft-tissues are usually preserved by substrate microfabrics, phosphate crystals grow directly in decay sites, requiring high readily phosphate contents from external sources[9,30]. Therefore the lack of phosphatized tissues can be explained by three main factors. Firstly, as already mentioned, BL has low C_{org} and associated phosphate accumulation[30,35], which controls mineralization[36] preventing enough phosphate accumulation to inhibit calcite formation[30]. Secondly, phosphatization is enhanced at Ca-depleted continental basins[43], which is not the case of the Crato palaeolake. Finally, high phosphate concentration buffers sulphide genesis[36], so it must have been low to enable pyritization. Interestingly, Crato Member pterosaur phosphatized soft-tissues[3] suggest that this process was taxon-controlled and localized in certain tissues, though palaeoenvironmental influence cannot be discarded.

Kerogenized Fishes

We consider that GL fish carbonaceous soft-tissues underwent kerogenization[44], evidenced by soft-tissue black colour, C composition[16], lack of microfabrics, and isotropy at crossed nicols[44]. Moreover, micro-Raman data reveal D and G bands of disordered carbon (Supplementary Figure 3), here considered kerogen since the association of the carbonaceous material to a well-known biogenic source and the low thermal imprint in the Crato unit[38] make other processes of disordered carbonaceous material genesis[45] very unlikely.

Cement filled vertebrae and inter-bone gaps have Mn concentration, just like matrix, revealing cement composition is either derived from matrix dissolution-reprecipitation during diagenesis and/or might reflect weathering-formed pyrolusite, which is frequently seen in Crato limestones[2]. Moreover, we interpret Zn-bone enrichment as remnant of original bone composition. As already alleged for Zn correlation to *Archaeopteryx* bones[46], Zn is highly-restricted to fish bones, thus not

showing evidence for Zn migration from surrounding sediment. Indeed, extant fish retain Zn in bones[47], which might reflect dietary availability also influencing physiological processes[48]. Furthermore, Fe and Cu are concentrated in some soft-tissue regions, in which high intensities of both elements are usually correlated (Fig. 2b,c). Regarding that evidence for mineralization has not been found, we interpret that Fe and Cu were incorporated to muscles during life, which is seen in extant fishes[47,49].

Preservational Model

Here, we propose some controls that have either inhibited mineralization or favoured kerogenization. Firstly, according to petrography, GL facies has likely greater organic matter/clay, further evidenced by its darker colour[50]. This more pronounced organic content accounts for both disseminated pyrite and lack of fish pervasive pyritization (as already explained), thus revealing how carcasses passed through SRZ without being extensively pyritized[6]. Nevertheless, differential C_{org} contents cannot explain kerogenization alone. Secondly, the two main mechanisms for resistant organic matter preservation[51], degradation-recondensation and selective preservation, are not sufficient to explain fish muscle preservation. However, muscle lipid free aliphatic and ester-bound molecules can origin degradation-lasting polymeric components during diagenesis, yielding kerogen. Moreover, more labile -issues undergo structural changes[52], which might account for muscle kerogenization.

A model predicting Neoproterozoic-Palaeozoic exceptional preservation by a kerogenization-pyritization gradient has been proposed[6]. This gradient is controlled by carcass residence time in distinct sediment anaerobic microbial zones[6], particularly anoxic-sulphidic (pyrite production) and non-sulphidic (methanogenesis) occurring below water-sediment interface[53,54]. Residence time is controlled by sedimentation rate. Slow rates increase residence time in SRZ yielding soft-tissue pyritization, while faster rates lead to short residence time in this zone, favouring kerogenization in methanogenesis zone[6]. Fatty acids with more than two carbons and aromatic chains are not degradable by methanogens, therefore, fermentation helps to break-up C_{org}[55]. Crato carbonate genesis had intense microbial influence, including SR bacteria and methanogens[14]. GL facies, with kerogenized fish soft-tissues, has evidence for higher terrigenous influx to the lacustrine setting (e.g. clay/organic matter levels and peloids), which increased burial rates (Fig. 6). The rounded peloids are restricted to specific

layers, suggesting that they were deposited during sedimentary pulses[50]. Alternatively, their round shape might point to *in situ* formation by microbial precipitation[50]. In fact, the variable terrigenous input has been controlled by climatic conditions (humid *versus* arid)[14,15]. Even taking that clay contribution has probably not yielded thick deposits at short intervals, the explanation above is sound. Indeed, it is known that slight depth changes (mm/cm-scale) are enough to change geochemical zones through sediment[54,56].

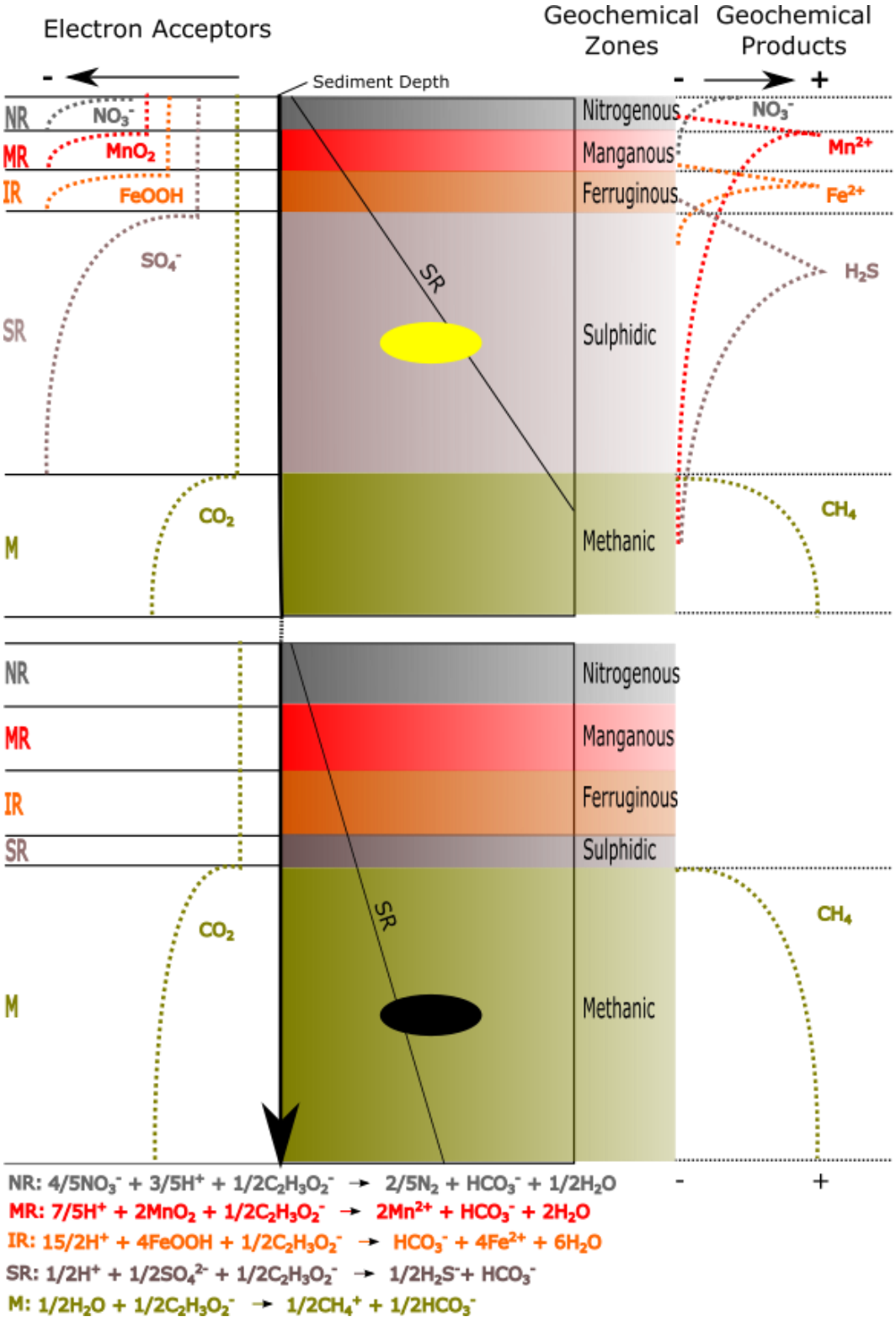

Figure 6. Taphonomic proposal for pyritization and kerogenization in the Crato Member. The upper and lower diagrams show bacterial respiration processes (NR – Nitrate Reduction, MR – Manganese Reduction, IR – Iron Reduction, SR – Sulphate Reduction, M - Methanogenesis) on the left. The correspondent reactions are seen at figure bottom. Electron acceptor curves used in these respiration processes are depicted, showing electron acceptor depletion from right to left (indicated by arrow at figure top). Sediment depth is represented by vertical arrow. Either pyritized (upper diagram) or kerogenized (lower diagram) fossils are represented by an ellipsis, located in the correspondent simplified sediment geochemical zone (sulphidic or methanic). Curves of respiration geochemical products are depicted on the right, showing increase from left to right. We propose that BL (upper diagram) has been deposited at lower sedimentation rates than GL (lower diagram) facies, as evidenced by greater terrigenous clay/organic matter content and peloid levels in GL. Variable sedimentation rates are explained by transgressive-regressive climatic cycles[15]. As a consequence, carcasses in BL have remained longer in the sulphidic zone, whereas carcasses in GL have both entered more rapidly and spent more time in the methanic zone, respectively yielding pyritized and kerogenized labile-tissues. In addition, variable cement contents in different carbonate facies[38] plus clay in GL facies could have diminished sulphate percolation downwards, narrowing the sulphidic zone. The hypotheses we propose are based on references 6, 57. Microbial respiration process zonation and reactions, geochemical zonation, plus electron acceptor and geochemical product curves are based on reference 54.

Besides the differential sedimentation rate hypothesis, Crato carbonate facies have varied cement contents[38], which altogether with clay in GL facies, possibly have diminished sulphate percolation downwards, narrowing SRZ[6]. The low microspar porosity might have enhanced this effect, also contributing to narrow other microbial zones, eliminating the need of very high sediment amounts to move carcasses through these zones. This would have led to premature sulphate exhaustion by SR, both hasting methanogenesis onset[53] and preventing sulphide migration downwards and pyrite precipitation in the methanogenesis zone[54]. This mechanism of cement-triggered bed-capping affecting sulphate diffusion has been proposed for Burgess Shale-type preservation[57]. Anyway, a sedimentological-controlled preservational-fidelity gradient

does exist since pyritization has recorded 3D muscle tissues, sarcolemma, putative cell nuclei, tendons, and eyes while kerogenization has yielded connective tissues, integument, and compressed/distorted muscle fibres.

Material and methods

We have analyzed samples and thin sections (Supplementary Table) of the fossil fish *Dastilbe crandalli*. Although the exact provenance of this material was not specified after collection, it belongs to the Crato Member (Santana Formation, Araripe Basin, north-east Brazil) and is deposited in the Palaeontological Scientific Collection of the Institute of Geosciences of the University of São Paulo (USP).

Thin sections cross-cutting rock lamination and fossils were prepared. While 30 µm-thick thin sections with cover slips were used for rock and soft-tissue description, thin sections, thicker than 30 µm (ca. 50 µm) devoid of cover slips were employed in geochemical and scanning electron microscopy analyzes. The latter present more rock volume than usual 30 µm thin sections, yielding enhanced signal for mapping[5]. We took images from thin sections in transmitted light mode.

Energy dispersive X-ray fluorescence (EDXRF) analyzes were performed in the Institute of Physics of USP (IF-USP). We used a portable equipment setup that consists of a mini Amptek X-ray tube of Ag anode and a silicon drift detector (SDD), with 125 eV FWHM for the 5.9 keV line of Mn. The measurements were carried out with 30 kV voltage and 5 µA current and with an excitation/detection time of 100 s. Data were then processed in the software WinQXAS and Microsoft Excel®. The SR-µXRF measurements were made at the XRF beamline of the Brazilian Synchrotron Light Laboratory (LNLS)[58] in micro-beam mode, using polychromatic excitation, filtered with Fe and Al foil. A KB focusing system was employed to achieve a beam size of approximately 12 x 25 µm. Mappings were made with 20 µm steps. The accumulation time was of 0.2 s per point, and acquisition was made in fly-scan mode. Control spectra were collected in both the glass slide and the glue used for thin-section preparation, as well as in untreated fossils and their host rock to ensure that fossils real data were actually being measured in thin sections. All data were treated using the PyMca software[59] for the creation of elemental concentration qualitative maps.

Soft-tissue micro-investigation was carried out by Scanning Electron Microscopy (SEM), using a JEOL JSM-6010 LA microscope and a FEI Quanta 650

FEG microscope at the Brazilian Nanotechnology National Laboratory (LNNano) and at the Laboratory of Technological Plasmas (LaPTec) of the São Paulo State University (UNESP). In order to avoid surface charging during micrograph acquisition, some samples were coated with a thin layer of gold-palladium in a DESK-V HP Cold Etch/Sputter system. We used an X-ray Dry SD Hyper (EX-94410T1L11) detector for Energy-Dispersive X-ray Spectroscopy (EDS) microanalysis. We yielded point spectra and maps of samples and thin sections, enabling the evaluation of elemental distribution among distinct fossil regions. We avoided EDS of coated samples.

Raman spectroscopy was performed both at the Research Unity in Astrobiology, Laboratory of Astrobiology (NAP/Astrobio-USP) and at the Laboratory of Molecular Spectroscopy (LEM) of the Institute of Chemistry of USP. Raman data were collected in micro mode with two different Renishaw inVia micro-Raman systems coupled to confocal light microscopes, one with 532 nm excitation laser line, and another with 785 nm excitation line. Equipment was set to provide spectral resolutions of about 4 cm^{-1}, being calibrated by the Si band at 520.7 cm^{-1}. We used a 20X objective lens, exposure times of 10s and 15s, and laser powers of 0.05 % and 5%. Point spectra were produced using both Renishaw WiRE™ 4.1 and Origin®8 software. Data were interpreted using the RRUFF database.

References

1. Seilacher A., Reif W.-E. & Westphal F. Sedimentological, ecological and temporal patterns of fossil lagerstätten. *Philos. Trans. R. Soc. Lond. B Biol. Sci*. **311,** 5-23 (1985).

2. Martill, D. M., Bechly, G. & Loveridge, R. *The Crato Fossil Beds of Brazil: Window To An Ancient World* (Cambridge University Press, New York, 2007).

3. Pinheiro, F. L., Horn, B. L. D., Schultz, C. L., de Andrade, J. A. F. G. & Sucerquia, P. A. Fossilized bacteria in a Cretaceous pterosaur headcrest. *Lethaia* **45,** 495–499 (2012).

4. Fielding, S., Martill, D. M. & Naish, D. Solnhofen-style soft-tissue preservation in a new species of turtle from the Crato Formation (early Cretaceous, Aptian) of north-east Brazil. *Palaeontology* **48,** 1301-1310 (2005).

5. Davis, S. P. & Martill, D. M. The gonorynchiform fish *Dastilbe* from the lower Cretaceous of Brazil. *Palaeontology* **42,** 715–740 (1999).

6. Schiffbauer, J. D et al. A unifying model for Neoproterozoic–Palaeozoic exceptional fossil preservation through pyritization and carbonaceous compression. *Nat. Commun*. **5:5754** doi: 10.1038/ncomms6754 (2014).

7. Chayen N. E., Rowlerson, A. M. & Squire, J. M. Fish muscle structure: fibre types in flatfish mullet fin muscles using histochemistry and antimyosin antibody labelling. *J. Muscle Res. Cell Motil.* **14,** 533-542 (1993).

8. Schweitzer, M. H. Soft Tissue preservation in terrestrial Mesozoic vertebrates. *Annu. Rev. Earth Planet. Sci*. **39,** 187–216 (2011).

9. Wilby, P. R. & Briggs, D. E. G. Taxonomic trends in the resolution of detail preserved in fossil phosphatized soft tissues. Geobios **20,** 493-502 (1997).

10. Sawlowicz, Z. Pyrite framboids and their development: a new conceptual mechanism. *Geol. Rundsch*. **82.** 148-156 (1993).

11. Delgado, A. de O. et al. Paleometry: a brand new area in Brazilian science. *Mater. Res*. **17,** 1434-1441 (2014).

12. Silva, A. L. *Estratigrafia Física e Deformação do Sistema Lacustre Carbonático (Aptiano-Albiano) da Bacia do Araripe em Afloramentos Selecionados* (Dissertação de Mestrado, Universidade Federal de Pernambuco, Recife, 2003).

13. Dias-Brito, D. & Tibana, P. *Calcários Lacustres Crato, Laminados e Não Laminados: Bacia do Araripe, Aptiano Superior (Alagoas Superior)* (IGCE/UNESP, UNESPetro Obra 1, Rio Claro, 2015).

14. Catto, B., Jahnert, R. J., Warren, L. V., Varejao, F. G., Assine, M. L. The microbial nature of laminated limestones: lessons from the Upper Aptian, Araripe Basin, Brazil. *Sediment. Geol.* doi: 10.1016/j.sedgeo.2016.05.007 (2016).

15. Neumann, V. H. M. L. *Estratigrafia, Sedimentologia, Geoquimica y Diagenesis de los Sistemas Lacustres Aptiense-Albienses de la Cuenca de Araripe (Noreste De Brasil)* (Tesis de Doctorado, Universitat de Barcelona, Barcelona, 1999).

16. Gabbott, S. E., Xian-guang, H., Norry, M. J. & Siveter, D. J. Preservation of early Cambrian animals of the Chengjiang biota. *Geology* **32,** 901-904 (2004).

17. Wilkin, R. T. & Barnes, H. L. Formation processes of framboidal pyrite. *Geochim. Cosmochim. Acta* **61,** 323-339 (1997).

18. Butler, I. B., Rickard D. Framboidal pyrite formation via the oxidation of iron (II) monosulphide by hydrogen sulphide. *Geochim. Cosmochim. Acta* **64,** 2665-2672 (2000).

19. Wilkin, R. T., Barnes, H. L., & Brantley, S. L. The size distribution of framboidal pyrite in modern sediments: an indicator of redox conditions. *Geochim. Cosmochim. Acta* **60,** 3897-3912 (1996).

20. Wacey et al. Uncovering framboidal pyrite biogenicity using nano-scale CNorg Mapping. *Geology* doi:10.1130/G36048.1 (2014).

21. Grimes, S.T. et al. Fossil plants from the Eocene London Clay: the use of pyrite textures to determine the mechanism of pyritization. *J. Geol. Soc.* **159,** 493-501 (2002).

22. Szczepanik, P., Sawlowicz, Z. & Bąk, M. Pyrite framboids in pyritized skeletons (mid-Cretaceous of the Pieniny Klippen Belt, Western Carpathians, Poland). *Ann. Soci. Geol. Pol.* **74,** 35-41 (2004).

23. Peterson, J. E., Lenczewski, M. E., Scherer, R. P. Influence of microbial biofilms on the preservation of primary soft tissue in fossil and extant archosaurs. *PLoS ONE* **5(10): e13334** doi:10.1371/journal.pone.0013334 (2010).

24. MacLean, L. C. W. et al. A high-resolution chemical and structural study of framboidal pyrite formed within a low-temperature bacterial biofilm. *Geobiology* **6,** 471–480 (2008).

25. Briggs et al. Controls on pyritization of exceptionally preserved fossils: an analysis of the Lower Devonian Hunsrück Slate of Germany. *Am. J. Sci.* **296,** 633–663 (1996).

26. Wang, B., Zhao, F., Zhang, H., Fang, Y. & Zheng D. Widespread pyritization of insects in the early Cretaceous Jehol biota. *Palaios* **27,** 707-711 (2012).
27. Lambrez, M. et al. Formation of sphalerite (ZnS) deposits in natural biofilms of sulfate-reducing bacteria. *Science* **290,** 1744-1777 (2000).

28. Kan, J. et al. Apatite and chitin amendments promote microbial activity and augment metal removal in marine sediments. *Open. J. Met*. **3,** 51-61 (2013).

29. Huerta-Diaz, M. A. & Morse, J. A. Pyritization of trace metals in anoxic marine sediments. Geochim. Cosmochim. Acta. 56, 2681-2702 (1992).

30. Briggs, D. The role of decay and mineralization in the preservation of soft-bodied fossils. *Annu Rev. Earth Planet. Sci*. **31,** 275-301 (2003).

31. Briggs, D. E. G., Bottrell, S. H. & Raiswell, R. Pyritization of soft-bodied fossils: Beecher's Trilobite Bed Upper Ordovician, New York State. *Geology* **19,** 1221-1224 (1991).

32. Gehling, J. G. Microbial mats in terminal Proterozoic siliciclastics: Ediacaran death masks. *Palaios Res. Rep*. **14,** 40-57 (1999).

33. Pan, Y., Sha, J. & Fürsich, F. T. A model for organic fossilization of the early Cretaceous Jehol lagerstätte based on the taphonomy of *Ephemeropsis trisetalis*. *Palaios* **29,** 363-377 (2014).

34. Callow, R. H. T. & Brasier, M. D. Remarkable preservation of microbial mats in Neoproterozoic siliciclastic settings: implications for Ediacaran taphonomic models. *Earth-Sci. Rev*. **96,** 207–219 (2009).

35. Allison, P. A. Konservat-Lagerstatten: cause and classification. *Paleobiology* **14,** 331-344 (1988).

36. Sagemann, J., Bale, S. J., Briggs, D. E. G & Parkes, R. J. Controls on the formation of authigenic minerals in association with decaying organic matter: an experimental approach. *Geochim. Cosmochim. Acta* **63,** 1083–1095 (1999).

37. Canfield, D. E. & Raiswell, R. *Pyrite Formation and Fossil Preservation Ch 7* (Plenum Press, New York, 1991).

38. Heimhofer, U. et al. Deciphering the depositional environment of the laminated Crato fossil beds (early Cretaceous, Araripe Basin, north-eastern Brazil). *Sedimentology* **57,** 677-694 (2010).

39. Coleman, M. L., Hedrick, D. B., Lovley, D. R., White, D. C. & Pye, K. Reduction of Fe (III) in sediments by sulphate-reducing bacteria. *Nature* **361,** 436-438 (1993).

40. Westrich, J. T. & Berner, R. A. *Limnol. Oceanogr.* **29,** 236-249 (1984).

41. Neumann, V. H., Borrego A. G., Cabrera I. & Dino, R. Organic matter composition and distribution through the Aptian-Albian lacustrine sequences of the Araripe Basin, northeastern Brazil. *Int. J. Coal. Geol.* **54,** 21-40 (2003).

42. Sansom, R. S., Gabbott, S. E. & Purnell, M. A. Atlas of vertebrate decay: a visual and taphonomic guide to fossil interpretation. *Palaeontology* **56,** 457–474 (2013).

43. Martínez-Delclòs, X., Briggs, D. E. G. & Peñalver, E. Taphonomy of insects in carbonates and amber. *Palaeogeogr. Palaeoclimatol. Palaeoecol.* **203,** 19-64 (2004).

44. Butterfield, N. J. Organic preservation of non-mineralizing organisms and the taphonomy of the Burgess Shale. *Paleobiology* **16,** 272-286 (1990).

45. Pasteris, J. D. & Wopenka B. Necessary, but not sufficient: Raman identification of disordered carbon as a signature of ancient life. *Astrobiology* **3,** 727-738 (2003).

46. Bergmann, U. et al. *Archaeopteryx* feathers and bone chemistry fully revealed via synchrotron imaging. *Proc. Natl. Acad. Sci. USA.* **107,** 9060-9065 (2010).

47. Staniskiene, B., Matusevicius, P., Budreckiene, R. & Skibniewska, K. A. Distribution of heavy metals in tissues of freshwater fish in Lithuania. *Polish. J. Environ. Stud.* **15,** 585-591 (2006).

48. Ramseyer, L., Garling, D., Hill, G. & Link, J. Effect of dietary zinc supplementation and phytase pre-treatment of soybean meal or corn gluten meal on growth, zinc status and zinc-related metabolism in rainbow trout, *Oncorhynchus mykiss. Fish Physiol. Biochem*. **20,** 251–261 (1999).

49. El-Moselhy, Kh. M., Othman, A. I., El-Azem, H. A. & El-Metwally, M. E. A. Bioaccumulation of heavy metals in some tissues of fish in the Red Sea, Egypt. *Egypt. J. Bas. Appl. Sci. 1* **1(2),** 97-105 (2014).

50. Flügel, E. *Microfacies of Carbonate Rocks: Analysis, Interpretation and Application* (Springer-Verlag, Berlin, 2004).

51. Vandenbroucke, M. & Largeau, C. Kerogen origin, evolution and structure. *Organ. Geochem.* **38,** 719–833 (2007).

52. Stankiewicz, B. A. et al. Alternative origin of aliphatic polymer in kerogen. *Geology* **28,** 559–562 (2000).

53. Berner, R. A. A new geochemical classification of sedimentary environments. *J. Sediment. Petrol.* 51, 359-365 (1981).

54. Canfield, D. E. & Thamdrup, B. Towards a consistent classification scheme for geochemical environments, or, why we wish the term 'suboxic' would go away. *Geobiology* **7,** 385–392 (2009).

55. Konhauser, K. O. *Introduction to Geomicrobiology* (Blackwell Publishing, Padstow, 2007).

56. Pfeffer, C. et al. Filamentous bacteria transport electrons over centimetre distances. *Nature* **491,** 218-221 (2012).

57. Gaines, R. R. et al. Mechanism for Burgess Shale-type preservation. *Proc. Natl. Acad. Sci. USA* **109,** 5180-5184 (2012).

58. Perez, C. A., Radtke, M., Sánchez, H. J., Tolentino, H., Neuenshwander et al. Synchrotron radiation X-ray fluorescence at the LNLS: beamline instrumentation and experiments. *X Ray Spectrom*. **28,** 320-326 (1999).

59. Sole, V. A., Papillon, E., Cotte, M., Walter, P. & Susini, J. A multiplatform code for the analysis of energy-dispersive X-ray fluorescence spectra. *Spectrochim. Acta Part B At. Spectrosc*. **62,** 63-68 (2007).

Acknowledgements

Luiz Anelli gave insightful suggestions for presenting the taphonomic model. We thank Heitor Figueiredo and Francisco Oliveira for stimulating discussions, and Rafael Ribeiro and Jessica Gonçalves for SEM/EDS. Carlos Pérez provided careful advice during SR-µXRF measurements. Renato Carvalho skilfully prepared thin sections. We thank IF-USP (EDXRF), LNLS (SR-µXRF, proposal 20150110), LaPTec (SEM/EDS), LNNano (SEM, project Quanta-18363), and LEM and NAP/Astrobio (micro-Raman). The latter was upgraded by São Paulo Research Foundation (FAPESP) funding (project 2012/18936-0), which also funded EDXRF equipment acquisition (process 2012/00202-0). We acknowledge CNPq (process 154062/2014-6) for G. Osés scholarship and Izabel Ladeira (EFY) for language revision.

Supplementary information

Supplementary Table – List of analyzed samples and thin sections

Samples	**Thin sections**	**Facies (GL - grey limestones; BL - beige limestones)**
GP/2E 9666	GP/L 16, GP/L 17	GL
GP/2E 9006	GP/L 18, GP/L 19	GL
GP/2E 7781g	GP/L 20, GP/L 21	BL
GP/1E 9435	GP/L 172	BL
GP/2E 9005		GL
GP/2E 9014		BL
GP/2E 7786f		BL
GP/2E 7913e		BL
GP/2E 7782j		BL
GP/2E 7780e		BL

Geological context: General overview

Located in north-eastern Brazil, the Araripe Basin (Supplementary Figure 1a,b) is a rift basin formed during the break-up of Gondwana[1]. The Aptian-Albian Santana Formation[2,3] is the most studied unit in the Araripe Basin, especially owing to its abundant fossil record and its rock commercial value[4]. This formation lies above the Aptian-Albian[2] Barbalha Formation, and below the Mesoalbian Araripina Formation. In addition, the Santana Formation is divided into two subunits: in the bottom, the Late Aptian Crato Member (with the Ipubi Layers at top), and in the top, the Late Aptian-Early Albian Romualdo Member[1,2]. Additionally, exceptional preservation occurs in both members, conferring them a status of Konservat- and Konzentrat-Lagerstätten[5,6,7], and references therein.

The Crato Member (Supplementary Figure 1c), wherein the studied fossils were unearthed, is composed of six carbonate lacustrine beds (clay-carbonate rythmites overlaid by laminated limestones) interbedded with deltaic shales, siltstones, and sandstones[1,8]. Evidence for preserved microfossils, EPS, and organomineralization suggest that the Crato carbonates were precipitated primarily by microbial activity[9]. Carbonate facies, which have varied organic matter contents, were deposited in a restricted basin under low energy in anoxic or dysoxic bottom water conditions, as evidenced by well-preserved palynomorphs, amorphous organic matter preservation and iron oxide-hydroxides after pyrite[9,10]. In addition, the analysis of the limestone facies suggests six transgressive-regressive cycles, controlled mainly by climate cycles (humid and dry conditions) and tectonics[8,9]. Located above the Crato Member, the Ipubi Layers record evidence for a transitional setting (evaporitic/lacustrine to lagoon/marine), where thick (ca. 30 m) beds of gypsum and anhydrite occur and are overlaid by shales and sandstones[1,11].

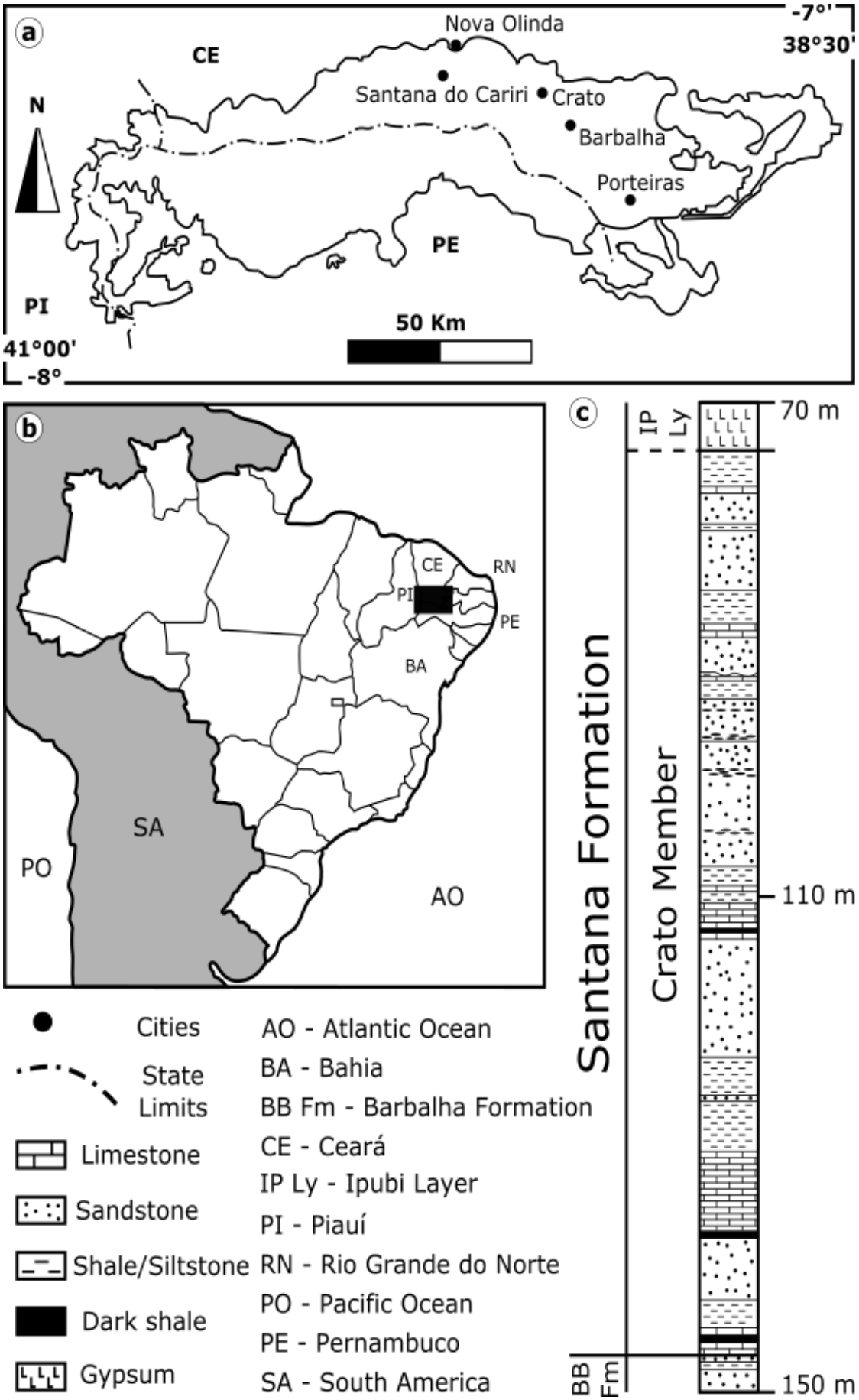
a
Nova Olinda
CE
-7°
38°30'
N
Santana do Cariri
Crato
Barbalha
Porteiras
PE
PI
50 Km
41°00'
-8°
b
CE
RN
PI
PE
BA
SA
PO
AO
c
IP
Ly
70 m
Santana Formation
Crato Member
110 m
BB Fm
150 m
Cities
State Limits
Limestone
Sandstone
Shale/Siltstone
Dark shale
Gypsum
AO - Atlantic Ocean
BA - Bahia
BB Fm - Barbalha Formation
CE - Ceará
IP Ly - Ipubi Layer
PI - Piauí
RN - Rio Grande do Norte
PO - Pacific Ocean
PE - Pernambuco
SA - South America

Supplementary Figure 1. Geologic unit of the studied fossils. a, The Araripe Basin. **b**, Localization of the Araripe Basin in Brazil. **c**, Representative lithostratigraphic column of the Crato Member. **c** is modified from ref. 9.

Supplementary note 1 – General overview of *Dastilbe crandalli*

Dastilbe crandalli (Gonorynchiformes: Chanidae) is the most common fish from the Crato Member. Its standard length is ca. 100 mm, although specimens up to 210 mm are also found. *D. crandalli* also occurs in the following Brazilian north-eastern sedimentary basins: Sergipe-Alagoas, Parnaíba, São Francisco, Tucano, Pernambuco-Paraíba, besides in Rio Benito, Equatorial Guinea[12]. A Middle Cretaceous vicariance involving the Chanidae clade, particularly between South America (*Tharrhias*, *Dastilbe*) and Africa (*Parachanos*) has been detected[13]. Freshwater fish dispersal was a common event since several marine barriers were still very narrow and probably subject to width variations due to sea level fluctuations[13]. Although several works deal with *Dastilbe* morphology and palaeogeographic distribution, very few use this fish as a taphonomic tool. In this way, the understanding of labile-tissue preservation sheds light on palaeoenvironmental aspects of *Dastilbe* habitats.

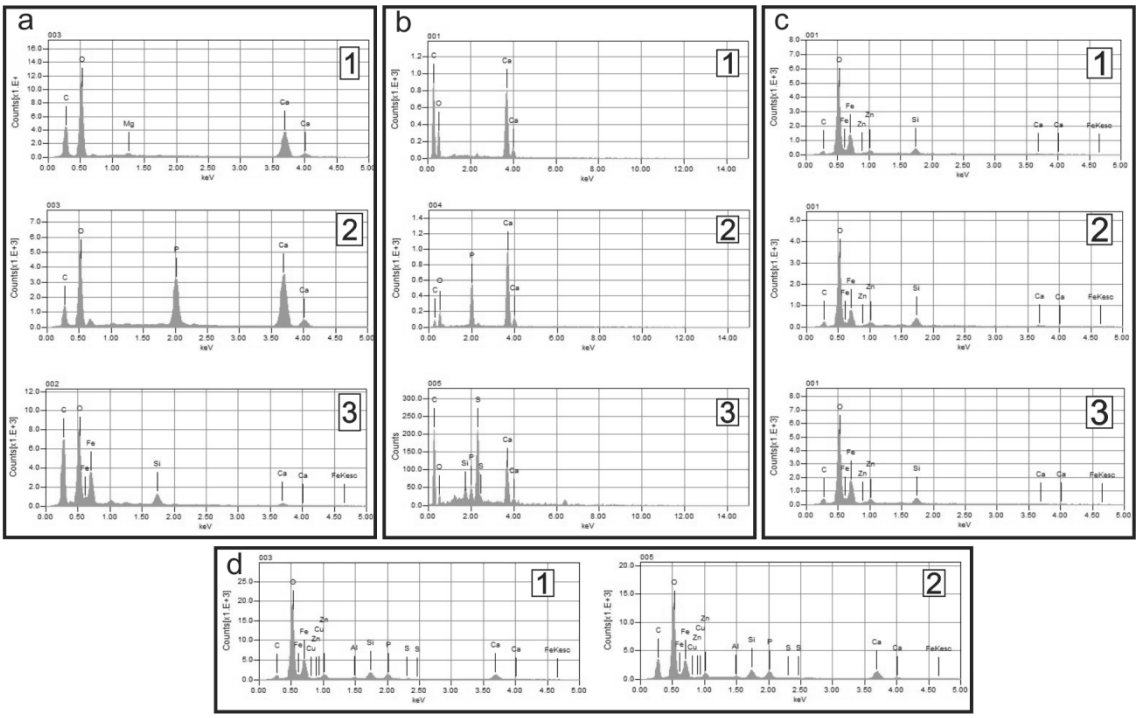

Supplementary Figure 2. EDS point spectra. Thin sections GP/L 20 (a) and GP/L 16 (b) and specimens GP/2E 7786f (c) and GP/2E 7913e (d). a, 1 – calcite cement, 2 – bone, 3 – soft-tissue. b, 1 – calcite cement, 2 – bone, 3 – soft-tissue. c, Muscle

microfabric composition: 1 – base of caudal fin, 2 – base of dorsal fin, 3 – muscles attached to vertebral column. d, 1 – microfabric, 2 – putative EPS.

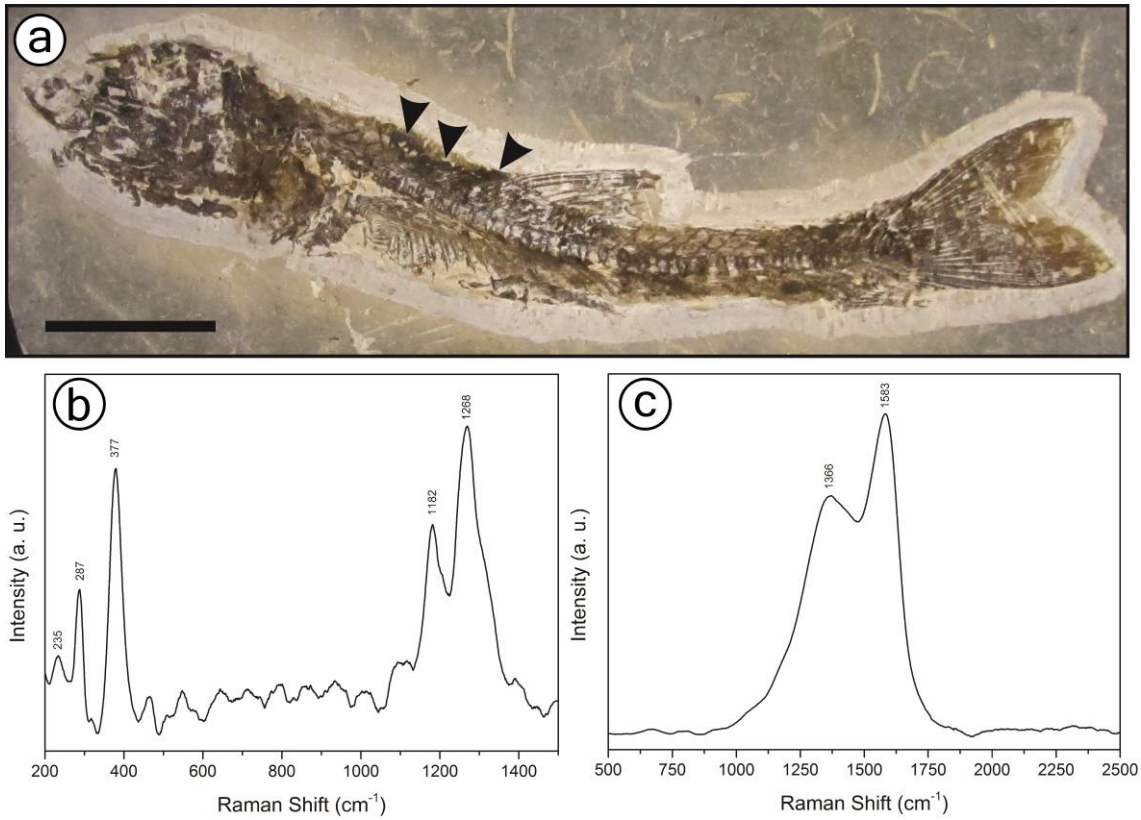

Supplementary Figure 3. Micro-Raman spectra of soft-tissues. a, Specimen GP/2E 9005. Soft-tissues are indicated by arrow heads. Scale bar is 30 mm. **b**, Spectrum of goethite (peaks at 235, 287, and 377 cm^{-1}) of BL fish GP/2E 7786f (Supplementary Figure 7). **c**, Spectrum of kerogen (D band – ca. 1366 cm^{-1}; G band – ca. 1583 cm^{-1}) of fossil in **a**. Intense bands (D and G bands) plus the lack of shoulder associated with the G band suggest that the analyzed material is both highly disordered and poorly geochemical mature, maybe implying that original composition has been little altered[14,15].

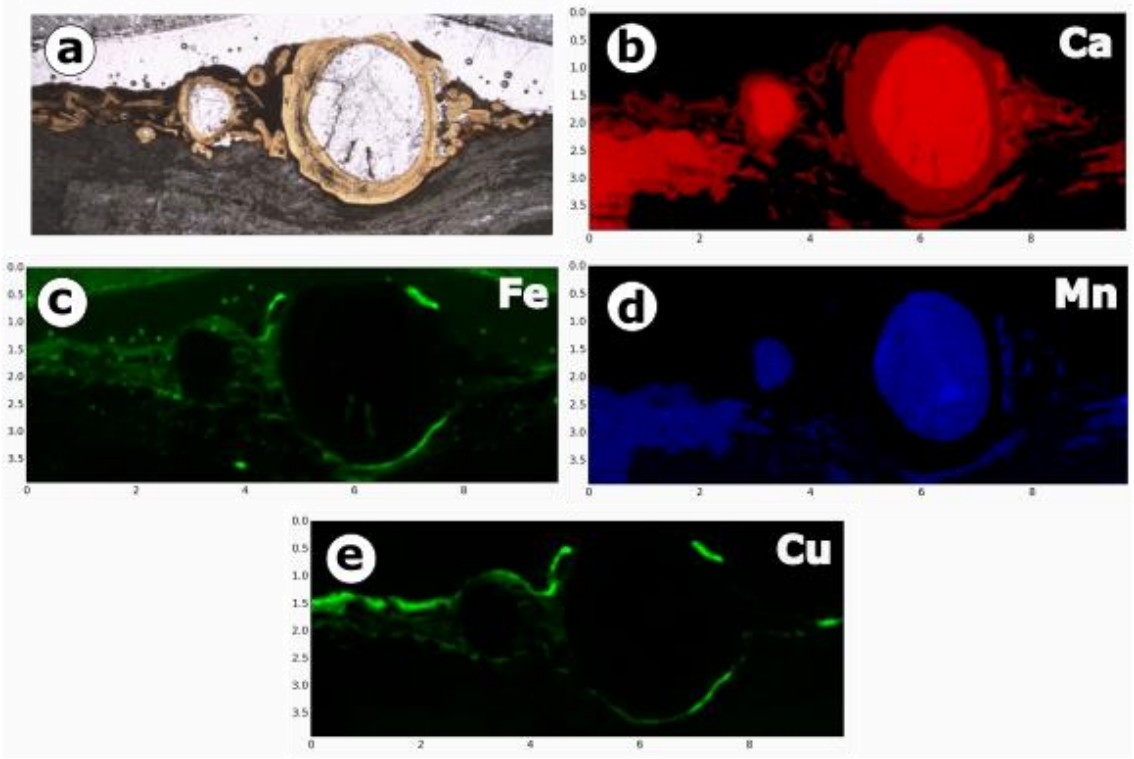

Supplementary Figure 4. SR-µXRF maps of fish (GP/2E 9666) with preserved carbonaceous soft-tissues. a, Area mapped by SR-µXRF of the thin section GP/L 16. **b-e**, SR-µXRF maps. Image brightness is proportional to element concentration, and both map horizontal and vertical scale axes are in mm.

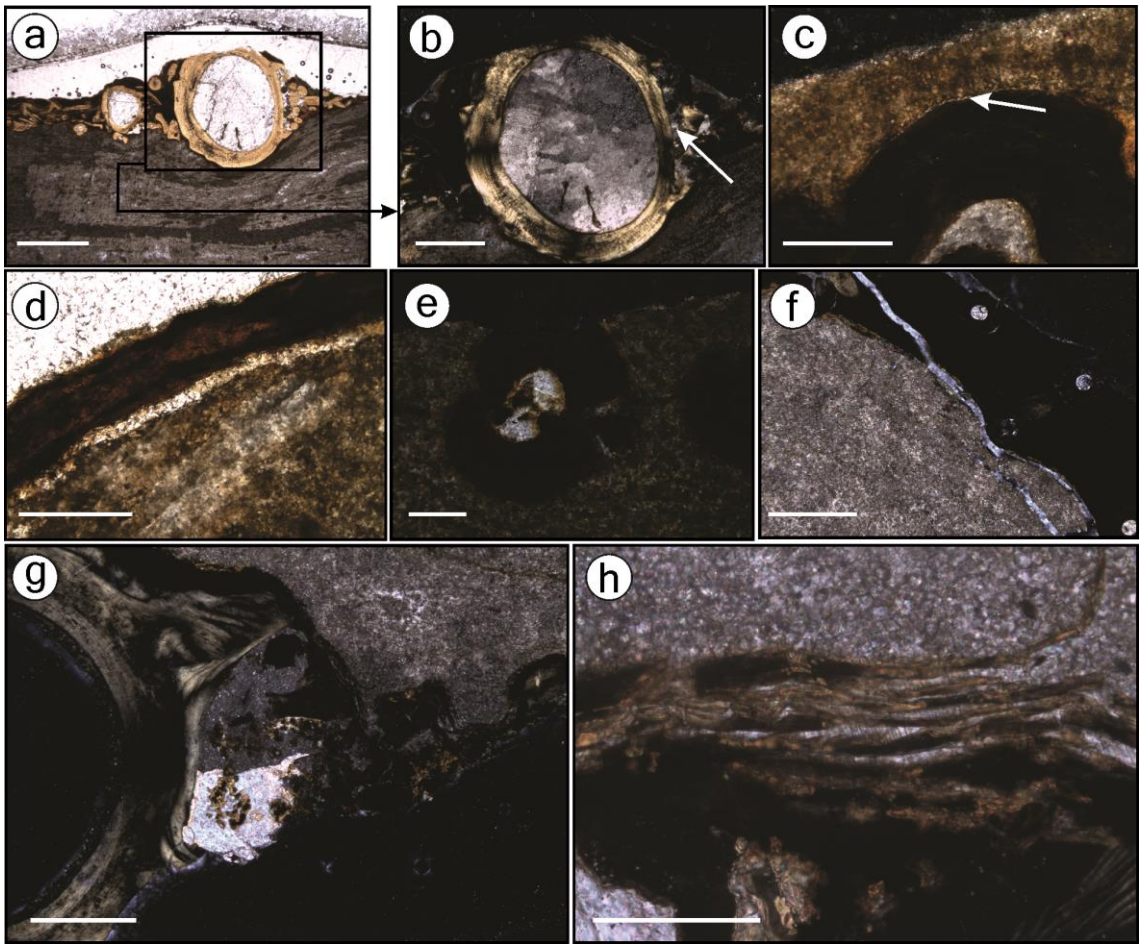

Supplementary Figure 5. Cement types in carbonaceous fish. Thin sections GP/L 16 (**a**-**e**) and GP/L 17 (**f**-**h**). **a**, Microfault in right half. **b**, Equigranular sparry calcite in mosaic filling the vertebrae, and poikilotopic sparry calcite filling tissue empty spaces around vertebra (arrow). **c**, Sparry calcite outlining bones (arrow). **d**, Sparry calcite outlining soft-tissues. **e**, Sparry calcite filled bones and their fractures. **f**, Apatite veins sometimes outline soft-tissue outer margin (lower half) and cut it inward (upper half). **g**, Poikilotopic sparry calcite around vertebra. **h**, Sparry calcite between scales. Scale bars: **a** – 2 mm; **b** – 1 mm; **c**-**e** – 0.2 mm; **f**, **g** – 0.5 mm; **h** – 0.1 mm.

Supplementary note 2 - Comments on integument preservation

While Crato Member pyritized fishes have rarely preserved integument, kerogenized specimens commonly display scales interlayered with skin remains. In the case of pyritization, the integument was the first massive source for microbial decay (by sulphate-reducing bacteria, SR), yielding high sulphide concentrations, even if considering integument to be less decay-prone than muscles. That very high sulphate

reduction rates only prompt pyrite coatings around carcasses and soft-tissues[16] accounts for the red halo that usually surrounds fossils as well as the lack of integument preserved in beige limestone (BL) fishes. Labile-tissue pyrite coating is uneventful among Konservat-Lagerstätten, being recorded in Beecher's Trilobite Bed and Hunsrück Slate[17]. However, Crato Member fish muscles and sometimes eyes have been preserved in 3D, implying that SR has not been widespread (i.e. SR rates have not been exceedingly high) and pyritization was more concentrated in some tissues. In this way, integument preservation in kerogenized fishes is coherent with methanogen degradation of C_{org} since methanogenesis yields less degradation than SR[18]. Additionally, the lack of skin preservation in BL specimens could be a consequence of *post mortem* rupture near head base, as seen in several specimens (Supplementary Figures 6-8). Gas escape, as reported in Romualdo Member (Santana Formation) fishes[19], is not likely an explanation for the case of *Dastilbe crandalli*. Taphonomic experiments on lacustrine fishes (Series Otophysi, related to Series Anotophysi, in which *D. crandalli* is classified) have shown that gases produced after decay escape from original openings[20]. Therefore, the head-neck rupture described above can be considered a case of tetany (i.e. severe muscular contraction), regarding that rupture was not likely caused by transport[20]. Tetany is caused by (1) thermic abrupt variation, (2) salinity/alkalinity, or (3) anoxia. Based on the fact that among these three possibilities, the second results in body deformation, we considered that salinity is the most plausible cause for head-neck rupture in *D. crandalli* specimens. This hypothesis is in agreement with hypersalinity episodes in the Crato palaeolake[6].

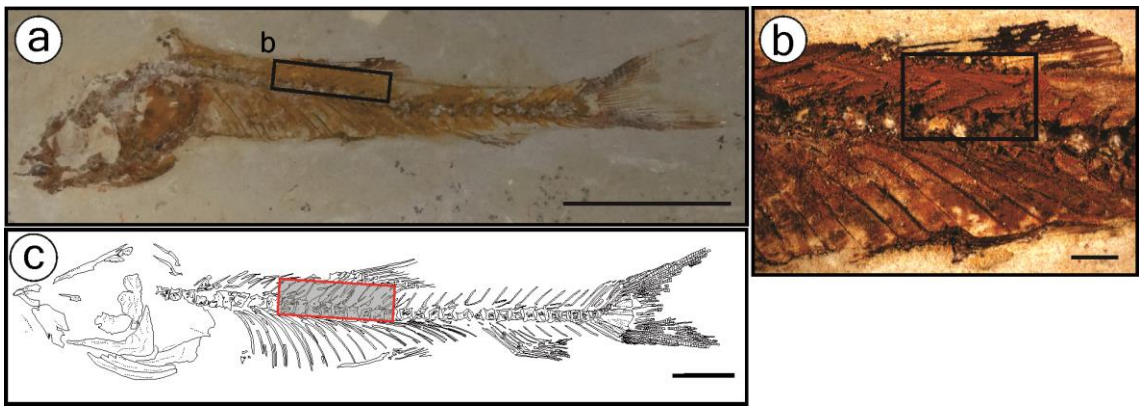

Supplementary Figure 6. Localization of soft-tissues analyzed by SEM. a, Fossil GP/2E 7782j. **b**, Myomeres below dorsal fin (at top). Area analyzed by SEM is highlighted by the rectangle. **c**, General scheme depicting area marked in **a**. Scale bars: **a** – 10 mm; **b** – 1 mm; **c** – 10 mm.

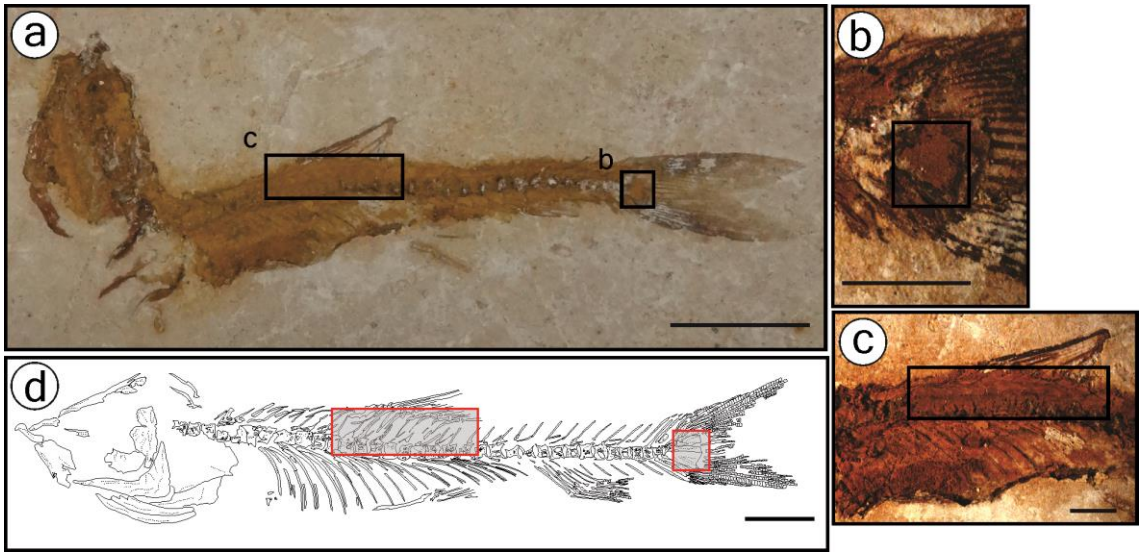

Supplementary Figure 7. Localization of soft-tissues analyzed by SEM. a, Specimen GP/2E 7786f. **b**, **c**, Regions imaged by SEM are highlighted by rectangles. **d**, General scheme depicting regions marked in **a**. Scale bars: **a** – 10 mm; **b** – 2 mm; **c** – 2 mm; **d** – 10 mm.

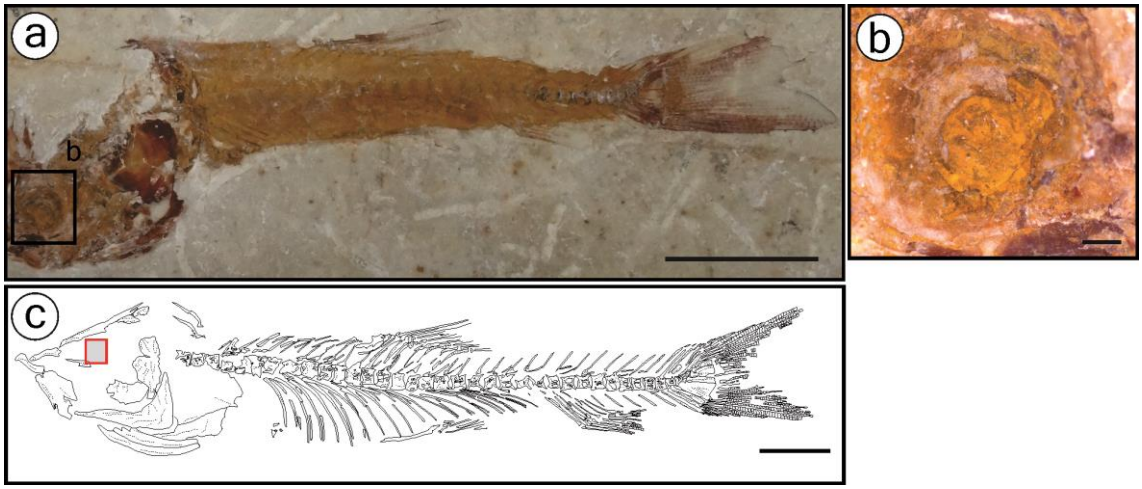

Supplementary Figure 8. Localization of soft-tissues analyzed by SEM. a, Fossil GP/2E 7780e. **b**, Detail of the eye analyzed by SEM. **c**, General scheme depicting area marked in **a**. Scale bars: **a** – 10 mm; **b** – 0.5 mm; **c** – 10 mm.

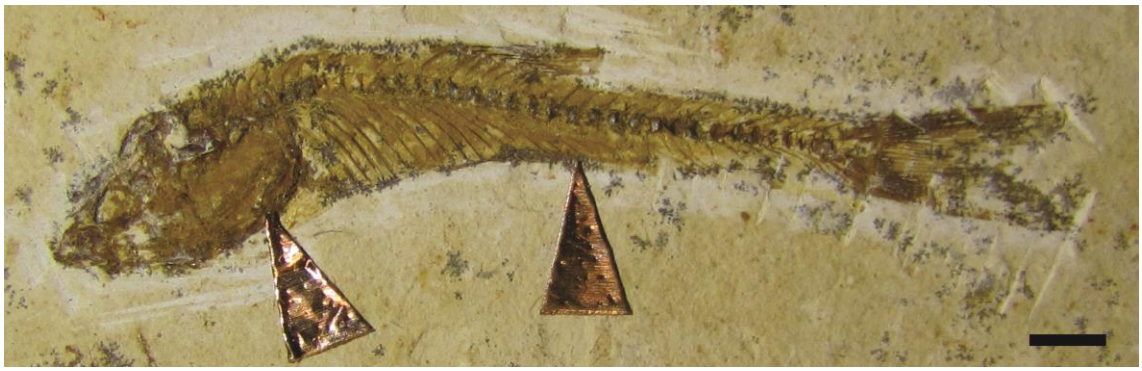

Supplementary Figure 9. Specimen GP/2E 7913e. Scale bar is 3 mm.

Supplementary References

1. Assine M. L. Bacia do Araripe. *Bol. Geoc. Petr*. **15,** 371-389 (2007).

2. Coimbra, J. C., Arai, M. & Carreño, A. L. Biostratigraphy of lower Cretaceous microfossils from the Araripe Basin, northeastern Brazil. *Geobios* **35,** 687-698 (2002).

3. Rios-Netto, A. D. M., Regali, M. D. S. P., Carvalho, I. D. S. & Freitas, F. I. D. Palinoestratigrafia do intervalo Alagoas da Bacia do Araripe, Nordeste do Brasil. *Rev. Bras. Geoc.* **42,** 331-342 (2002).

4. Campos, D. A., Vidal, F. W. H. & Castro, N. F. *Quarrying limestones and saving fossils of the Araripe Basin, Brazil* (Pacini Editore, Pisa, 2008).

5. Maisey, J. G. *Santana fossils: an illustrated atlas* (T.F.H. Publications, Neptune City, 1991).

6. Martill, D. M., Bechly, G. & Loveridge, R. *The Crato Fossil Beds of Brazil: Window To An Ancient World* (Cambridge University Press, New York, 2007).

7. Barling, N., Martill, D. M., Heads, S.W. & Gallien, F. High fidelity preservation of fossil insects from the Crato Formation (lower Cretaceous) of Brazil. *Cret Res*. **52,** 605-622 (2015).

8. Neumann, V. H. M. L. *Estratigrafia, Sedimentologia, Geoquimica y Diagenesis de los Sistemas Lacustres Aptiense-Albienses de la Cuenca de Araripe (Noreste De Brasil)* (Tesis de Doctorado, Universitat de Barcelona, Barcelona, 1999).

9. Catto, B., Jahnert, R. J., Warren, L. V., Varejao, F. G., Assine, M. L. The microbial nature of laminated limestones: lessons from the Upper Aptian, Araripe Basin, Brazil. *Sediment. Geol.* doi: 10.1016/j.sedgeo.2016.05.007 (2016).

10. Heimhofer, U. et al. Deciphering the depositional environment of the laminated Crato fossil beds (early Cretaceous, Araripe Basin, north-eastern Brazil). *Sedimentology* **57,** 677-694 (2010).

11. Silva, M. A. M. Evaporitos do Cretáceo da Bacia do Araripe: ambientes de deposição e história diagenética. *Bol. Geoc. Petr.* **2,** 53-63 (1988).

12. Brito, P. M., Amaral, C. R. L. *An overview of the specific problems of Dastilbe JORDAN, 1910 (Gonorynchiformes: Chanidae) from the Lower Cretaceous of western Gondwana* (Verlag, Munich, 2008).

13. Cavin, L. Palaeobiogeography of Cretaceous bony fishes (Actinistia, Dipnoi and Actinopterygii). *Geol. Soc. Spec. Publ.* **295,** 165-183 (2008).

14. Pasteris, J. D. & Wopenka B. Necessary, but not sufficient: Raman identification of disordered carbon as a signature of ancient life. *Astrobiology* **3,** 727-738 (2003).

15. Schopf, J. W., Kudryavtsev, A. B. Confocal laser scanning microscopy and Raman imagery of ancient microscopic fossils. *Prec. Res.* **173,** 39-49 (2009).

16. Canfield, D. E. & Raiswell, R. *Pyrite Formation and Fossil Preservation Ch 7* (Plenum Press, New York, 1991).

17. Allison, P. A. Konservat-Lagerstatten: cause and classification. *Paleobiology* **14,** 331-344 (1988).

18. Berner, R. A. A new geochemical classification of sedimentary environments. *J. Sediment. Petrol.* 51, 359-365 (1981).

19. Martill, D. M. Preservation of fish in the Cretaceous Santana Formation of Brazil. *Palaeontology* **31,** 1-18 (1988).

20. Elder, R. L. *Principles of aquatic taphonomy with examples from the fossil record* (Thesis, University of Michigan, Ann Arbor, 1985).

7. Conclusions

The genesis of the Crato Member carbonate beds has been extensively investigated (Heimhofer et al., 2010; Catto et al., 2016). It is now accepted that calcite precipitation has been driven chiefly by a microbial mat-dwelling microbiota, including cyanobacteria and/or sulphate-reducing and methanogenic microorganisms (Catto et al., 2016). These authors support their conclusions based on preserved microfossils and EPS. The results here shown are in agreement with the conclusions of Catto et al. (2016), given that EDXRF, SEM/EDS, micro-Raman, and PIXE reveal pseudomorphs of framboidal pyrite (Delgado et al., 2014) in association with EPS, replacing both insect cuticles and soft-tissues and fish labile-tissues, such as muscle cells and eyes. Such evidence point to pyrite organomineralization by sulphate-reducing bacteria (SRB). On the basis of the observation that framboidal pseudomorphs vary in size when comparing insect cuticle and inner areas or soft tissues, it is proposed here the balance between ion diffusion rates and nucleation rates of pyrite through the decaying carcasses accounts for this size variation. EDS and synchrotron micro-XRF further suggest that insects may have also been phosphatized, albeit with minor contribution than pyrite. Moreover, SEM, EDS, and micro-Raman show that fish muscles, skin, and connective tissues are kerogenized, which is interpreted here as a result of methanogen activity.

EDXRF, EDS and PIXE geochemical data reveal that originally pyritized insects and fishes have higher Cu and Zn concentrations in comparison with their host carbonate. This has most likely occurred because of Cu/Zn incorporation in pyrite crystals during nucleation (Huerta-Diaz and Morse, 1992). Nevertheless, biofilms could have enhanced element-fixing in decaying carcasses (Kan et al., 2013), particularly those around/within insects since chitin has chemical affinity with Cu and Zn (Neugebauer, 1986). Regardless of the previous hypotheses, these elements are shown to bond to organic matter (Šípková et al., 2013). Anyway, the importance of metal fixation in decaying carcasses undoubtedly enhances mineralization. On the other hand, Zn is concentrated in the bones of kerogenized fishes, while Fe and Cu occur in some soft-tissue regions and seem to be correlated. Such patterns are interpreted here as derived from metal accumulation during life, mainly considering that no evidence for mineralization has hitherto been found in kerogenized fishes.

The following evidence suggest sediment anoxic conditions: (1) lack of bioturbation (Heimhofer and Martill, 2007), (2) pyritized fossils, and (3) possibly microbial mats (Catto et al., 2016) that could have sealed the substrate, reducing O_2 diffusion (Gehling, 1999). Therefore, well-known factors that control exceptional fossil preservation helped in soft-tissue preservation in the Crato Member. In addition, it is a consensus that sediment has a key role in fossil mineralization (Gehling, 1999; Sagemann et al., 1999), which is the main control of labile-tissue fossilization (Allison, 1988). Following this rationale, the absence of bioturbation (and substrate oxygenation) provided a shallow sulphate reduction zone, thus favouring pyritization (Callow and Brasier, 2009). Moreover, low organic contents in the laminated limestones (Neumann et al., 2003) explain widespread insect and fish pyritization. There have to be few nucleation sites (i.e. low widespread organic matter contents) within sediment to enable fixation of SRB-produced sulphide by Fe^{2+} in decaying carcasses sites, leading to pyritization (Allison, 1988). It is here considered that organic matter mineralization (pyritization) and kerogenization have taken place, respectively, within anoxic-sulphidic and anoxic-non-sulphidic sedimentary zones. In addition, low microspar porosity plus varied cement contents among carbonate beds (Heimhofer et al., 2010), along with clay, might have led to the narrowing of microbial zones owing to the limitation of migration of both electron acceptors and microbial respiration geochemical products downwards, thus controlling mineralization (Gaines et al., 2012; Schiffbauer et al, 2014).

In the particular case of fishes, the hypothesis of palaeoenvironmental-driven taphonomic variation has been tested. Light petrography, geochemical, and SEM data reveal two preservational pathways - pyritization and kerogenization - that have accounted for exceptional soft-tissue fossilization. Petrographic thin sections of carbonates bearing distinctly preserved fossils show variations in clay and organic matter contents, thus indicating two different facies: (1) beige limestones (BL), which bear originally pyritized fossils, thinner and less frequent dark clay/organic matter rich laminae than (2) grey limestones (GL), which host kerogenized fishes. It is proposed that GL were deposited under higher terrigenous influence than BL, implying that sedimentary rates have most likely been higher in the former. As a consequence, fish decaying carcasses would have been buried faster in GL, placing carcasses faster within the methanogenesis zone, where kerogenization took place. On the other hand, fishes would have been buried more slowly in BL, making them spend more time in the

sulphate-reduction zone, yielding ubiquitous pyrite precipitation. Schiffbauer et al. (2014) proposed this pyritization-kerogenization gradient for Precambrian metazoan fossilization.

It is noteworthy that pyritized soft-tissues follow a preservational-fidelity degree, with some regions being dominated by scattered goethite pseudomorphs, and 3D muscle fibres organized in myomeres, at both extremes of the preservational gradient. Finally, pyritized and kerogenized labile-tissues also reveal a preservational-quality gradient, besides selectivity of preserved tissues. While the former have 3D muscle tissues, sarcolemma, putative cell nuclei, tendons, and eyes, the latter display connective tissues, integument, and compressed/distorted muscle fibres. This pattern agrees both with the well-known preference of kerogenization of more recalcitrant tissues and mineralization of labile-tissues (Butterfield, 1995), and with the time elapsed between both processes.

Finally, some questions raised during this research still remain open for debate, such as (1) whether chemical elements (e.g. Zn, Cu, Pb) are isolated, incorporated in pyrite crystals, or associated to other minerals; (2) search for apatite crystals replacing insects; (3) test the pyritization-kerogenization preservational gradient hypothesis for insects and plants, for example, with controlled sampling in multiple locations; (4) test the influence of cement bed-capping to pyritization; and (5) further understand the influence of distinct taphonomic pathways to preservational fidelity.

References

Abbate M, Vicentin FC, Compagnon-Cailhol V, Rocha MC, Tolentino HCN. The soft X-ray spectroscopy beamline at the LNLS: technical description and commissioning results. J Synchrotron Radiat. 1999; 6 (5): 964-972.

Allison PA. Konservat-Lagerstatten: cause and classification. Paleobiology. 1988; 14: 331-344.

Allison PA. Phosphatized soft-bodied squids from the Jurassic Oxford Clay. Lethaia. 1988; 21 (4): 403-410.

Allison PA, Bottjer DJ. Taphonomy: bias and process through time. In: Allison PA, Bottjer DJ, editors. Taphonomy: bias and process through time, Topics in Geobiology 32, Springer, New York; 2011. Chap. 1, p. 1-17.

Assine ML. Bacia do Araripe. Bol. Geoc. Petr. 2007; 15 (2): 371-389.

Barling N, Martill DM, Heads SW, Gallien F. High fidelity preservation of fossil insects from the Crato Formation (lower Cretaceous) of Brazil. Cret Res. 2015; 52 (B): 605-622.

Bergmann U, Morton RW, Manning PL, Sellers WI, Farrar S, Huntley KG, et al. *Archaeopteryx* feathers and bone chemistry fully revealed via synchrotron imaging. Proc Natl Acad Sci U S A. 2010; 107 (20): 9060-9065.

Berner RA. A new geochemical classification of sedimentary environments. J. Sediment. Petrol. 1981; 51: 359-365.

Berner RA. Sedimentary pyrite formation: an update. Geochim Cosmochim Acta. 1984; 48: 605-615.

Bertazzo S. et al. Fibres and cellular structures preserved in 75-million-year-old dinosaur specimens. Nat. Commun. 2015; 6:7352 doi: 10.1038/ncomms8352.

Beurlen K. As condições ecológicas e faciológicas da Formação Santana na Chapada do Araripe (Nordeste do Brasil). An. Acad. Bras. C. 1971; 43 (supl.): 411-415.

Beurlen K. Geologia da Chapada do Araripe. An Acad Bras Cienc. 1962; 34 (3): 365-370.

Brasier MD, Antcliff J, Saunders M, Wacey D. Changing the picture of Earth's earliest fossils (3.5–1.9 Ga) with new approaches and new discoveries. Proc Natl Acad Sci U S A. 2015; 112(16): 4859-4864.

Briggs D. The role of decay and mineralization in the preservation of soft-bodied fossils. Annu Rev Earth and Planet Sci. 2003; 31: 275-301.

Briggs DEG, Bottrell SH, Raiswell R. Pyritization of soft-bodied fossils: Beecher's Trilobite Bed Upper Ordovician, New York State. Geology. 1991; 19: 1221-1224.

Briggs DEG, Erwin DH, Collier FJ. The fossils of the Burgess Shale, Smithsonian Institution Press, Washington and London; 1994. 256 pp.

Briggs DEG, Kear AJ. Fossilization of soft tissue in the laboratory. Science. 1993; 259: 1439-1442.

Briggs DEG, McMahon S. The role of experiments in investigating the taphonomy of exceptional preservation. Palaeontology. 2016; 59: 1-11.

Briggs DEG, Moore RA, Shultz JW, Schweigert G. Mineralization of soft-part anatomy and invading microbes in the horseshoe crab *Mesolimulus* from the Upper Jurassic lagerstätte of Nusplingen, Germany. Proc Biol Sci. 2005; 272: 627–632.

Briggs DEG, Summons RE. Ancient biomolecules: their origin, fossilization and significance in revealing the history of life. Bioessays. 2014; 36: 482-490.

Briggs DEG, Wilby PR. The role of the calcium carbonate-calcium phosphate switch in the mineralization of soft-bodied fossils. J Geol Soc London. 1996; 153: 665-668.

Briggs et al. Controls on pyritization of exceptionally preserved fossils: an analysis of the Lower Devonian Hunsrück Slate of Germany. Am. J. Sci. 1996; 296: 633–663.

Brito PM, Amaral CRL. An overview of the specific problems of *Dastilbe* JORDAN, 1910 (Gonorynchiformes: Chanidae) from the Lower Cretaceous of western Gondwana. In: Arratia G, Schultze H-P, Wilson MVH, editors. Mesozoic Fishes 4 – Homology and Phylogeny. Verlag, Munich; 2008. pp. 279-294.

Brito-Neves BB. A Bacia do Araripe no contexto geotectônico regional. In: Atas do I Simpósio sobre a Bacia do Araripe e Bacias Interiores do Nordeste; 1990. 1: 21-33.

Brock F, Parkes RJ, Briggs DEG. Experimental pyrite formation associated with decay of plant material. Palaios. 2006; 21: 499-506.

Buck PV. Paleometria aplicada ao estudo de fósseis brasileiros: implicações evolutivas e tafonômicas. Monografia de Conclusão de Curso, Universidade Federal de São Carlos, Sorocaba; 2013.

Butler IB, Rickard D. Framboidal pyrite formation via the oxidation of iron (II) monosulphide by hydrogen sulphide. Geochim Cosmochim Acta. 2000; 64 (15): 2665-2672.

Butterfield NJ. Organic preservation of non-mineralizing organisms and the taphonomy of the Burgess Shale. Paleobiology. 1990; 16: 272-286.

Butterfield NJ. Secular distribution of Burgess-Shale-type preservation. Lethaia. 1995; 28: 1-13.

Callow RHT, Brasier MD. Remarkable preservation of microbial mats in Neoproterozoic siliciclastic settings: Implications for Ediacaran taphonomic models. Earth-Sci. Rev. 2009; 96: 207–219.

Campos DA, Vidal FWH, Castro NF. Quarrying limestones and saving fossils of the Araripe Basin, Brazil. In: Dimension Stones – ICDS: XXI Century Challenges – Proceedings of the Second International Congress. Pacini Editore, Pisa; 2008. pp. 63-69.

Canfield DE, Raiswell R. Pyrite formation and fossil preservation. In: Allison PA, Briggs DEG, editors. Topics in Geobiology. Plenum Press; 1991, pp. 337–387.

Canfield DE, Thamdrup B. Towards a consistent classification scheme for geochemical environments, or, why we wish the term ‘suboxic’ would go away. Geobiology. 2009; 7: 385–392.

Castro JL, Valença LMM, Neumann VH. Ciclos e seqüências deposicionais das formações Rio da Batateira e Santana (Andar Alagoas), Bacia do Araripe, Brasil. Geoc. UNESP. 2006; 25(3): 289-296.

Catto B, Jahnert RJ, Warren LV, Varejao FG, Assine ML. The microbial nature of laminated limestones: lessons from the Upper Aptian, Araripe Basin, Brazil. Sediment Geol. 2016; doi: 10.1016/j.sedgeo.2016.05.007.

Cavin L. Palaeobiogeography of Cretaceous bony fishes (Actinistia, Dipnoi and Actinopterygii). Geol. Soc. Spec. Publ. 2008; 295: 165-183.

Characklis WG, Wilderer PA. Glossary. In: Characklis WG, Wilderer PA (eds) Structure and function of biofilms. Wiley, Chichester; 1989. pp. 369-371.

Chayen NE, Rowlerson AM, Squire JM. Fish muscle structure: fibre types in flatfish mullet fin muscles using histochemistry and antimyosin antibody labelling. J. Muscle Res. Cell Motil. 1993; 14: 533-542.

Chen L, Xiao S, Pang K, Zhou C, Yuan X. Cell differentiation and germ-soma separation in Ediacaran animal embryo-like fossils. Nature. 2014; 516: 238-241.

Coimbra JC, Arai M, Carreño AL. Biostratigraphy of lower Cretaceous microfossils from the Araripe Basin, northeastern Brazil. Geobios. 2002; 35 (6): 687-698.

Coleman ML, Hedrick DB, Lovley DR, White DC, Pye K. Reduction of Fe (III) in sediments by sulphate-reducing bacteria. Nature. 1993; 361: 436-438.

Davis SP, Martill DM. The gonorynchiform fish *Dastilbe* from the lower Cretaceous of Brazil. Palaeontology. 1999; 42: 715–740.

Défarge C, Trichet J, Jaunet A-M, Robert M, Tribble J, Sansone FJ. Texture of microbial sediments revealed by cryo-scanning electron microscopy. J Sediment Res. 1996; 66 (5): 935-947.

Delgado A de O, Buck PV, Osés GL, Ghilardi RP, Rangel EC, Pacheco MLAF. Paleometry: a brand new area in Brazilian science. Mater Res. 2014; 17: 1434-1441.

Dias-Brito D, Tibana P. Calcários lacustres Crato, laminados e não laminados: Bacia do Araripe, Aptiano superior (Alagoas superior). In: Dias-Brito D, Tibana P., editors. Calcários do Cretáceo do Brasil: um atlas, IGCE/UNESP, UNESPetro Obra 1, Rio Claro; 2015. p. 121-129.

Dias-Brito D, Tibana P, Assine ML, Rossetti DF. Laminitos lacustres organo-calcários neoaptianos ricos em ostracodes no nordeste do Brasil: Bacias do Araripe, Potiguar e Parnaíba, Aptiano Superior (Alagoas Superior). In: Dias-Brito D, Tibana P., editors. Calcários do Cretáceo do Brasil: um atlas, IGCE/UNESP, UNESPetro Obra 1, Rio Claro; 2015. p. 49-119.

Duncan IJ, Briggs DEG. Three-dimensionally preserved insects. Nature. 1996; 381: 30-31.

Dupraz C, Reid RP, Braissant O, Decho AW, Norman RS, Visscher PT. Processes of carbonate precipitation in modern microbial mats. Earth-Sci Rev. 2008; 96 (3): 141-162.

Elder RL. Principles of aquatic taphonomy with examples from the fossil record. Thesis, University of Michigan, Ann Arbor; 1985.

El-Moselhy KhM, Othman AI, El-Azem HA, El-Metwally MEA. Bioaccumulation of heavy metals in some tissues of fish in the Red Sea, Egypt. Egypt. J. Bas. Appl. Sci. 2014; 11(2): 97-105.

Engel MS, Grimaldi D & Krishna K. Primitive termites from the Early Cretaceous of Asia (Isoptera). Stuttgarter Beiträge zur Naturkunde, Serie B (Geologie und Paläontologie). 2007; 371: 1-32.

Faria DLA, Lopes FN. Heated goethite and natural hematite: can Raman spectroscopy be used to differentiate them? Vib Spectrosc. 2007; 45: 117-121.

Fielding S, Martill DM, Naish D. Solnhofen-style soft-tissue preservation in a new species of turtle from the Crato Formation (early Cretaceous, Aptian) of north-east Brazil. Palaeontology. 2005; 48: 1301-1310.

Filho FES. Aplicação de técnicas físicas na paleontologia: um estudo de fósseis da Formação Ipubi – Bacia Sedimentar do Araripe. Tese de Doutorado, Universidade Federal do Ceará, Fortaleza; 2011.

Flügel E. Microfacies of Carbonate Rocks: Analysis, Interpretation and Application. Springer-Verlag, Berlin; 2004. 984 p.

Gabbott SE, Xian-guang H, Norry MJ, Siveter DJ. Preservation of early Cambrian animals of the Chengjiang biota. Geology. 2004; 32 (10): 901-904.

Gaines RR et al. Mechanism for Burgess Shale-type preservation. Proc Natl Acad Sci USA. 2012; 109: 5180-5184.

Gehling JG. Microbial mats in terminal Proterozoic siliciclastics: ediacaran death masks. Palaios Res. Rep. 1999; 14: 40-57.

Gierlowski-Kordesch EH. Lacustrine carbonates. In: Alonso-Zarza AM, Tanner LH, editors. Carbonates in Continental settings: facies, environments and processes, Elsevier, Oxford; 2010. Chap. 1, pp. 1-101.

Gonzalez-Davila M, Millero FJ. The adsorption of copper to chitin in seawater. Geochim Cosmochim Acta. 1990; 54*:* 761-768.

Greenwalt DE, Goreva YS, Siljeström SM, Rose T, Harbach RB. Hemoglobin-derived porphyrins preserved in a middle Eocene blood-engorged mosquito. Proc Natl Acad Sci U S A. 2013; 110(46): 18496–18500.

Grimaldi D, Maisey J. Introduction. In: Gimaldi D, editor. Insects from the Santana Formation, Lower Cretaceous, of Brazil. Bull. AMNH; 1990. pp. 1-15.

Grimes ST, Davies KL, Butler IB, Brock F, Edwards D, Rickard D, et al. Fossil plants from the Eocene London Clay: the use of pyrite textures to determine the mechanism of pyritization. J Geol Soc. 2002; 159: 493-501.

Gueriau, P.; Mocuta, C.; Dutheil, D.B.; Cohen, S.X.; Thiaudière, D.; The OT1 Consortium; Charbonnier, S.; Clément, G.; Bertrand, L. Trace Elemental Imaging of Rare Earth Elements Discriminates Tissues at Microscale in Flat Fossils. PLoS One. 2014; 9(1): e86946. doi:10.1371/journal.pone.0086946.

Heimhofer U, Ariztegui D, Lenniger M, Hesselbo SP, Martill DM, Rios-Netto AM. Deciphering the depositional environment of the laminated Crato fossil beds (early Cretaceous, Araripe Basin, north-eastern Brazil). Sedimentology. 2010; 57: 677-694.

Heimhofer U, Martill DM. The sedimentology and depositional environment of the Crato Formation. In: Martill DM, Bechly G, Loveridge R, editors. The Crato fossil beds of Brazil: window to an ancient world. Cambridge University Press; 2007. pp. 44-62.

Huerta-Diaz MA, Morse JA. Pyritization of trace metals in anoxic marine sediments. Geochim. Cosmochim. Acta. 1992; 56: 2681-2702.

Jarzembowski EA, Ross AJ. Insect Origination and Extinction in the Phanerozoic. In: Hart MB, editor. Biotic Recovery from Mass Extinction Events. Geological Society Special Publication; 1996, nº 102, pp. 65-78.

Kalliokoski J, Cathles L. Morphology, mode of formation, and diagenetic changes in framboids. Bull Geol Soc Fin. 1969; 41: 152—133.

Kan J, Obraztsova A, Wang Y, Leather J, Scheckel KG, Nealson KH. Apatite and chitin amendments promote microbial activity and augment metal removal in marine sediments. Open J. Met. 2013; 3: 51-61.

Kellner AWA. Membro Romualdo da Formação Santana, Chapada do Araripe, CE: um dos mais importantes depósitos fossíliferos do Cretáceo brasileiro. In: Schobbenhaus C, Campos DA, Qeiroz ET, Winge M, Berbert-Born MLC, editors. Sítios geológicos e paleontológicos do brasil, Departamento Nacional da Produção Mineral/Companhia de Pesquisa de Recursos Minerais/Comissão Brasileira de Sítios Geológicos e Paleobiológicos; 2002. pp. 121- 130.

Konhauser KO. Introduction to Geomicrobiology. Blackwell Publishing, Padstow; 2007.

Labandeira C. Why did Terrestrial Insect Diversity Not Increase During the Angiosperm Radiation? Mid-Mesozoic, Plant-Associated Insect Lineages Harbor Clues. In: Pontarotti P, editor. Evolutionary Biology: Genome Evolution, Speciation, Coevolution and Origin of Life. Springer International Publishing Switzerland; 2014, pp. 261-299.

Labandeira C, Eble GJ. The fossil record of insect diversity and disparity. In: Anderson J, de Wit M, Thackeray F, van Wyk B, editors. Gondwana alive: biodiversity and the evolving biosphere, Witwatersrand University Press; 2000.

Laflamme M, Schiffbauer JD, Narbonne JM, Briggs DEG. Microbial biofilms and the preservation of the Ediacara biota. Lethaia. 2011; 44: 203-213.

Lambrez M, Druschel GK, Thomsen-Ebert T, Gilbert B, Welch SA, Kemner KM, et al. Formation of sphalerite (ZnS) deposits in natural Biofilms of sulfate-reducing bacteria. Science. 2000; 290: 1744-1777.

Leng Y. Materials characterization: introduction to microscopic and spectroscopic methods, John Wiley & Sons, Singapore; 2008. 337 pp.

Leri AC, Hay MB, Lanzirotti A, Rao W, Myneni SCB. Quantitative determination of absolute organohalogen concentrations in environmental samples by X-ray absorption spectroscopy. Anal Chem. 2006; 78: 5711-5718.

Lidgard S, Crane PR. Quantitative analyses of the early angiosperm radiation. Nature. 1988; 331: 344-346.

Love LG. Micro-organic material with diagenetic pyrite from the lower Proterozoic Mount Isa shale and a carboniferous shale. Proc York Geol Soc. 1965; 35 (2), 9: 187-202.

MacLean LCW, Tyliszczak T, Gilbert PU, Zhou D, Pray TJ, Onstott TC, et al. A high-resolution chemical and structural study of framboidal pyrite formed within a low-temperature bacterial biofilm. Geobiology. 2008; 6: 471–480.

Maisey JG. Santana fossils: an illustrated atlas. T.F.H. Publications, Neptune City; 1991.

Martill DM. Preservation of fish in the Cretaceous Santana Formation of Brazil. Palaeontology 31, 1-18 (1988).

Martill DM, Bechly G, Loveridge R. The Crato fossil beds of Brazil: window to an ancient world, Cambridge University Press, New York; 2007a. 625 pp.

Martill DM, Loveridge RF, Heimhofer U. Dolomite pipes in the Crato Formation fossil lagerstätte (Lower Cretaceous, Aptian), of northeastern Brazil. Cret. Res. 2008; 29: 79-86.

Martill DM, Loveridge RF, Heimhofer U. Halite pseudomorphs in the Crato Formation (early Cretaceous, late Aptian) Araripe Basin, northeast Brazil: further evidence for hypersalinity. Cret. Res. 2007b; 28 (4): 613-620.

Martill DM, Wilby PR. Stratigraphy. In: Martill DM, editor. Fossils of the Santana and Crato Formations, Brazil, The Palaeontological Association, London; 1993. Chap. 3, p. 20-50.

Martínez-Delclòs X, Briggs DEG, Peñalver E. Taphonomy of insects in carbonates and amber. Palaeogeogr. Palaeoclimatol. Palaeoecol. 2004; 203: 19-64.

Martínez-Delclòs X, Martinell J. The oldest known record of social insects. J Paleontol. 1995; 69: 594-599.

McNamara ME. The taphonomy of colour in fossil insects and feathers. Palaeontology. 2013; 56: 557-575.

Melendez I, Grice K, Trinajstic K, Ladjavardi M, Greenwood P, Thompson K. Biomarkers reveal the role of photic zone euxinia in exceptional fossil preservation: an organic geochemical perspective. Geology. 2012 Nov 06. doi:10.1130/G33492.1.

Menon F, Martill DM. Taphonomy and Preservation of Crato Formation Arthropods. In: Martill DM, Bechly G, Loveridge R, editors. The Crato fossil beds of Brazil: window to an ancient world. Cambridge University Press; 2007. pp. 79-96.

Narbonne GM. The Ediacara Biota: Neoproterozoic origin of animals and their ecosystems. Annu. Rev. Earth Planet. Sci. 2005; 33: 421–42.

Neugebauer E. The krill chitin and some aspects of metals transport in antarctic sea water. Pol. Polar Res. 1986; 371-376.

Neumann, V. H. M. L. Estratigrafia, Sedimentologia, Geoquimica y Diagenesis de los Sistemas Lacustres Aptiense-Albienses de la Cuenca de Araripe (Noreste De Brasil). Tesis de Doctorado, Universitat de Barcelona, Barcelona; 1999.

Neumann VH, Aragão MANF, Valença LMM, Leal JP. Ambientes lacustres. In: Silva AJCLP, Aragão MANF, Magalhães AJC, organizers. Ambientes de sedimentação siliciclástica do Brasil, Editora Becca, São Paulo; 2008. Chap. V, p. 132-169.

Neumann VH, Borrego AG, Cabrera I, Dino R. Organic matter composition and distribution through the Aptian-Albian lacustrine sequences of the Araripe Basin, northeastern Brazil. Int J Coal Geol. 2003; 54: 21-40.

Neumann VH, Cabrera L. Características hidrogeológicas gerais, mudanças de salinidade e caráter endorréico do sistema lacustre Cretáceo do Araripe, NE Brasil. Rev. Geol. 2002; 15: 43-54.

Neumann VH, Cabrera L, Mabesoone JM, Valença LMM, Silva AL. Ambiente sedimentar e fácies da seqüência lacustre Aptiana-Albiana da Bacia do Araripe, NE do Brasil. In: Boletim do 6º Simpósio sobre o Cretáceo do Brasil. 6º Simpósio sobre o Cretáceo do Brasil, São Pedro. 2002; p. 37-41.

Neuville DR, Ligny D, Henderson GS. Advances in Raman spectroscopy applied to Earth and material sciences. In: Henderson GS, Neuville DR, Downs RT, editors. Spectroscopy methods in mineralogy and materials sciences, Reviews in mineralogy and geochemistry, v. 78, Mineralogical Society of America, Chantilly; 2014. Chap. 13, p. 509-541.

Nicholson DB, Mayhew PJ, Ross AJ. Changes to the Fossil Record of Insects Through Fifteen Years of Discovery. PLoS ONE. 2015; 10(7): e0128554. doi:10.1371/journal.pone.0128554.

Noffke N, Gerdes G, Klenke T, Krumbein WE. Microbially induced sedimentary structures-a new category within the classification of primary sedimentary structures. J. Sediment. Res. 2001; 71 (5): 649-656.

Ohfuji H, Rickard D. Experimental syntheses of framboids—a review. Earth-Sci Rev. 2005; 71: 147-170.

Oliveira et al. Large-field electron imaging and X-ray elemental mapping unveil the morphology, structure, and fractal features of a Cretaceous fossil at the centimeter scale. Anal. Chem. 2015; 87, 10088–10095.

Orr PJ, Briggs DEG, Kearns S. Taphonomy of exceptionally preserved crustaceans from the upper Carboniferous of southeastern Ireland. Palaios. 2008; 23: 298-312.

Osés GL. Artrópodes fósseis do Membro Crato (Formação Santana, Bacia do Araripe, Eocretáceo, NE do Brasil): levantamento taxonômico, tafonômico e paleoecológico utilizando técnicas não-destrutivas. Monografia de Formatura, Universidade de São Paulo, São Paulo; 2013.

Pacheco MLAF et al. Insights into the skeletonization, lifestyle, and affinity of the unusual Ediacaran fossil *Corumbella*. PLoS One. 2015; 10: e0114219. doi:10.1371/journal.pone.0114219.

Pan Y, Sha J, Fürsich FT. A model for organic fossilization of the early Cretaceous Jehol lagerstätte based on the taphonomy of ‘‘*Ephemeropsis trisetalis*’’. Palaios. 2014; 29: 363-377.

Pasteris JD, Wopenka B. Necessary, but not sufficient: Raman identification of disordered carbon as a signature of ancient life. Astrobiology. 2003; 3: 727-738.

Perez CA, Radtke M, Sánchez HJ, Tolentino H, Neuenshwander et al. Synchrotron radiation X-ray fluorescence at the LNLS: beamline instrumentation and experiments. X Ray Spectrom. 1999; 28: 320-326.

Peterson JE, Lenczewski ME, Scherer RP. Influence of microbial biofilms on the preservation of primary soft tissue in fossil and extant archosaurs. PLoS ONE. 2010; 5 (10): e13334. doi:10.1371/journal.pone.0013334.

Pfeffer C. et al. Filamentous bacteria transport electrons over centimetre distances. Nature. 2012; 491: 218-221.

Pinheiro FL, Horn BLD, Schultz CL, de Andrade JAFG, Sucerquia PA. Fossilized bacteria in a Cretaceous pterosaur headcrest. Lethaia. 2012; 45: 495–499.

Ponte FC, Ponte-Filho FC. Estrutura geológica e evolução da Bacia do Araripe, DNPM, 4º e 10º Distritos Regionais, Recife. 1996; 68 pp.

Popa R, Kinkle BK, Badescu A. Pyrite framboids as biomarkers for iron-sulfur systems. Geomicrobiol J. 2004; 21 (3): 193-206.

Raff EC, Schollaert KL, Nelson DE, Donoghue PCJ, Thomas C-W, Turner FR, et al. Embryo fossilization is a biological process mediated by microbial biofilms. Proc Natl Acad Sci U S A. 2008; 105 (49): 19360–19365.

Ramseyer L, Garling D, Hill G, Link J. Effect of dietary zinc supplementation and phytase pre-treatment of soybean meal or corn gluten meal on growth, zinc status and zinc-related metabolism in rainbow trout, *Oncorhynchus mykiss.* Fish Physiol. Biochem. 1999; 20: 251–261.

Rios-Netto ADM, Regali MDSP, Carvalho IDS, Freitas FID. Palinoestratigrafia do intervalo Alagoas da Bacia do Araripe, Nordeste do Brasil. Rev. Bras. Geoc. 2002; 42: 331-342.

Riquelme F, Alvarado-Ortega J, Ruvalcaba-Sil JL, Aguilar-Franco M, Porras-Múzquiz H. Chemical fingerprints and microbial biomineralization of fish muscle tissues from the late Cretaceous Múzquiz Lagerstätte, Mexico. Rev. Mex. C. Geol. 2013; 30(2): 417-435.

Riquelme F, Ruvalcaba-Sil JL, Alvarado-Ortega J. Palaeometry: non-destructive analysis of fossil materials. Bol Soc Geol Mex. 2009; 61(2): 177-183.

Sagemann J, Bale SJ, Briggs DEG, Parkes RJ. Controls on the formation of authigenic minerals in association with decaying organic matter: an experimental approach. Geochim Cosmochim Acta. 1999; 63 (7/8): 1083–1095.

Sansom RS, Gabbott SE, Purnell MA. Atlas of vertebrate decay: a visual and taphonomic guide to fossil interpretation. Palaeontology. 2013; 56: 457–474.

Sawlowicz Z. Pyrite framboids and their development: a new conceptual mechanism. Geol Rundsch. 1993; 82: 148-156.

Sawlowicz Z, Kaye TG. Replacement of iron sulphides by oxides in the dinosaur bone from the Lance Fm. (Wyoming, USA) – preliminary study. Min. Pol. Spec. Pap. 2006; 29, 184-187.

Schaal S, Ziegler W, editors. Messel: an insight into the history of life and of the Earth, Oxford University Press; 1992. 322pp.

Schiffbauer JD, Xiao S, Cai Y, Wallace AF, Hua H, Hunter J. A unifying model for Neoproterozoic–Palaeozoic exceptional fossil preservation through pyritization and carbonaceous compression. Nat Commun. 2014; 5: 5754. doi: 10.1038/ncomms6754.

Schopf JW. Microfossils of the early Archean Apex chert: new evidence of the antiquity of life. Science. 1993; 260: 640–646.

Schopf JW, Kudryavtsev AB. Confocal laser scanning microscopy and Raman imagery of ancient microscopic fossils. Prec. Res. 2009; 173: 39-49.

Schwark L. Exceptional preservation of microbial lipids in Paleozoic to Mesoproterozoic sediments. Geology. 2013; 41: 287-288.

Schweitzer MH. Soft Tissue preservation in terrestrial Mesozoic vertebrates. Annu. Rev. Earth Planet. Sci. 2011; 39: 187–216.

Seilacher A, Reif W-E, Westphal F. Sedimentological, ecological and temporal patterns of fossil lagerstätten. Philos Trans R Soc Lond B Biol Sci. 1985; 311: 5-23.

Silva AL. Estratigrafia Física e Deformação do Sistema Lacustre Carbonático (Aptiano-Albiano) da Bacia do Araripe em Afloramentos Selecionados**.** Dissertação de Mestrado, Universidade Federal de Pernambuco, Recife; 2003.

Silva AL, Neumann VH, Cabrera L. Facies carbonáticas laminadas da Formação Crato (Aptiano), Bacia do araripe: litofácies, microfácies e microestruturas. In: Boletim do 6º Simpósio sobre o Cretáceo do Brasil. 6º Simpósio sobre o Cretáceo do Brasil, São Pedro. 2002; p.31-36.

Silva MAM. Evaporitos do Cretáceo da Bacia do Araripe: ambientes de deposição e história diagenética. Bol. Geoc. Petr. 1988; 2: 53-63.

Šípková A, Száková J, Tlustoš P. Affinity of Selected Elements to Individual Fractions of Soil Organic Matter. Water, Air & Soil Poll. 2013; 225: 1802.

Skei JM. Formation of framboidal iron sulfide in the water of a permanently anoxic fjord-Framvaren, South Norway. Mar Chem. 1988; 23: 345-352.

Soares LPCM, Kerber BB, Osés GL, de Oliveira AM, Pacheco MLAF. Paleobiologia e evolução: o potencial do registro fossilífero brasileiro. Rev. Esp. 2013; 2: 24-40.

Sole VA, Papillon E, Cotte M, Walter P, Susini J. A multiplatform code for the analysis of energy-dispersive X-ray fluorescence spectra. Spectrochim. Acta Part B At. Spectrosc. 2007; 62: 63-68.

Staniskiene B, Matusevicius P, Budreckiene R, Skibniewska KA. Distribution of heavy metals in tissues of freshwater fish in Lithuania. Polish. J. Environ. Stud. 2006; 15: 585-591.

Stankiewicz BA et al. Alternative origin of aliphatic polymer in kerogen. Geology. 2000; 28: 559–562.

Szczepanik P, Sawłowicz Z, Bak M. Pyrite framboids in pyritized radiolarian skeletons (Mid-Cretaceous of the Pieniny Klippen Belt, Western Carpathians, Poland). An Soc Geol Pol. 2004; 74: 35–41.

Toporski JKW, Steele A, Westall F, Avci R, Martill DM, McKay DS. Morphologic and spectral investigation of exceptionally well-preserved bacterial biofilms from the

Oligocene Enspel formation, Germany. Geochim Cosmochim Acta. 2002; 66: 1773–1791.

Trewin NH. History of research on the geology and palaeontology of the Rhynie area, Aberdeenshire, Scotland. Trans. R. Soc. Edinb.: Earth Sci. 2003; 94: 285-297.

Vandenbroucke M, Largeau C. Kerogen origin, evolution and structure. Organ. Geochem. 2007; 38: 719–833.

Verma HR. Atomic and nuclear analytical methods: XRF, Mössbauer, XPS, NAA and Ion-Beam Spectroscopic techniques. Springer-Verlag, Berlin; 2007, 376 pp.

Viana MS, Neumann VH. O Membro Crato da Formação Santana: riquíssimo registro de fauna e flora do Cretáceo. In: Schobbenhaus C, Campos DA, Qeiroz ET, Winge M, Berbert-Born MLC, editors. Sítios geológicos e paleontológicos do brasil, 5. Departamento Nacional da Produção Mineral/Companhia de Pesquisa de Recursos Minerais/Comissão Brasileira de Sítios Geológicos e Paleobiológicos; 2000. pp. 113-120.

Wacey D, Kilburn MR, Saunders M, Cliff J, Brasier MD. Microfossils of sulphur-metabolizing cells in 3.4-billion-year-old rocks of Western Australia. Nat. Geosc. 2011; 4: 698-702.

Wacey et al. Uncovering framboidal pyrite biogenicity using nano-scale CNorg
Wang B, Zhao F, Zhang H, Fang Y, Zheng D. Widespread pyritization of insects in the early Cretaceous Jehol biota. Palaios. 2012; 27: 707-711.

Wang B, Zhao F, Zhang H, Fang Y, Zheng D. Widespread pyritization of insects in the early Cretaceous Jehol biota. Palaios. 2012; 27: 707-711.

Westall F, de Vries ST, Nijman W, Rouchon V, Orberger B, Pearson V, et al. The 3.466 Ga ‘Kitty’s Gap Chert,’ an early Archean microbial ecosystem. Geol Soc Am Spec Pap. 2006; 405: 105–131.

Westrich JT, Berner RA. Limnol. Oceanogr. 1984; 29: 236-249.
White SN. Laser Raman spectroscopy as a technique for identification of seafloor hydrothermal and cold seep minerals. Chem. Geol. 2009; 259(3-4): 240-252.

Wilby PR, Briggs DEG. Taxonomic trends in the resolution of detail preserved in fossil phosphatized soft tissues. Geobios. 1997; 20: 493-502.

Wilby PR, Briggs DEG, Bernier P, Gaillard C. Role of microbial mats in the fossilization of soft tissues. Geology. 1996; 24 (9): 787-790.

Wilkin RT, Barnes HL. Formation processes of framboidal pyrite. Geochim. Cosmochim. Acta. 1997; 61: 323-339.

Wilkin RT, Barnes HL, Brantley SL. The size distribution of framboidal pyrite in modern sediments: an indicator of redox conditions. Geochim. Cosmochim. Acta. 1996; 60: 3897-3912.

Appendix 1 – Article “Paleometry: a brand new area in Brazilian science”.

Materials Research. 2014; 17(6): 1434-1441
DOI: http://dx.doi.org/10.1590/1516-1439.288514

Paleometry: A Brand New Area in Brazilian Science

Adriana de Oliveira Delgado[a]*, Pedro Victor Buck[b], Gabriel Ladeira Osés[c], Renato Pirani Ghilardi[d], Elidiane Cipriano Rangel[e], Mirian Liza Alves Forancelli Pacheco[b]

[a]Centro de Ciências e Tecnologias para Sustentabilidade, Universidade Federal de São Carlos – UFSCar, Rod. João Leme dos Santos, Km 110, CEP 18052-780, Sorocaba, SP, Brazil
[b]Centro de Ciências Humanas e Biológicas, Universidade Federal de São Carlos – UFSCar, Rod. João Leme dos Santos, Km 110, CEP 18052-780, Sorocaba, SP, Brazil
[c]Instituto de Geociências, Universidade de São Paulo – USP, Rua do Lago, 562, Cidade Universitária, CEP 05508-080, São Paulo, SP, Brazil
[d]Faculdade de Ciências, Universidade Estadual Paulista "Júlio de Mesquita Filho" – UNESP, Av. Eng. Luiz Edmundo Carrijo Coube, 14-01, CEP 17033-360, Bauru, SP, Brazil
[e]Universidade Estadual Paulista "Júlio de Mesquita Filho" – UNESP, Campus Experimental de Sorocaba, Avenida Três de Março, 511, CEP 18087-180, Sorocaba, SP, Brazil

Received: April 8, 2014; Revised: December 18, 2014

Paleometry is a promising research field that brings together different areas, such as physics and chemistry, applied to paleobiological issues. In spite of being recognized abroad, it is a new research field in Brazil. The most important characteristic is the application of mostly non-destructive techniques to the study of fossils. This work compiles some paleometrical applications to different geological contexts, such as the synthesis of hard skeleton in *Corumbella werneri*, geochemical aspects about fresh water bivalves from the Bauru Group and the exceptional preservation of arthropods from the Crato Member. Diffuse Reflectance Infrared (DRIFT) and Energy Dispersive X-ray Spectroscopy (EDX) were complementary to elucidate the types of skeletogenesys in *Corumbella*. In the case of the bivalves, DRIFT revealed to be important to elucidate aspects about death and fossilization. Among arthropods, morphological analysis with Scanning Electron Microscopy (SEM) associated with EDX was more profitable to understand fossilization process and paleoenvironmental implications.

Keywords: *paleometry, FTIR, SEM, EDX, calcite, fossilization*

1. Introduction

Paleobiology studies the history and evolution of life on Earth by the means of fossil record. However, this is not an easy task. During the fossilization process, taphonomy (everything that occurs after the death of an organism, until its burial and discovery by the paleontologist)[1] can alter the morphology of the organism, hide important structures and build artifacts that can lead paleontologists to misinterpretations[2-4].

Worldwide, in just a few years, the use of a series of advanced and/or high resolution techniques, mostly non-destructive, has proved to be important for the study of very old and rare well preserved fossils, in order to assist the work of paleontologists. The application of these techniques (*e.g.* Raman and FT-IR spectroscopies[5,6], X ray microCT[7-9], NanoSIMs[10]) to the study of fossils has expanded research in paleobiology and led it to a higher level of sophistication, and it is called paleometry[11].

Inspired in the well established Brazilian archaeometry which studies archaeological, etnographical and the so called patrimonial materials[12-16], the application of paleometrical techniques to the study of many Brazilian fossils is still growing[17-21] and opening new perspectives to deepen our knowledge of the biological affinities and paleoecological aspects. Some exceptionally well-preserved fossils (e.g. the Ediacaran Corumbá Group and the Cretaceous Araripe Basin) have become, in fact, scientific challenges to the development of twenty-first century Brazilian paleobiology. Now, our new paleontology requires, not only the basic description of the oldest forms of life on Earth, but also an understanding and foundation of most modern concepts and methodological assumptions to bring extinct contexts to life. For Brazilian paleontologists, paleometrical techniques have proved to be important, for example, both for the elucidation of the chemical composition of paleoinvertebrate skeletons[22,23], and to understand the processes of fossilization and paleoenvironment in contexts of climate and geochemical changes in the past[20].

In this work, the potential of some of these techniques to the study of invertebrate fossils collected in different and important paleontological sites in Brazil, as seen in Figure 1: *Corumbella werneri* from the Corumbá group (Ediacaran); Unionoida freshwater mollusk from the Bauru Group (Cretaceous); and insects of the Crato Formation from the Araripe Basin (Cretaceous) is presented. The data here compiled is important both to the paleobiological insights

*e-mail: adelgado@ufscar.br

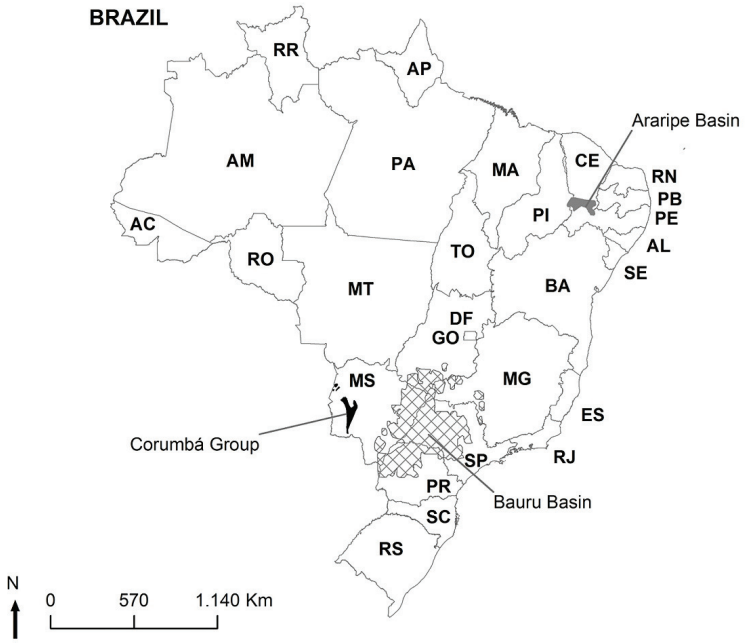

Figure 1. Brazil map with the locations of geological settings where fossils used in this work occur.

and in the field of materials characterization in order to boost paleometry in Brazil.

2. Paleontological Aspects and Motivation

Corumbella werneri (Ediacaran, Corumbá Group) is a fossil preserved in marls and shales. It was considered as an elongated polyhedral tube: a kind of fixed life form of cnidarian medusas that lived ca. 543 million years ago[22]. Their fossils were firstly documented in Ladário and Corumbá, Brazil[24]. Since it was one of the first animals on Earth capable of building a real skeleton, studies with *Corumbella* are important to understand the origin and evolution of skeletonized animals on Earth.

Unionoida mollusks (Cretaceous, Bauru Group) are typically preserved in freshwater sandstones, indicative of energetic processes in paleoenvironmental reconstructions[25]. Our samples were collected in the municipality of Monte Alto, SP, Brazil. Paleometrical analysis has proved to be important to elucidate how these bivalves died and why the vast majority of specimens have articulated valves with sedimentary matrix inside.

The fossil insects from the Crato Formation (Cretaceous, Araripe Basin) are worldwide known for their high level of preservation in carbonates, including three-dimensional specimens with soft tissues preserved[26-28]. These fossils have important paleobiological and paleoenvironmental information and it is, therefore, crucial to understand the taphonomic processes that led to their exceptional preservation. Despite having been briefly discussed in previous studies[26,29], the taphonomy of the insects of the Crato Formation is still an unresolved question.

3. Experimental

The fossils have been characterized at the Laboratory of Characterization of Materials (LMCMat) at UNESP (Sorocaba, Brazil), in collaboration with the Group of Plasmas and Materials and at the Brazilian Nanotechnology National Laboratory (LNNano) at CNPEM (Campinas, Brazil).

The chemical composition of *Corumbella werneri*, (Figure 2a) and the Unionoida freshwater mollusk (Figure 2b) were investigated by using Diffuse Reflectance Infrared Fourier Transform Spectroscopy (DRIFT) at LMCMat. DRIFT analysis revealed to be the most appropriate for IR spectroscopy due to the small amount of available samples and to the configuration of the spectrometer sample holder. For the analysis, grated powder of the fossils and the respective rock matrices were collected and dried at 50 °C. The dried powder was placed in a cylindrical sample cup that was partially filled with KBr powder, forming an upper layer with the material of interest. According to J. Ji et al.[30], the use of unmixed layers saves a significant amount of time and does not interfere with the sensitivity to carbonates and sandstones, which are the main components in the analyzed fossils. The ratio of the amount of sample and KBr powder was kept approximately to 1:9. The layers were carefully pressed into the cup for the measurement of the sample spectra and another sample cup filled with only KBr powder was used for the measurement of the background spectrum. The analyses were carried out with a *Jasco FT-IR 410* spectrometer in the range of 600-4000 cm^{-1}, with a resolution of 4 cm^{-1} and average of 100 scans.

The micromorphology characterization of *Corumbella werneri* was performed at LNNano, with an electron

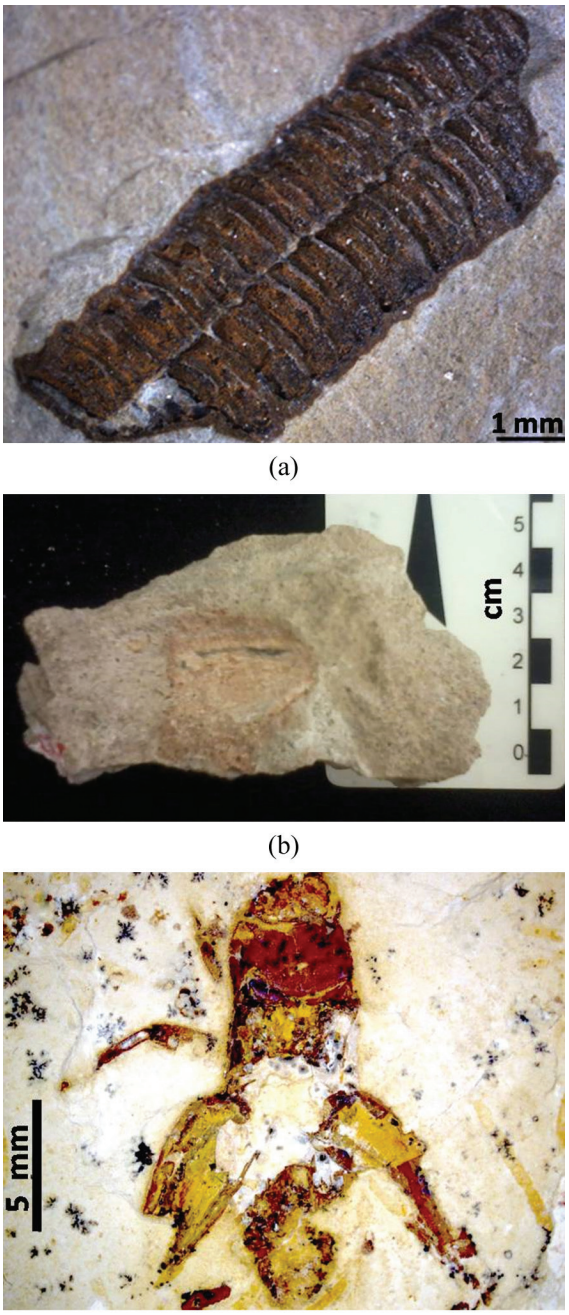

Figure 2. Studied fossils: (a) *Corumbella werneri* (Ediacaran, Corumbá Group); (b) Unionoida freshwater mollusk (Cretaceous, Bauru Group). (c) Cricket (Cretaceous, Araripe Basin) from IGc/USP collection, specimen n. GP/1E-7105.

microscope *FEI Quanta 650 FE* in the mode of secondary electrons detection, with acceleration voltages of 10 kV. Energy Dispersive X-ray Spectroscopy (EDX) was also carried out using an *X-Max* detector in semi-quantitative and mapping mode, in order to identify the distribution of chemical elements and compare it to FTIR results.

The fossil cricket of the Crato Formation (Figure 2c) was kindly lent to the researchers by IGc/USP collection (specimen n. GP/1E-7105). Its ultrastructure was characterized at LMCMat, analyzed by Scanning Electron Microscopy (SEM), with a *Jeol JSM6010* microscope, with acceleration voltage of 10 kV[20]. The fossil samples were coated with Au/Pd thin layer in order to improve the quality of the micrographs. EDX measurements with a *Jeol Dry SD Hyper Detector* were also applied to the sample, in order to identify the chemical composition of the observed structures on the fossil surface and inside the specimen[20].

4. Results and Discussion

4.1. Corumbella werneri

Diffuse reflectance analyses, in Figure 3, give us information about the ultrastructure of the carapace of *Corumbella werneri* and the respective rock matrix. The main IR bands are indicated in Figure 3 and correspond to calcite[30-32]. It is worth pointing out that in the reflectance spectrum, the weak IR bands appear stronger than expected for the absorption and transmission spectra. This stems from the fact that in reflectance spectra there is no linear relationship between band intensity and concentration (as it occurs in transmission), and quantitative analyses by the DRIFT method are therefore rather complicated. The band in 2509 cm^{-1}, for example, is described as very weak and weak in the transmission spectra presented in works of Miller and Wilkins[33] and Huang and Kerr[31], respectively, while it can be considered strong in our work in consistence with the reflectance data presented by Ji et al.[30]. Since the quantitative approach is not necessary at this point of our study, our research will focus on qualitative analysis that can provide paleobiologists with new important information.

Table 1 presents the comparison between the IR reflectance bands of the fossil of *C. werneri* and its rock matrix (Figure 3). The bands in the IR region from 600 to 1500 cm^{-1} occur due to the four fundamental modes of vibration of the carbonate ion (CO_3^{-2}): ν_1 is the symmetrical stretching of CO (ν_s); ν_2 is the out-of-plane bending of CO_3 (γ); ν_3 is the asymmetrical stretching of CO (ν_{as}); and ν_4 is the in-plane bending of OCO (δ)[31,34] . The ν_1 mode should be inactive in FTIR spectra due to the symmetry of the molecule[31,35], but since the studied sample (rock + fossil) presents several other minor constituents and impurities (common in sedimentary rocks), it is possible that bands at 1010 cm^{-1} for the fossil and 1160 cm^{-1} for the rock matrix are due to the ν_1 mode, which theoretically would occur at 1087 cm^{-1}. The vibrations at 875 and 711 cm^{-1} correspond to out-of-plane and in-plane bending, respectively. Both are observed in the carapace reflectance spectrum, but not in the rock matrix spectrum, despite being a marl (kind of shale carbonate rich rock). From the difference in spectra of the fossil and the rock, we can wonder if the synthesis of this hard exoskeleton leads to higher concentrations of the calcite in the carapace than in the surrounding rock medium. Finally, the asymmetrical stretching mode occurs at 1452 cm^{-1} as a broad band in the fossil reflectance spectrum with no obvious correspondent band in the rock spectrum. This band is actually a double degenerated band that is observed for pure materials as a doublet. The mixture of minor components in the matrix can be responsible for the

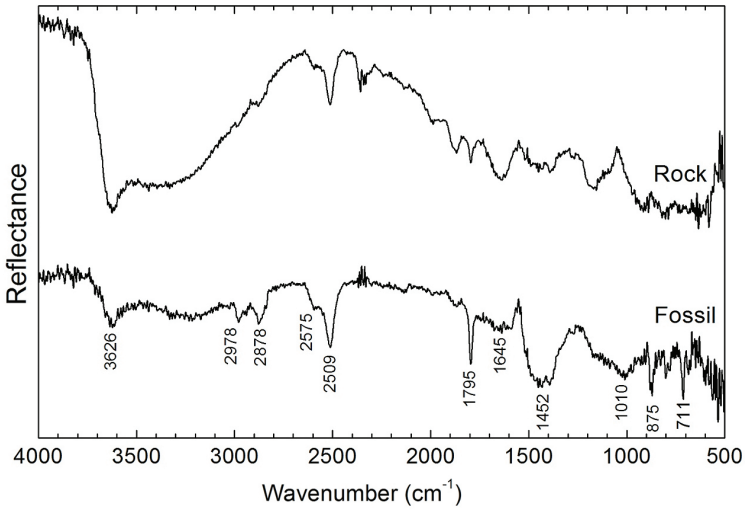

Figure 3. Diffuse reflectance infrared spectra of *Corumbella werneri* carapace and rock matrix. The positions of the absorption bands are indicated in the figure.

Table 1. Comparison of IR reflectance bands for analyzed fossils and their rock matrices.

Wavenumber (cm^{-1})			
C. werneri	**matrix**	**molusk**	**matrix**
3626	3622	3617	3668
2978	2983	2948	*
2878	2878	2877	*
2575	2594	2588	*
2509	2511	2508	*
---	2360	2362	*
1795	1796	*	*
1645	1641	*	*
1452	*	*	*
1010	1160	*	*
875	*	863-836	*
711	---	700	*

*refers to undistinguished bands of continuous noise.

enlargement of each line of the doublet, in a manner that they cannot be interpreted. The other observed bands of IR Reflectance are all regarded as vibrations of the carbonate ion in overtone modes and combinations of the fundamental modes[30,36]. Most of them appear both in the reflectance spectra of the *Corumbella* and in the rock with different relative intensities.

On the other hand, the large shoulders observed in 1000-1200 cm^{-1} and 1600-1800 cm^{-1} can be putative chitin, when compared with the reflectance data of analyzed chitin from black corals[37]. These shoulders are clearly not present in the spectrum of rock matrix, hence the assignment and interpretation of these will be further investigated in future work.

The EDX mapping (Figure 4) supports the assumption that there is higher concentration of calcium (attributed to calcite) in the carapace of *Corumbella* in comparison with the rock matrix. It is also possible to see in Figure 4c, that Fe atoms are more concentrated (density in gray scale) in the rock than in the fossil. Si, Al and O atoms were also detected by EDX and presented the same surface distribution as Fe atoms. The existence of O is related to the oxides present in the matrix. On the other hand, in Figure 4d, it is seen that Ca ions present a higher concentration in the carapace, with C atoms accompanying this tendency. The presence of Ca and C in the carapace denotes the presence of calcite in an organic carapace and, together with IR reflectance analysis, gives us evidence of a biomineralized exoskeleton.

As a technique for elemental characterization, EDX is important to complement IR Reflectance or FTIR Absorption spectroscopy. Moreover, the EDX mapping analysis allows the investigation of the distribution of element concentration with higher resolution than it could be achieved with IR spectroscopy.

The collected results from DRIFT and EDX spectroscopies reinforce, if not an entirely organic tegument[23], at least, a weakly mineralized *Corumbella* carapace[22], among one of the first skeletonized animals. The evolution of animal skeletogenesis could be linked to environmental changes, such as the oceanic chemistry, as well as selective pressures correlated with the appearance of new ecological relations, such as predator/prey ones[38].

4.2. Unionoida bivalve

The same approach previously described was applied to the bivalve. The identified IR reflectance bands are indicated in the spectrum in Figure 5 and listed in Table 1.

It is noticeable that the IR spectrum of rock does not contain any information about its chemical composition, since the continuous noise is quite high when compared to candidates to reflection bands. This occurs due to the fact that sedimentary rocks, such as sandstones, can be composed of different kinds of minerals and organic matter.

The IR reflectance spectrum of the fossil, on the other hand, presents bands that are attributed to calcite, as seen in Table 1. Since the reddish internal part of the mollusk should correspond to soft tissue fossilized in the interior

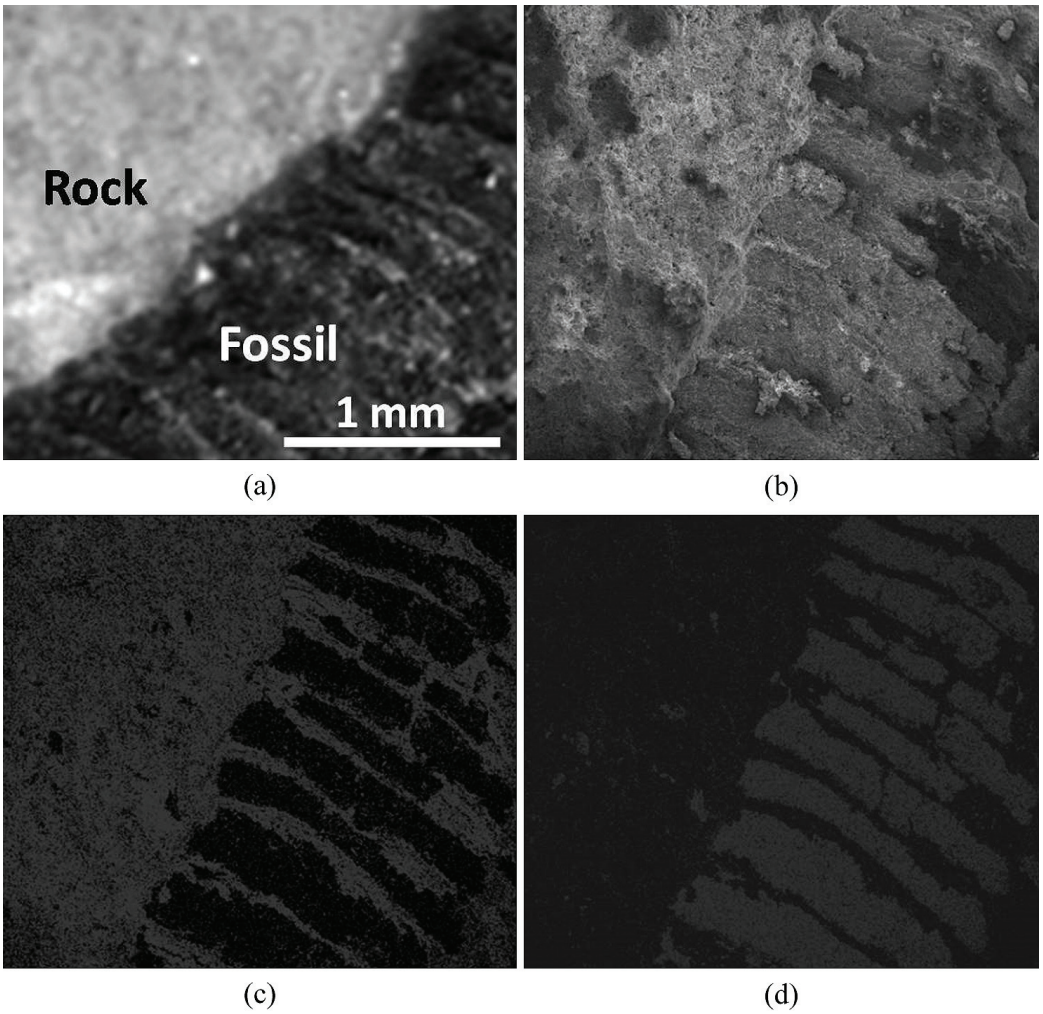

Figure 4. SEM/EDX analysis of *Corumbella werneri*: (a) Image of the analyzed portion of carapace and rock matrix. The scale in photograph refers to the all four images. (b) SEM micrograph of fossil and rock; (c) EDX map of the distribution of Fe on the sample; (d) EDX map of the distribution of Ca on the sample. For the figures (c) and (d), the lighter spots indicate higher concentration of elements, while the dark regions indicate the absence of the element.

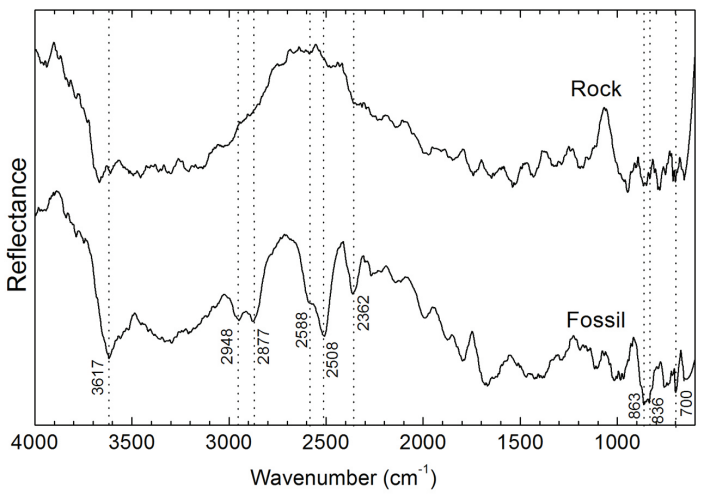

Figure 5. Diffuse reflectance infrared spectra of inner part of Unionoida bivalve and surround rock matrix. The positions of absorption bands that can be distinguish of the noise of spectrum of fossil are indicated in the figure.

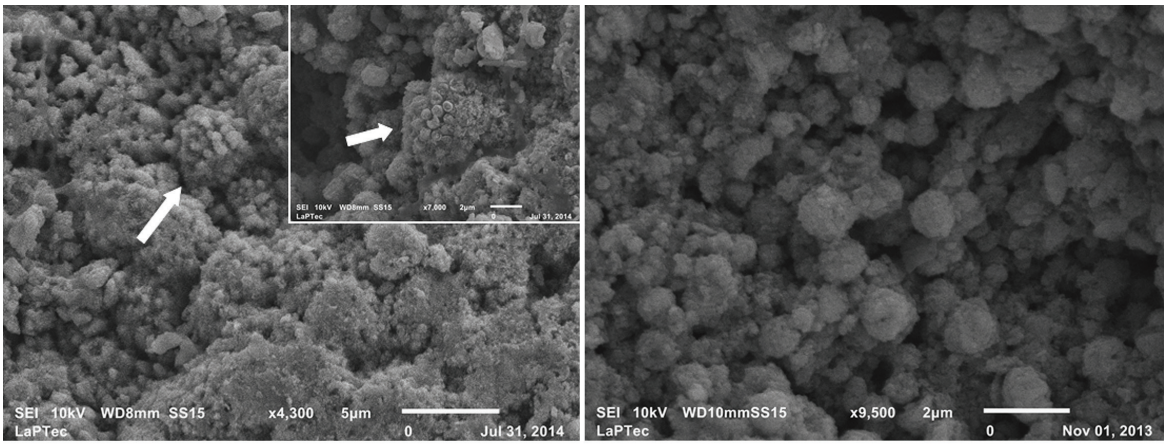

(a) (b)

Figure 6. Photomicrographs of the minerals which constitute the fossils from the Crato Formation. (a) Exoskeleton replaced by pseudomorphs of framboidal pyrite (indicated by arrow; detail of a well preserved pseudomorph). (b) Interior of the fossil, with preserved framboidal pyrite pseudomorps.

of the shell, the presence of calcite suggests models of fossilization via incorporation of calcite available in the internal part of the shell[39,40]. This can occur when the specimen is fossilized with closed and articulated valves, creating an internal system isolated from the environment. After death, in decomposition, closed valves may have solubilized, and calcite might have been trapped in the sediment within the valves.

4.3. Insect of the Crato Formation

SEM analysis of the fossil cricket from the Crato Formation was performed in order to investigate the characteristics of the minerals that replaced the original organic matter. It was found that the texture of the exoskeleton or carapace (Figure 6a) is different from the inner part of the specimen (Figure 6b). While the exoskeleton consists of pseudomorphs of framboidal pyrite >5µm in diameter, the inner portion of the fossil is filled with framboidal pyrite pseudomorphs with ca. 1µm of diameter. Pyrite is a metallic mineral with chemical formula FeS_2 (iron sulfide).The observed grains are interpreted as being pseudomorphs since their EDX analysis (Table 2) does not show the presence of sulfur in chemical composition. The pseudomorphs are covered with pliable structures here interpreted as mineralized extracellular polymeric substance (EPS) (Figure 7).

Data presented in Table 2, should be interpreted as an estimation of the chemical composition of the exoskeleton and the inner part of the fossil. Despite not being a quantitative analysis, the data gives valuable information about the presence or absence of key elements that can be associated with taphonomic and environmental processes.

EDX data supports that both external and internal portions of the fossils have iron and oxygen, suggesting that pyrite has been replaced by iron oxides/hydroxides due to weathering[20]. Furthermore, the inner part of the insects also presents small amounts of phosphorous and magnesium, that are not observed in the exoskeleton. These elements must be further investigated since there are is no definite evidence

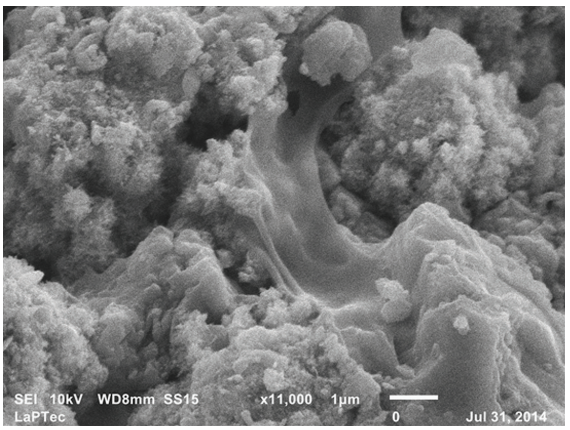

Figure 7. Pseudomorphs of framboidal pyrite covered by mineralized EPS.

Table 2. Estimated chemical composition of the exoskeleton and inner part of the insect of Crato Formation. Data were obtained with EDX in semi-quantitative mode. The errors were automatic calculated by the analysis software.

Atomic composition (%)		
element	**exoskeleton**	**inner part**
C	23.735 ± 0.010	24.697 ± 0.010
O	56.60 ± 0.04	60.63 ± 0.05
Na	0.575 ± 0.021	0.523 ± 0.021
Mg	---	0.369 ± 0.021
Al	0.914 ± 0.021	0.503 ± 0.021
Si	2.14 ± 0.03	1.067 ± 0.021
P	---	1.78 ± 0.03
Ca	5.51 ± 0.06	8.29 ± 0.07
Fe	10.533 ± 0.020	2.13 ± 0.13

that could relate them with intrinsic characteristics of the organisms neither extrinsic conditions of the environment or with taphonomic processes[41].

The textural differences verified between the carapace and the inner portion of the fossil might occur due to distinct

mechanisms of fossilization. The presence of framboidal pyrite pseudomorphs, replacing and infilling the fossil , which possibly indicates the oxidation of previously precipitated pyrite framboids, as well as their coating by EPS, strongly suggest the activity of sulfate reducing bacteria during diagenesis, as suggested elsewhere[29]. The very small size of the minerals may also account for the high degree of fidelity of preservation of the Crato Formation fossil insects[20].

5. Conclusion and Perspective

IR Reflectance and SEM/EDX analysis were successfully applied to the study of Brazilian fossils from different geological contexts contributing to the progress and broadening of paleometry in Brazil. The use of IR Reflectance instead of Transmittance allowed the observation of the bands that would appear weaker in transmission/absorption modes, which can be a great advantage for complex materials such as rocks and fossils. The EDX mapping showed to be an important complementary technique to: (a) Reflectance spectroscopy, bringing information about the distribution of elements on fossil surface enabling even higher resolution with IR analysis; (b) SEM morphological characterization, allowing elemental analysis of specific biological structures. Interpretative results contributed to clarify outstanding questions still open in paleobiology and in taphonomy, such as: (1) the understanding of evolutionary and geochemical trends that led to the origin and diversification of skeletonized animals such as the *Corumbella*; (2) the establishment of specific conditions that culminated in different types of fossilization in high energy environments, such as the Bauru Group; (3) the interpretation and comprehension of exceptional and rare well preserved soft parts, just like the case of insects from the Crato Formation. In this sense, paleometry has shed new light on material sciences studies and has opened a window to a brand new and exciting past for paleobiologists.

Acknowledgements

We would like to acknowledge Rafael Parra from LMCMat for SEM micrographs of insects and Professor Setembrino Petri from the University of São Paulo for having supported part of this work by supervising Gabriel L. Osés' final undergraduate monograph.

We also acknowledge LNNano/CNPEM for the use of SEM (Quanta) microscope; Fapesp (proc. 2009/02312-4; 2013/16545-6, 2013/06719-7 and 2013/06718-0) and CNPq for the financial support and M. Amália S. Ladeira and Izabel M. S. Ladeira from English for You (São Paulo, Brazil) for the language revision.

References

1. Behrensmeyer AK and Hook RW. Paleoenvironmental contexts and taphonomic modes in the terrestrial fossil record. In: Behrensmeyer AK, Damuth JD, DiMichele WA, Potts R, Hans-Dieter S and Wing SL. *Terrestrial ecosystems through time: evolutionary paleoecology of terrrrestrial plants and animals*. Chicago: University of Chicago Press; 1992. p. 15-136.
2. Waggoner BM. Interpreting the earliest metazoan fossils: What can we learn? *American Zoologist*. 1998; 38(6):975-982.
3. Lucas SG. Taphotaxon. *Lethaia*. 2001; 34(1):30. http://dx.doi.org/10.1080/002411601300068198.
4. Simões M, Rodrigues S, Leme JM and Van Iten H. Some Middle Paleozoic Conulariids (Cnidaria) as possible examples of taphonomic artifats. *Journal of Taphonomy*. 2003; 1(3):165-186.
5. Schopf JW and Kudryavtsev AB. Confocal laser scanning microscopy and Raman imagery of ancient microscopic fossils. *Precambrian Research*. 2009; 173(1-4):39-49. http://dx.doi.org/10.1016/j.precamres.2009.02.007.
6. Igisu M, Ueno Y, Shimojima M, Nakashima SM, Awramik SM, Ohta H, et al. Micro-FTIR spectroscopic signatures of bacterial lipids in proterozoic microfossils. *Precambrian Research*. 2009; 173(1-4):19-26. http://dx.doi.org/10.1016/j.precamres.2009.03.006.
7. Chen JY, Bottjer DJ, Davidson EH, Li G, Gao F, Cameron RA, et al. Phase contrast synchrotron X-ray microtomography of Ediacaran (Doushantuo) metazoan microfossils: phylogenetic diversity and evolutionary implications. *Precambrian Research*. 2009; 173(1-4):191-200. http://dx.doi.org/10.1016/j.precamres.2009.04.004.
8. Pidassa B. *High-resolution X-ray imaging of fossil samples*. [Thesis]. Munich: Technische Universität München; 2013.
9. Pacheco MLAF, Galante D, Leme J, Rodrigues F, Bidola P, Hagadorn W, et al. Insights into the skeletonization, lifestyle, and affinity of the unusual Ediacaran fossil Corumbella. *PLoS ONE*. 2014; (in press)
10. Oehler DZ, Robert F, Walter MR, Sugitani K, Allwood A, Meibom A, et al. NanoSIMS: Insights to biogenicity and syngeneity of Archean carbonaceous structures. *Precambrian Research*. 2009; 173(1-4):70-78. http://dx.doi.org/10.1016/j.precamres.2009.01.001.
11. Riquelme F, Ruvalcaba-Sil JL and Alvarado-Ortega J. Palaeometry: Non-destructive analysis of fossil materials. *Boletín de la Sociedad Geológica Mexicana*. 2009; 61(2):177-183.
12. Rosalie David A, Edwards HGM, Farwell DW and De Faria DLA. Raman Spectroscopic Analysis of Ancient Egyptian Pigments. *Archaeometry*. 2001; 43(4):461-473. http://dx.doi.org/10.1111/1475-4754.00029.
13. Silva FA, Appoloni CR, Quiñones FRE, Santos AO, Da Silva LM, Barbieri PF, et al. A arqueometria e a análise de artefatos cerâmicos: um estudo de fragmentos cerâmicos etnográficos e arqueológicos por fluorescência de Raios X (EDXRF) e transmissão Gama. *Revista de Arqueologia*. 2004; 17(1):41-61.
14. Rizzuto MA, Tabacniks MH, Added N, Barbosa MDL, Curado JF, Pascholati PR, et al. Pixe externo para análises de objetos de arte e arqueologia. *Revista Brasileira de Arqueometria, Restauração e Conservação*. 2007; 1:309 -312.
15. Lima SC, Rizzutto MA, Added N, Barbosa MDL, Trindade GF and Fleming MIDA. Pre-Hispanic ceramics analyzed using PIXE and radiographic techniques. *Nuclear Instruments & Methods in Physics Research. Section B, Beam Interactions with Materials and Atoms*. 2011; 269(24):3025-3031. http://dx.doi.org/10.1016/j.nimb.2011.04.064.
16. Jamieson RW, Hancock RGV, Beckwith LA and Pidruczny AE. Neutron activation analysis of Inca and colonial ceramics from

central highland Ecuador. *Archaeometry*. 2013; 55(2):198-213. http://dx.doi.org/10.1111/j.1475-4754.2012.00683.x.

17. Lima RJC, Saraiva AAS, Lanfredi S, Nobre MAL, Freire PTC and Sasaki JM. Caracterização espectroscópica de peixe do período cretáceo (Bacia do Araripe). *Quimica Nova*. 2007; 30(1):22-24. http://dx.doi.org/10.1590/S0100-40422007000100005.
18. Fairchild TR, Sanchez EAM, Pacheco MLAF and Leme JM. Evolution of Precambrian life in the Brazilian geological record. *International Journal of Astrobiology*. 2012; 11(4):309-323. http://dx.doi.org/10.1017/S1473550412000183.
19. Freire PTC, Abagaro BTO, Sousa Filho FE, Silva JH, Saraiva AAF, Brito DDS, et al. Pyritization of fossils from the Lagerstätte Araripe Basin, Northeast Brazil, from the Cretaceous Period. In: Whitley N and Vinsen PT, editors. *Pyrite: synthesis, characterization and uses*. New York: Nova Science Publishers Inc; 2013. p. 123-140.
20. Osés GL. *Artrópodes fósseis do Membro Crato (Formação Santana, Bacia do Araripe, Eocretáceo, NE do Brasil): levantamento taxonômico, tafonômico e paleoecológico utilizando técnicas não-destrutivas*. [Monografia]. São Paulo: Universidade de São Paulo; 2013.
21. Buck PV. *Paleometria aplicada ao estudo de fósseis brasileiros: implicações evolutivas e tafonômicas*. [Monografia]. Sorocaba: Universidade Federal de São Carlos; 2013.
22. Pacheco MLAF, Leme J and Machado A. Taphonomic analysis and geometric modelling for the reconstitution of the Ediacaran metazoan *Corumbella werneri* Hahn *et al*. 1982 (Tamengo Formation, Corumbá Basin, Brazil). *Journal of Taphonomy*. 2011; 9(4):269-283.
23. Warren LV, Pacheco MLAF, Fairchild TR, Simões MG, Riccomini C, Boggiani PC, et al. The Dawn of animal skeletogenesis: ultrastructural analysis of Ediacaran metazoan *Corumbella werneri. Geology*. 2012; 40(8):691-694. http://dx.doi.org/10.1130/G33005.1.
24. Hahn G, Hahn R, Leonardos OH, Pflug HD and Walde DHG. Kfrperlich erhaltene Scyphozoen Reste aus dem Jungprekambrium Brasiliens. *Geologica et Paleontologica*. 1982; 16:1-18.
25. Ghilardi RP, D'Ágosta FCP, Alves K and Campos ACA. Tafonomia de moluscos fósseis do Grupo Bauru (Cretáceo Superior, bacia Bauru), na região do Município de Monte Alto, São Paulo, Brasil. *Boletim do Museu Paraense Emílio Goeldi. Ciências Naturais*. 2011; 6(2):197-206.
26. Grimaldi D. *Insects from the Santana Formation, lower cretaceous, of Brazil*. New York: Bulletin of the AMNH; 1990.
27. Grimaldi D. The Santana Formation insects. In: Maisey JG. *Santana fossils: an illustrated atlas*. Neptune City: T.F.H. Publications; 1991. p. 379-406.
28. Martill DM. *Fossils of the Santana and Crato Formations, Brazil*. London: Palaeontological Association; 1993.
29. Menon F and Martill DM. Taphonomy and preservation of Crato Formation arthropods. In: *The crato fossil beds of brazil: window to an ancient world*. Cambridge: Cambridge University Press; 2007, p. 79-96.. http://dx.doi.org/10.1017/CBO9780511535512.008.
30. Ji J, Ge Y, Balsam W, Damuth JE and Chen J. Rapid identification of dolomite using a Fourier Transform Infrared Spectrophotometer (FTIR): A fast method for identifying Heinrich events in IODP Site U1308. *Marine Geology*. 2009; 258(1-4):60-68. http://dx.doi.org/10.1016/j.margeo.2008.11.007.
31. Huang CK and Kerr PF. Infrared study of the carbonate minerals. *The American Mineralogist*. 1960; 45(3-4):311-324.
32. National Institute of Standards and Technology. *Calcium carbonate (calcite)*. Material measurement laboratory; 2011. Available from: <http://www.nist.gov/mml/>. Access in: 24/03/2014.
33. Miller FA and Wilkins CF. Infrared spectra and characteristic frequencies of inorganic Ions. *Analytical Chemistry*. 1952; 24(8):1253-1294. http://dx.doi.org/10.1021/ac60068a007.
34. Bessler KE and Rodrigues LC. Os Polimorfos de carbonato de cálcio: Uma síntese fácil de aragonita. *Quimica Nova*. 2008; 31(1):178-180. http://dx.doi.org/10.1590/S0100-40422008000100032.
35. Reichenbächer M and Popp J. *Challenges in molecular structure determination*. Springer; 2012.. http://dx.doi.org/10.1007/978-3-642-24390-5.
36. Clark RN. Spectroscopy of rocks and minerals, and principles of spectroscopy. In: Rencz AN, editors. *Remote sensing for the earth sciences – Manual of remote sensing*. New York: John Wiley & Sons; 1999. p. 3-58. v. 3.
37. Bo M, Bavestrello G, Kurek D, Paasch S, Brunner E, Born R, et al. Isolation and identification of chitin in the black coral Parantipathes larix (Anthozoa: Cnidaria). *International Journal of Biological Macromolecules*. 2012; 51(1-2):129-137. http://dx.doi.org/10.1016/j.ijbiomac.2012.04.016. PMid:22546360
38. Wood RA. Paleoecology of the earliest skeletal metazoan communities: Implications for early biomineralization. *Earth-Science Reviews*. 2011; 106(1-2):184-190. http://dx.doi.org/10.1016/j.earscirev.2011.01.011.
39. Jacob DE, Wirth R, Soldati AL, Wehrmeister U and Schreiber A. Amorphous calcium carbonate in the shells of adult Unionoida. *Journal of Structural Biology*. 2011; 173(2):241-249. http://dx.doi.org/10.1016/j.jsb.2010.09.011. PMid:20850546
40. Yang W, Kashani N, Li XW, Zhang GP and Meyers MA. Structural characterization and mechanical behavior of a bivalve shell (Saxidomus purpuratus). *Materials Science and Engineering C*. 2011; 31(4):724-729. http://dx.doi.org/10.1016/j.msec.2010.10.003.
41. Holz, M. and Simões, MG. *Elementos fundamentais de tafonomia*. Porto Alegre: Ed. da UFRJ; 1993.

Appendix 2 – List of specimens and thin sections

Sample	Brief description	Facies (GL - grey limestones; BL - beige limestones)
GP/2E 9666	*Dastilbe crandalli*	GL
GP/2E 9005	*Dastilbe crandalli*	GL
GP/2E 9006	*Dastilbe crandalli*	GL
GP/2E 9014	*Dastilbe crandalli*	BL
GP/2E 7781g	*Dastilbe crandalli*	BL
GP/2E 7786f	*Dastilbe crandalli*	BL
GP/2E 7913e	*Dastilbe crandalli*	BL
GP/2E 7782j	*Dastilbe crandalli*	BL
GP/2E 7780e	*Dastilbe crandalli*	BL
GP/1E 9435	Insect	BL
GP/1E 7105	Insect - Orthoptera	BL
GP/1E 8440	Insect - Hemiptera	BL
GP/1E 8397	Insect - Orthoptera	BL
GP/1E 8827	Insect - Orthoptera	BL
GP/1E 6820	Insect - Indetermined exoskeleton	BL
GP/1E 10368	Insect - Orthoptera	BL
GP/1E 9137	Insect - Blattodea	BL

Sample	Thin section	Brief description
GP/2E 9666	GP/L 16, GP/L 17	Thin section cross-cutting rock lamination and fish
GP/2E 9006	GP/L 18, GP/L 19	Thin section cross-cutting rock lamination and fish
GP/2E 7781g	GP/L 20, GP/L 21	Thin section cross-cutting rock lamination and fish
GP/1E 9435	GP/L 172	Thin section cross-cutting rock lamination and insect

Appendix 3 – Submission receipts of the articles in chapters 5 and 6.

Gmail

Gabriel Osés <gabriel.ladeiraoses@gmail.com>

[PeerJ] Your submission: "Deciphering the Preservation of Fossil Insects: a Case Study from the Crato Member, Early Cretaceous of Brazil" (#2016:07:12183:0:0:CHECK)

1 mensagem

PeerJ <info@peerj.com> 19 de julho de 2016 12:15
Responder a: PeerJ <info@peerj.com>
Para: Gabriel Osés <gabriel.ladeiraoses@gmail.com>

PeerJ

Dear Gabriel,

Thank you for submitting your article for review - Deciphering the Preservation of Fossil Insects: a Case Study from the Crato Member, Early Cretaceous of Brazil.

It will now be checked by PeerJ staff, who will email you if any changes are required.

After passing checks, it will be assigned to an Academic Editor, who will invite reviewers to carry out peer-review.

You will receive email updates at each stage of this process, and you can check the status of your article at any time:

View your Submission

This is a great time to complete your PeerJ profile. Even the basics of a profile photo and institutional info will leave readers with a richer, more rounded understanding of who you are, helping you and your research stand out in their minds.

Complete your Profile

In under 3 minutes

With kind regards,
The PeerJ Team

Some useful advice

If your submission receives a **revise** or **accept** decision, you will need to upload your figures and tables as separate files. We strongly suggest backing these files up now, to have them ready to upload at resubmission!

Article ID: 12183

Need help? Just reply to this email.

Manuscript #	SREP-16-28643-T
Current Revision #	0
Submission Date	19th July 16
Current Stage	Quality Check Started
Title	Deciphering pyritization-kerogenization gradient for fish soft-tissue preservation
Manuscript Type	Original Research
Corresponding Author	Mr. Gabriel Osés (gabriel.ladeiraoses@gmail.com) (University of São Paulo)
Contributing Authors	Dr. Setembrino Petri , Dr. Cibele Voltani , Mr. Gustavo Prado , Dr. Douglas Galante , Dr. Marcia Rizzutto , Dr. Isaac Rudnitzki , Mr. Evandro Silva , Dr. Fabio Rodrigues , Dr. Elidiane Rangel , Dr. Paula Sucerquia , Dr. Mírian Pacheco
Authorship	Yes
Abstract	Soft-tissue preservation provides palaeobiological information otherwise lost during fossilization. In Brazil, the Early Cretaceous Santana Formation has fishes with integument, muscles, connective tissues, and eyes still preserved. Thin-section petrography, geochemistry, and electron microscopy have been employed to test if such labile structures are the result of distinct palaeoenvironment-controlled pathways. Our study reveals that soft-tissues were pyritized or kerogenized in different facies, yielding distinct preservational fidelities. Indeed, new data provide the first record so far of vertebrate pyritized muscles and eyes. We propose that distinct sedimentation rates yielded two different facies in which buried carcasses underwent varied residence times in sulphate-reduction and methanogenesis zones, thus yielding pyritized or kerogenized soft-tissues, as suggested by Ediacaran fossil preservation.
Techniques	Physical sciences techniques; Physical sciences techniques, Microscopy techniques [Scanning electron microscopy]; Physical sciences techniques, Spectroscopy [Raman spectroscopy];
Subject Terms	Earth and environmental sciences/Solid Earth sciences/Geology Earth and environmental sciences/Solid Earth sciences/Palaeontology Earth and environmental sciences/Solid Earth sciences/Sedimentology Earth and environmental sciences/Solid Earth sciences/Geochemistry
Competing Financial Interest	There is **NO** Competing Interest.
Applicable Funding Source	Brazilian Synchrotron Light Laboratory (20150110), Brazilian Nanotechnology National Laboratory (Quanta-18363), São Paulo Research Foundation (FAPESP) (2012/18936-0), São Paulo Research Foundation (FAPESP) (2012/00202-0), CNPq (154062/2014-6) [Osés] Brazilian Synchrotron Light Laboratory (20150110), Brazilian Nanotechnology National Laboratory (Quanta-18363), São Paulo Research Foundation (FAPESP) (2012/18936-0), São Paulo Research Foundation (FAPESP) (2012/00202-0), CNPq (154062/2014-6) [Petri] Brazilian Synchrotron Light Laboratory (20150110), Brazilian Nanotechnology National Laboratory (Quanta-18363), São Paulo Research Foundation (FAPESP) (2012/18936-0), São Paulo Research Foundation (FAPESP) (2012/00202-0), CNPq (154062/2014-6) [Voltani] Brazilian Synchrotron Light Laboratory (20150110), Brazilian Nanotechnology National Laboratory (Quanta-18363), São Paulo Research Foundation (FAPESP) (2012/18936-0), São Paulo Research Foundation (FAPESP) (2012/00202-0), CNPq (154062/2014-6) [Prado] Brazilian Synchrotron Light Laboratory (20150110), Brazilian Nanotechnology National Laboratory (Quanta-18363), São Paulo Research Foundation (FAPESP) (2012/18936-0), São Paulo Research Foundation (FAPESP) (2012/00202-0), CNPq (154062/2014-6) [Galante] Brazilian Synchrotron Light Laboratory (20150110), Brazilian Nanotechnology National Laboratory (Quanta-18363), São Paulo Research Foundation (FAPESP) (2012/18936-0), São Paulo Research Foundation (FAPESP) (2012/00202-0), CNPq (154062/2014-6) [Rizzutto] Brazilian Synchrotron Light Laboratory (20150110), Brazilian Nanotechnology National Laboratory (Quanta-18363), São Paulo Research Foundation (FAPESP) (2012/18936-0), São Paulo Research Foundation (FAPESP) (2012/00202-0), CNPq (154062/2014-6) [Rudnitzki] Brazilian Synchrotron Light Laboratory (20150110), Brazilian Nanotechnology National Laboratory (Quanta-18363), São Paulo Research Foundation (FAPESP) (2012/18936-0), São Paulo Research Foundation (FAPESP) (2012/00202-0), CNPq (154062/2014-6)

	[Silva] Brazilian Synchrotron Light Laboratory (20150110), Brazilian Nanotechnology National Laboratory (Quanta-18363), São Paulo Research Foundation (FAPESP) (2012/18936-0), São Paulo Research Foundation (FAPESP) (2012/00202-0), CNPq (154062/2014-6) [Rodrigues] Brazilian Synchrotron Light Laboratory (20150110), Brazilian Nanotechnology National Laboratory (Quanta-18363), São Paulo Research Foundation (FAPESP) (2012/18936-0), São Paulo Research Foundation (FAPESP) (2012/00202-0), CNPq (154062/2014-6) [Rangel] Brazilian Synchrotron Light Laboratory (20150110), Brazilian Nanotechnology National Laboratory (Quanta-18363), São Paulo Research Foundation (FAPESP) (2012/18936-0), São Paulo Research Foundation (FAPESP) (2012/00202-0), CNPq (154062/2014-6) [Sucerquia] Brazilian Synchrotron Light Laboratory (20150110), Brazilian Nanotechnology National Laboratory (Quanta-18363), São Paulo Research Foundation (FAPESP) (2012/18936-0), São Paulo Research Foundation (FAPESP) (2012/00202-0), CNPq (154062/2014-6) [Pacheco]

Manuscript Items

1. Author Cover Letter PDF (46KB) Source File (DOCX) 62KB
2. Merged File containing manuscript text and 6 Figure files. PDF (63851KB)
    a. Article File PDF (127KB) Source File (DOCX) 74KB
    b. Figure 1 PDF (15780KB) Source File (TIF) 13469KB
    c. Figure 2 PDF (3142KB) Source File (TIF) 11673KB
    d. Figure 3 PDF (17565KB) Source File (TIF) 24329KB
    e. Figure 4 PDF (16964KB) Source File (TIF) 24016KB
    f. Figure 5 PDF (9914KB) Source File (TIF) 11554KB
    g. Figure 6 PDF (362KB) Source File (TIF) 24747KB
3. Supplementary Information PDF (1459KB) Source File (PDF) 1459KB
4. Catto et al. (2016) PDF (2941KB) Source File (PDF) 2941KB

More Manuscript Info and Tools

Send Manuscript Correspondence

Check Status

Appendix 4 – Permission Letter.

Dear Gabriel LadeiraOsés

On behalf of the journal Materials Research, I permit that you publish a modified version of Figure 2c from Delgado et al.(2014), on the open-access journal PeerJ (manuscript "Deciphering the Preservation of Fossil Insects from the Early Cretaceous of Brazil"), under the CC-BY 4.0 license (http://creativecommons.org/licenses/by/4.0/).

Kind regards,

Walter J. Botta

Materials Research Editor

Reference

Delgado A de O, Buck PV, Osés GL,Ghilardi RP, Rangel EC, Pacheco MLAF.Paleometry: a brand new area in Brazilian science. Mater Res. 2014; 17: 1434-1441.